Dissertation

submitted to the

Combined Faculties of the Natural Sciences and Mathematics

of the Ruperto-Carola-University of Heidelberg. Germany

for the degree of

Doctor of Natural Sciences

Put forward by

Alexander Dück

born in Schortandy, Kasachstan

Oral examination: February 6th 2013

Phenomenology of Neutrinos and Possible SO(10) Origins of Fermion Masses and Mixings

Referees:

Dr. Werner Rodejohann

Prof. Dr. Tilman Plehn

Phänomenologie von Neutrinos und mögliche SO(10) Ursprünge von Fermionmassen und -mischungen

Wichtige, aber bisher unbeantwortete, Fragen in der Neutrinophysik sind die Neutrinomassenhierarchie, präzise Messung der Mischungsparameter und CP-Verletzung. Ein in der Literatur detailliert untersuchtes Schema für Mischungsparameter ist Tri-Bimaximale Mischung. In der vorliegenden Arbeit wird die Wichtigkeit von alternativen Mischungsschemata betont, viele von ihnen analysiert, und ihre Vorhersagen mit aktuellen Messdaten zu Neutrinomischungen konfrontiert. Wo notwendig zeigen wir wie Störungen der Vorhersagen erster Ordnung zu einem phänomenologisch akzeptablen Mischungsschema führen. Des Weiteren erforschen wir die Aussicht die invertierte Hierarchie mit neutrinolosem doppeltem Betazerfall zu testen. Ein Ergebnis ist, dass das untere Limit der effektiven Neutrinomasse, die relevant für diesen Prozess und somit die Aussicht die invertierte Hierarchie experimentell auszuschließen ist, sensitiv vom Neutrinomischungswinkel θ_{12} abhängt. Weiterhin beziehen wir Unsicherheiten aus der Kernphysik mit in die Analyse ein. Als nächstes analysieren wir die Möglichkeit den Ursprung von Fermionmassen und -mischungen sowie die Baryonasymmetrie im Rahmen renormierbarer großer vereinheitlichter Theorien basierend auf der Gruppe $SO(10)$ zu erklären und berücksichtigen dabei Effekte des Renormierungsgruppenlaufens. Modelle mit verschiedenen Higgsdarstellungen werden betrachtet. Nachdem die Modellparameter anhand experimenteller Daten eingeschränkt worden sind, präsentieren wir Vorhersagen der Modelle für bisher ungemessene Observablen. Für die leptonische CP-verletzende Phase geben wir zulässige Bereiche mit 68 % Konfidenz an.

Phenomenology of Neutrinos and Possible SO(10) Origins of Fermion Masses and Mixings

Important but yet unanswered questions in neutrino physics are the neutrino mass hierarchy, precision determination of mixings and CP violation. A widely studied mixing scheme upon which many models are based is tri-bimaximal mixing. We emphasize the importance of alternative mixing schemes and confront their predictions with current data on neutrino mixings. Where necessary we show how perturbations of the leading order predictions can result in viable schemes. Further we study the prospects to test the inverted hierarchy with neutrinoless double beta decay. We find that the lower limit of the effective neutrino mass relevant for this process and hence the prospects to experimentally exclude the inverted hierarchy are highly sensitive to the neutrino mixing angle θ_{12}. We further take into account uncertainties from nuclear physics. Next we analyze the possibility to explain the origin of fermion masses and mixings as well as the baryon asymmetry within renormalizable Grand Unified Theories based on $SO(10)$, including effects of renormalization group evolution. Models with different Higgs representations are considered. After constraining the model parameters with experimental data we give the model predictions for undetermined observables; for the leptonic CP violating phase we also show the ranges allowed at 68 % C.L.

Contents

Chapter 1

Introduction

This thesis is dedicated to the study of the phenomenology of neutrino physics and to the analysis of a possible $SO(10)$ origin of fermion masses and mixings.

With the unambiguous discovery of neutrino oscillations [1, 2], the field of neutrino physics brought to us the most firmly established experimental evidence for physics beyond the Standard Model (SM)[1], the SM being restricted here to a renormalizable $SU(3)_C \times SU(2)_L \times U(1)_Y$ theory without right-handed neutrinos. This discovery gives strong experimental support to look for a successor or at least an extension of the SM. Furthermore, it immediately opens up two central interrelated questions: (*i*) What is the origin of neutrino masses and mixings? (*ii*) Is the neutrino a Dirac or a Majorana particle? While the first question is to a large extent theoretical with experiments providing guidance, the second question can in principle be decided from experiments searching for neutrinoless double beta ($0\nu\beta\beta$) decay [5]. Generally, the potential impact of data from neutrino physics experiments is very high. This is very much due to the special properties of neutrinos as compared to the other SM particles. Firstly, as mentioned above, there is the possibility of being Majorana particles. Secondly, the mixings in the lepton sector are very different from those already known in the quark sector. While in the quark sector the off-diagonal elements of the Cabibbo–Kobayashi–Maskawa (CKM) mixing matrix are very small, in the corresponding Pontecorvo–Maki–Nakagawa–Sakata (PMNS) mixing matrix, important for neutrino experiments, all entries are of the same order of magnitude. Finally, the scale of neutrino masses is at least six orders of magnitude below that of charged leptons, which also distinguishes leptons from quarks. Therefore one can expect data from neutrino experiments to be especially important in constraining the possibilities to extend the SM and in giving hints which paths of theoretical research may turn out to be very fruitful.

A straightforward extension of the SM in order to incorporate neutrino masses is the inclusion of right-handed neutrinos, which must be SM singlets. This again opens up an intriguing possibility: through a mechanism known as thermal leptogenesis (see sec. 6.4 for details) the lightest of these new particles can produce the observed baryon asymmetry and thus answer the question of the origin of matter. Taken together, this is more than

[1] Dark Matter [3] being the other one, which can however also have an origin outside of particle physics [4]. In this thesis we will not be concerned with Dark Matter.

enough motivation to study the phenomenology of neutrinos.

The current main open questions in neutrino physics are the neutrino mass hierarchy and precision determination of mixings. Here we will be concerned with both of them.

From the theory side, the most widely studied mixing scheme is tri-bimaximal (TBM) mixing [6], which was first proposed as a purely phenomenological description of neutrino mixing data. Since then the quest for a theory explaining neutrino mixings was often tackled with flavor symmetry models [7], which try to reproduce the corresponding TBM form of the mass matrix. There are, however, many other possibilities to explain the observed data. It was shown that mass matrices that are significantly different from the mass matrix yielding TBM mixing are phenomenologically viable [8]. Hence, one should certainly ask the question as to whether there indeed exists some hidden flavor symmetry or whether the nearly observed TBM mixing is purely accidental. In particular, we will explore a plethora of alternatives to TBM and confront the predictions of these possibilities with current data on neutrino mixings.

One way to address the question of neutrino mass hierarchy is neutrinoless double beta ($0\nu\beta\beta$) decay [5]. This process violates lepton number by two units and hence would verify the Majorana nature of neutrinos [9]. The (as yet unobserved) $0\nu\beta\beta$ decay rate depends on a number of known and unknown neutrino parameters. Among the unknown parameters the neutrino mass hierarchy (i.e., the sign of the atmospheric mass-squared difference) is of particular interest. Neutrinoless double beta decay offers the fascinating possibility to rule out the inverted neutrino mass hierarchy. However, in practice this crucially depends on theoretical calculations of nuclear matrix elements for $0\nu\beta\beta$ decay and on the precise knowledge of the solar neutrino mixing angle (θ_{12}). In this thesis we focus on the particle physics aspects of $0\nu\beta\beta$ decay by precisely analyzing the latter dependence, but we also take into account uncertainties coming from nuclear matrix element calculations.

The fact that the prospects to exclude the inverted hierarchy with $0\nu\beta\beta$ decay experiments depend on θ_{12} gives a nice connection to the lepton mixing schemes that were described above and that are analyzed in this thesis. However, our world consists of leptons *and* quarks and one should wonder whether there is a connection between these two particle species. Grand Unified Theories (GUTs) [10] provide a compelling framework to establish and analyze possible relations between quarks and leptons. By reducing the number of multiplets to which observed particles are assigned it is possible to relate different parameters from the Yukawa sector, which are otherwise unrelated in the SM. Besides being suitable to establish relations between quarks and leptons, Grand Unified Theories can give an explanation for charge quantization [10], which is not understandable within the SM. Furthermore, in GUTs it is possible to relate the three SM gauge couplings to each other and thus unify all particle interactions. This motivation is further strengthened by the observed approximate unification of SM gauge couplings at a common high energy scale $M_{\rm GUT} \sim 10^{15} \div 10^{16}$ GeV. The fact that lepton number violation is a generic prediction of GUTs makes – in view of $0\nu\beta\beta$ decay– the Grand Unification paradigm even more attractive. Specifically, through either observing $0\nu\beta\beta$ decay or setting new limits on the process it is possible to constrain or exclude several GUT scenarios.

Among different Grand Unified Theories, models based on $SO(10)$ symmetry are particu-

larly interesting. $SO(10)$ GUTs have the advantage that all SM fermions of one generation plus a right-handed neutrino neatly fit into one 16-dimensional representation of $SO(10)$, giving strong relations between Yukawa couplings of quarks and leptons. In addition, one can argue that $SO(10)$ GUTs predict the existence of right-handed neutrinos. Furthermore, through the seesaw mechanism [11] $SO(10)$ explains in an elegant way why neutrinos are so light. Although there is no direct experimental hint (like proton decay) for a Grand Unified Theory, considering the list of arguments in favor of GUTs in general and $SO(10)$ in particular we will analyze renormalizable GUTs based on $SO(10)$ in the second part of this thesis.

The thesis is organized as follows. In the first part we are concerned with the phenomenology of neutrino physics. In particular, in chapter 2 we analyze many alternative scenarios to tri-bimaximal mixing and plot the allowed ranges for neutrino mixing angles in comparison with data. We also suggest a new scenario, "hexagonal mixing", not previously discussed in the literature. This scenario has later been shown to be derivable from a flavor symmetry [12]. Two of the schemes we considered, "hexagonal" and "bimaximal" mixing, display a high amount of symmetry but require moderate perturbations in order to bring them into compliance with the data, and we have examined the various ways for doing so. In chapter 3 we analyze the prospects of ruling out the inverted neutrino mass hierarchy with neutrinoless double beta decay experiments and emphasize the strong dependence on the value of the solar neutrino mixing angle. We give the required half-lives to exclude (and touch) the inverted hierarchy regime for all double beta decay isotopes with a Q-value above 2 MeV. The nuclear matrix elements from 6 different groups and, if available, their errors are used and compared. We carefully put the calculations on equal footing in what regards various convention issues. We also use our compilation of matrix elements to give the attainable values of the effective mass for a given half-life value. Note that chapters 2 and 3 have already been published together with coauthors as refs. [13] and [14], respectively, and are updated here due to the recent discovery of the non-zero reactor mixing angle (θ_{13}) [15–17], more precise data on the other mixing parameters now available, and new limits on $0\nu\beta\beta$ decay [18, 19]. Further work we performed on the phenomenology of neutrinos can be found in ref. [20]. Since it does not reflect the central theme it was not included in this thesis.

The second part of this thesis is concerned with numerical fits of fermion masses and mixings within renormalizable $SO(10)$ theories. Models with $10_H + \overline{126}_H$, $\overline{126}_H + 120_H$, and $10_H + \overline{126}_H + 120_H$ Higgs representations are analyzed in the case of type I seesaw dominance. Available literature heavily focuses on supersymmetric GUTs; in this thesis both supersymmetric as well as non-supersymmetric versions of the models are considered. For supersymmetric models we use three different values of $\tan\beta$ (50, 38, 10). To compare the models with data we include detailed 1-loop renormalization group evolution (RGE) in our analysis. Previous studies use input values for their analysis that have been evolved to high energies with some generic assumptions and then perform the fits at the scale of unification, $M_{\rm GUT}$. Evolving observables from low energies to high energies depends on model details, e.g., the seesaw scale or the Yukawa coupling matrix of neutrinos above the seesaw scale. Hence, studies that perform the analysis at $M_{\rm GUT}$ suffer from inherent

systematic uncertainties. We avoid these by including RGE into our fitting procedure. In addition we take into account effects from non-degenerate seesaw scales by integrating out heavy neutrinos one by one during RGE at their respective energy scale.

Performing RGE ourselves allows us to consider both possibilities, normal or inverted, for the neutrino mass hierarchy. This is only sensibly possible when including RGE into the analysis, since for the inverted hierarchy neutrino parameters are known to evolve sizably between high and low energies. This explains the strong focus on the normal hierarchy in the literature. By including RGE into our fitting procedure we can show that some models work only with the normal hierarchy and hence will be ruled out if the neutrino mass spectrum turns out to be inverted.

Observables commonly considered when analyzing GUTs are fermion masses and mixings. As a novel feature of our analysis we check the ability of the models to additionally reproduce the experimentally observed baryon asymmetry of the universe through thermal leptogenesis, also including flavor effects. A further novelty presented in this thesis is that we additionally constrain the non-supersymmetric models by fitting the mass of the Higgs boson (assuming recent discoveries of a new resonance at the Large Hadron Collider [21, 22] are indeed produced by a Higgs boson), which introduces severe tensions for all models under consideration. Finally, we give the predictions for as yet unmeasured quantities, namely the effective mass $\langle m_\nu \rangle$ relevant for neutrinoless double beta decay, the leptonic CP violating phase, δ^l_{CP}, the mass of the lightest neutrino, and the masses of the heavy neutrinos. Experiments in the near future will decide whether the atmospheric neutrino mixing angle corresponds to maximal mixing (i.e., $\theta_{23} = 45°$) or not. In addition the next question to be answered in neutrino physics is the value of δ^l_{CP}. Therefore we check whether fits to observables described above really fix these quantities to a tight interval or whether the models are compatible with a broad range of values. For δ^l_{CP} we provide confidence intervals, compare those derived with and without inclusion of RGE and find that the results are very different. Thus we stress the importance of including RGE especially when investigating model predictions.

Part I

Phenomenology of Neutrino Physics

Chapter 2

Alternatives to Tri-bimaximal Mixing

2.1 Introduction

The text in this chapter corresponds in large parts to the one in ref. [13] that has been published together with coauthors as C. H. Albright, A. Dueck, and W. Rodejohann, *"Possible Alternatives to Tri-bimaximal Mixing",* Eur. Phys. J. C 70 (2010) 1099–1110. It is updated here due to more precise data on neutrino mixing angles available now. Updates concern tbl. 2.1 and figs. 2.1–2.6.

The first discoveries of neutrino oscillations arose from observations of the depletions of atmospheric muon-neutrinos [1] and solar electron-neutrinos [2], relative to their expected predictions. In efforts to understand these findings, many theorists adopted top-down approaches in attempts to construct models which would explain the data. For this purpose, various forms of the neutrino and charged lepton mass matrices were postulated, some applied directly to the light left-handed neutrino mass matrix, while other more ambitious efforts invoked the seesaw mechanism partly using also the framework of grand unified models. Examples to constrain the mass matrices involved the assignment of texture zeros, the use of a vertical family symmetry group, and/or the selection of a horizontal flavor symmetry, usually of a continuous type such as $U(1)$, $SU(2)$ or $SU(3)$. The more complete models and their predictions differed by the choice of family and flavor symmetries, and the fermion and Higgs representation assignments made in the construction of the unknown Yukawa interactions needed to extend the Standard Model.

As the oscillation data became more accurate with refinements in the atmospheric [23,24] and solar [25–27] neutrino experiments and introduction of land-based reactor [28–30] and long baseline neutrino [31, 32] experiments, bottom-up approaches to construct models became more feasible. Among the first to realize the mixing data were pointing to a rather simple construction were Harrison, Perkins and Scott [6], who coined the phrase "tri-bimaximal mixing". In this scheme the atmospheric neutrino mixing angle (θ_{23}) is maximal (45°), the reactor neutrino mixing angle (θ_{13}) vanishes, while the solar neutrino mixing angle is $\theta_{12} \simeq 35.3°$, such that $\sin^2\theta_{12} = \frac{1}{3}$. With this tri-bimaximal mixing (TBM) texture in mind, many models have been constructed based on the discrete symmetry

groups such as S_3, A_4, S_4, T', etc., with a vast majority using A_4 (see refs. [7,33] for reviews on flavor symmetries, in particular A_4, and ref. [34] for a classification of all existing (50+) type I seesaw, type II seesaw and non-seesaw A_4 models). After the recent discovery of θ_{13} being non-zero [15–17], the leading order prediction of the tri-bimaximal mixing pattern ($\theta_{13} = 0$) is definitely excluded. Thus, with new data available our study presented in this chapter is even more relevant than at the time when it was originally conducted [13].

It is fair to say that TBM dominates the theoretical literature in flavor model building[1]. We remind the reader that attempts to explain the mixing data based on grand unified models using continuous flavor symmetry groups were also reasonably successful in explaining the mixing data (see ref. [35] for a list of 13 valid $SO(10)$ models in agreement with current data). This raises the issue whether there indeed exists some hidden flavor symmetry, such as A_4, or whether the nearly observed TBM mixing is accidental in nature. Ref. [35] tried to attack this issue from the point of perturbing the neutrino mass matrix $m_\nu^{\rm TBM}$ corresponding to TBM. It was argued that when relative corrections to the mass matrix entries are applied, the value of $|U_{e3}|$ can be crucial to distinguish TBM from grand unified theories. A very recent paper [8] has shown that mass matrices which are significantly different from $m_\nu^{\rm TBM}$ are also allowed. It is thus important not to focus solely on one particular mixing scheme, such as TBM, but to look for other options as well. In any case, it is apparent that very accurate experimental determinations of the neutrino mixing parameters will be required in order to pin down the source of the flavor mixing.

In the spirit of the above considerations, we point out in this chapter the existence of a plethora of alternatives to TBM and explore a number of other possibilities for the neutrino mixing matrix. We wish to stress that many of the mixing scenarios that we describe are allowed by the current data equally well. Some of them have been obtained in models with the flavor symmetry specified at the outset, and very often the choice of symmetry group is motivated by geometrical considerations. Good examples here are the two golden ratio possibilities for the solar neutrino mixing angle. Among the other examples we give is trimaximal mixing, where only the second column of the tri-bimaximal mixing matrix with equal flavor contributions is postulated. Variations of this theme make the invariant assumption for the first or third column or one of the three rows. Yet another hypothesis involves quark-lepton complementarity where the quark and neutrino mixing matrices are related. Obviously, one should try to disentangle the huge number of proposed flavor models in order to sort out the correct one, or at least rule out many of the incorrect ones [36–38].

We should also mention that it is not unlikely that corrections to mixing schemes may apply. Radiative corrections, effects of charged lepton rotations, soft breaking, or "NLO" effects of the underlying flavor models are possibilities. The magnitude of the corrections relies heavily on the models which realize the respective scenarios, and depend on a number of unknown parameters, such as neutrino masses or CP phases. Let us mention, however, that radiative corrections are small for a normal hierarchy of neutrino masses, and that

[1]The original suggestion of tri-bimaximal mixing was a purely phenomenological Ansatz and only later shown to be obtainable in dedicated flavor models.

charged lepton rotations play no role if the symmetry basis coincides with the charged lepton mass basis. In principle one could perform for each scenario to be discussed in the following a dedicated analysis of perturbations in analogy, e.g., to the model-independent study for TBM in ref. [39], or to studies for concrete models in refs. [40–43]. In the present thesis we neglect the study of these aspects, and rather focus on pointing out the existence of a variety of alternatives to TBM, their possible physics motivation, and the "unperturbed" predictions of the scenarios. In principle, for each scenario considered, one can use the bottom-up approach to determine the neutrino mass matrix and presumably to construct a model based on some discrete flavor symmetry which yields the desired mixing. This is well illustrated, for instance, in the case of tri-bimaximal mixing for which an extensive literature exists in which models based on one of the discrete symmetries mentioned above have been proposed.

2.2 Lepton Mixing Schemes

We begin with the Pontecorvo–Maki–Nakagawa–Sakata (PMNS) mixing matrix, which in general is given by

$$U = U_\ell^\dagger \, U_\nu \,, \tag{2.1}$$

where U_ℓ (U_ν) stems from diagonalization of the charged lepton (neutrino) mass matrix. The standard form of the PMNS matrix is

$$U = \begin{pmatrix} c_{12}\, c_{13} & s_{12}\, c_{13} & s_{13}\, e^{-i\delta} \\ -s_{12}\, c_{23} - c_{12}\, s_{23}\, s_{13}\, e^{i\delta} & c_{12}\, c_{23} - s_{12}\, s_{23}\, s_{13}\, e^{i\delta} & s_{23}\, c_{13} \\ s_{12}\, s_{23} - c_{12}\, c_{23}\, s_{13}\, e^{i\delta} & -c_{12}\, s_{23} - s_{12}\, c_{23}\, s_{13}\, e^{i\delta} & c_{23}\, c_{13} \end{pmatrix} P \,, \tag{2.2}$$

where $c_{ij} = \cos\theta_{ij}$, $s_{ij} = \sin\theta_{ij}$ with δ the unknown CP-violating Dirac phase. The two equally unknown Majorana phases appear in $P = \mathrm{diag}(1, e^{i\alpha}, e^{i\beta})$. While the phases are currently unconstrained, the present best-fit values of the mixing angles and their 1σ and 3σ ranges [44] are presented in tbl. 2.1 (other groups obtain very similar results [45, 46]). The above parameterization of U is obtained by three consecutive rotations:

$$U = R_{23}(\theta_{23})\, \tilde{R}_{13}(\theta_{13};\delta)\, R_{12}(\theta_{12}) \,, \quad \text{where, e.g.,} \tag{2.3}$$

$$R_{12}(\theta_{12}) = \begin{pmatrix} c_{12} & s_{12} & 0 \\ -s_{12} & c_{12} & 0 \\ 0 & 0 & 1 \end{pmatrix} , \quad \tilde{R}_{13}(\theta_{13};\delta) = \begin{pmatrix} c_{13} & 0 & s_{13}\, e^{-i\delta} \\ 0 & 1 & 0 \\ -s_{13}\, e^{i\delta} & 0 & c_{13} \end{pmatrix} . \tag{2.4}$$

The most popular mixing scenario approximating the current data is the tri-bimaximal one [6, 47–49]:

$$U_{\rm TBM} = \begin{pmatrix} \sqrt{\frac{2}{3}} & \sqrt{\frac{1}{3}} & 0 \\ -\sqrt{\frac{1}{6}} & \sqrt{\frac{1}{3}} & -\sqrt{\frac{1}{2}} \\ -\sqrt{\frac{1}{6}} & \sqrt{\frac{1}{3}} & \sqrt{\frac{1}{2}} \end{pmatrix} , \tag{2.5}$$

Parameter	Best-fit$\pm 1\,\sigma$	$3\,\sigma$ range
$\sin^2\theta_{12}$	0.30 ± 0.013	$0.27 \to 0.34$
$\sin^2\theta_{23}$	$0.41^{+0.037}_{-0.025}$	$0.34 \to 0.67$
$\sin^2\theta_{13}$	0.023 ± 0.0023	$0.016 \to 0.030$

Table 2.1: Mixing angles and their $1\,\sigma$ and $3\,\sigma$ ranges [44].

corresponding to[2]

$$\sin^2\theta_{12} = \frac{1}{3}\,, \quad \sin^2\theta_{23} = \frac{1}{2}\,, \quad |U_{e3}| = 0\,. \tag{2.6}$$

The overwhelming majority of the plethora of models (see [7, 33, 34] for a list of references) invokes the symmetry group A_4. One reason is that A_4 is rather economical: it is the smallest discrete group containing a three dimensional irreducible representation (IR). Furthermore, in the flavor basis it can be generated by two generators[3] S and T, one of which is diagonal and leaves the charged lepton mass matrix diagonal, while the other one leaves $m_\nu^{\rm TBM}$ invariant [7], where

$$m_\nu^{\rm TBM} = \begin{pmatrix} A & B & B \\ \cdot & \frac{1}{2}(A+B+D) & \frac{1}{2}(A+B-D) \\ \cdot & \cdot & \frac{1}{2}(A+B-D) \end{pmatrix} \tag{2.7}$$

is the most general neutrino mass matrix leading to TBM. A geometrical motivation is provided by noting that A_4 is the symmetry group of the regular tetrahedron, and the angle between two faces is $2\theta_{\rm TBM}$, where $\sin^2\theta_{\rm TBM} = \frac{1}{3}$. Models can be constructed in such a way that the Yukawa couplings, and hence the mass matrices, are invariant under certain group elements, which are generated by S and T, which in turn are connected to the symmetry of the geometrical object the group describes. In this way the connection between geometry and flavor physics can arise.

Tri-bimaximal mixing is a variant of the more general μ–τ symmetry, which leaves solar neutrino mixing unconstrained:

$$U_{\mu\text{–}\tau} = \begin{pmatrix} \cos\theta_{12} & \sin\theta_{12} & 0 \\ -\frac{\sin\theta_{12}}{\sqrt{2}} & \frac{\cos\theta_{12}}{\sqrt{2}} & -\sqrt{\frac{1}{2}} \\ -\frac{\sin\theta_{12}}{\sqrt{2}} & \frac{\cos\theta_{12}}{\sqrt{2}} & \sqrt{\frac{1}{2}} \end{pmatrix}, \tag{2.8}$$

corresponding to

$$\sin^2\theta_{23} = \frac{1}{2}\,, \quad |U_{e3}| = 0\,. \tag{2.9}$$

[2]To obtain this form of U, it is necessary to insert $\theta_{23} = -\pi/4$ in the standard parameterization (2.2) of the PMNS matrix. Compared to $\theta_{23} = +\pi/4$, the difference is unphysical, of course. In the following we will use $\theta_{23} = -\pi/4$ whenever we speak about maximal atmospheric mixing.

[3]Some groups require 3 generators.

From a theoretical point of view, θ_{12} is unconstrained by μ–τ symmetry and hence can be expected to be a number of order one. This is indeed in good agreement with data. A simple Z_2 or S_2 exchange symmetry acting on the neutrino mass matrix suffices to generate μ–τ symmetry. In fact, any symmetry having Z_2 or S_2 as a subgroup can be used, for instance, D_4 [50, 51].

We now turn to other mixing scenarios which serve as alternatives to the tri-bimaximal one. First consider trimaximal mixing and its variants [52–57] (see also [58]). Here a given row or column of U takes the same form as for tri-bimaximal mixing. The term "trimaximal" was originally used for the case of the second column of the PMNS matrix being identical to the TBM case. The analogous possibilities for the other rows and columns go under the same banner "trimaximal". The notation is such that if the ith column (row) of U has the same form as for TBM, then the scenario is called TM_i (TM^i). In case this applies to the first column of U, the condition is:

$$\mathrm{TM}_1: \quad \begin{pmatrix} |U_{e1}|^2 \\ |U_{\mu 1}|^2 \\ |U_{\tau 1}|^2 \end{pmatrix} = \begin{pmatrix} 2/3 \\ 1/6 \\ 1/6 \end{pmatrix}. \tag{2.10}$$

The implications of this Ansatz are [57]

$$\sin^2\theta_{12} = \frac{1}{3}\,\frac{1-3\,|U_{e3}|^2}{1-|U_{e3}|^2} \simeq \frac{1}{3}\,\left(1-2\,|U_{e3}|^2\right) \tag{2.11}$$

and

$$\cos\delta\,\tan 2\theta_{23} = -\frac{1-5\,|U_{e3}|^2}{2\sqrt{2}\,|U_{e3}|\,\sqrt{1-3\,|U_{e3}|^2}} \simeq \frac{-1}{2\sqrt{2}\,|U_{e3}|}\left(1-\frac{7}{2}\,|U_{e3}|^2\right). \tag{2.12}$$

For the second column the originally-named trimaximal condition is

$$\mathrm{TM}_2: \quad \begin{pmatrix} |U_{e2}|^2 \\ |U_{\mu 2}|^2 \\ |U_{\tau 2}|^2 \end{pmatrix} = \begin{pmatrix} 1/3 \\ 1/3 \\ 1/3 \end{pmatrix}, \tag{2.13}$$

leading to [52, 53, 57]

$$\sin^2\theta_{12} = \frac{1}{3}\,\frac{1}{1-|U_{e3}|^2} \geq \frac{1}{3} \tag{2.14}$$

and

$$\cos\delta\,\tan 2\theta_{23} = \frac{2\,\cos\theta_{13}\,\cot 2\theta_{13}}{\sqrt{2-3\,\sin^2\theta_{13}}} = \frac{1-2\,|U_{e3}|^2}{|U_{e3}|\,\sqrt{2-3\,|U_{e3}|^2}} \tag{2.15}$$

$$\simeq \frac{1}{\sqrt{2}}\,\frac{1}{|U_{e3}|}\left(1-\frac{5}{4}\,|U_{e3}|^2\right). \tag{2.16}$$

If we would insist that the third column of $U_{\rm TBM}$ remains invariant instead, i.e., $|U_{e3}|^2 = 0$, $|U_{\mu 3}|^2 = |U_{\tau 3}|^2 = \frac{1}{2}$, then $\theta_{13} = 0$, $\theta_{23} = \pi/4$, while θ_{12} is a free parameter and δ is arbitrary. This case (TM_3 in our notation) is nothing other than μ–τ symmetry.

It was argued [55,56] that models based on flavor symmetries which have A_4 as a subgroup should be possible for TM_2. For TM_1 and TM_3, these groups are S_4 and S_3, respectively. Models based on flavor symmetry groups $\Delta(27)$ [52, 53] and S_3 [54] have been constructed for the trimaximal scenario TM_2.

Now consider the case where one of the rows of the tri-bimaximal mixing matrix remains invariant [57]. We start with the case of the first row in $U_{\rm TBM}$ remaining invariant, denoting this by TM^1,

$$\mathrm{TM}^1: \qquad \left(|U_{e1}|^2\,,\ |U_{e2}|^2\,,\ |U_{e3}|^2\right) = \left(\frac{2}{3}\,,\ \frac{1}{3}\,,\ 0\right). \tag{2.17}$$

Here θ_{23} is a free parameter, while $\sin^2\theta_{12} = \frac{1}{3}$, as well as $\theta_{13} = \delta = 0$.

If we consider only the second or third row invariant, we can again correlate all four mixing parameters. Starting with the second row, i.e.,

$$\mathrm{TM}^2: \qquad \left(|U_{\mu 1}|^2\,,\ |U_{\mu 2}|^2\,,\ |U_{\mu 3}|^2\right) = \left(\frac{1}{6}\,,\ \frac{1}{3}\,,\ \frac{1}{2}\right), \tag{2.18}$$

one immediately finds from $|U_{\mu 3}|^2 = \frac{1}{2}$:

$$\sin^2\theta_{23} = \frac{1}{2\left(1 - |U_{e3}|^2\right)} \simeq \frac{1}{2}\left(1 + |U_{e3}|^2\right) \geq \frac{1}{2}\,, \tag{2.19}$$

with atmospheric neutrino mixing on the "dark side" ($\theta_{23} \geq \pi/4$). The second correlation among the mixing parameters is

$$\sin^2\theta_{12} \simeq \frac{1}{3} - \frac{2\sqrt{2}}{3}\,|U_{e3}|\,\cos\delta\, + \frac{1}{3}\,|U_{e3}|^2\,\cos 2\delta\,. \tag{2.20}$$

On the other hand, with the third row remaining invariant,

$$\mathrm{TM}^3: \quad \left(|U_{\tau 1}|^2\,,\ |U_{\tau 2}|^2\,,\ |U_{\tau 3}|^2\right) = \left(\frac{1}{6}\,,\ \frac{1}{3}\,,\ \frac{1}{2}\right), \tag{2.21}$$

the atmospheric neutrino mixing is now predicted on the "bright side," ($\theta_{23} \leq \pi/4$):

$$\sin^2\theta_{23} = \frac{1 - 2\,|U_{e3}|^2}{2\left(1 - |U_{e3}|^2\right)} \simeq \frac{1}{2}\left(1 - |U_{e3}|^2\right) \leq \frac{1}{2}\,, \tag{2.22}$$

while the solar neutrino mixing is correlated with $|U_{e3}|$ and δ according to

$$\sin^2\theta_{12} \simeq \frac{1}{3} + \frac{2\sqrt{2}}{3}\,|U_{e3}|\,\cos\delta\, + \frac{1}{3}\,|U_{e3}|^2\,\cos 2\delta\,. \tag{2.23}$$

We also note the recently proposed tetramaximal mixing scheme (T^{4}M) [59]. Its name stems from the fact that it can be obtained by four consecutive rotations, each having a maximal angle of $\pi/4$, and properly chosen phases associated with the rotations:

$$U_{\rm tetra} = R_{23}(\pi/4;\pi/2)\, R_{13}(\pi/4;0)\, R_{12}(\pi/4;0)\, R_{13}(\pi/4;\pi)\,. \tag{2.24}$$

The notation of the rotation matrices is defined in eqn. (2.3). The definite predictions are[4]

$$\delta = \pi/2, \quad \sin^2\theta_{23} = \frac{1}{2}\,, \quad \sin^2\theta_{12} = (\frac{5}{2}+\sqrt{2})^{-1} \simeq 0.255\,, \tag{2.25}$$

$$|U_{e3}|^2 = \frac{1}{4}\,(\frac{7}{4}-\sqrt{2})\,\sin^2\theta_{12} = \frac{1}{4}\,(\frac{3}{2}-\sqrt{2}) \simeq 0.021\,. \tag{2.26}$$

Another interesting possible property of U is that it might be symmetric: $U = U^T$. One can show that there follows one constraint on the mixing parameters [60]:

$$|U_{e3}| = \frac{\sin\theta_{12}\,\sin\theta_{23}}{\sqrt{1-\sin^2\delta\,\cos^2\theta_{12}\,\cos^2\theta_{23}}+\cos\delta\,\cos\theta_{12}\,\cos\theta_{23}}\,. \tag{2.27}$$

Scenarios in which this happens at lowest order, for instance, reflect "Quark-Lepton Universality" [61]. Here it is proposed that down quarks and charged leptons are diagonalized by the same matrix V and that the down quark mass matrix is hermitian. Furthermore, $m_D = m_{\rm up} = m_{\rm up}^T$, and M_R is also diagonalized by V, where m_D (M_R) is the Dirac (Majorana) mass matrix in the type I seesaw mechanism. With these assumptions it follows that the PMNS matrix is symmetric. In general, U is symmetric if $U_\ell = S\,U_\nu^\dagger$, where S is a symmetric and unitary matrix. Moreover, if m_ν^* and (symmetric) m_ℓ are diagonalized by the same matrix, again the PMNS matrix is symmetric.

Several proposed mixing matrices single out the solar mixing angle for special treatment. In the case of bimaximal mixing (BM), $\sin^2\theta_{12} = 1/2$, with the same atmospheric and reactor neutrino mixing angles as in the case of tri-bimaximal mixing or μ–τ symmetry. Hence the mixing matrix has the form [62–66]

$$U_{\rm BM} = \begin{pmatrix} \frac{1}{\sqrt{2}} & \frac{1}{\sqrt{2}} & 0 \\ -\frac{1}{2} & \frac{1}{2} & -\frac{1}{\sqrt{2}} \\ -\frac{1}{2} & \frac{1}{2} & \frac{1}{\sqrt{2}} \end{pmatrix}, \tag{2.28}$$

In [67] it has been shown that for instance one can use the discrete symmetry S_3 to construct such a mixing matrix. While the value $\sin^2\theta_{12} = \frac{1}{2}$ is ruled out by close to 10σ, this mixing scenario has recently been revived in the form of a model based on S_4 [68]. Here the two

[4] By multiplying a fifth maximal rotation $R_{12}(\pi/4;2\pi/3)$ to the right of $U_{\rm tetra}$ one could obtain "quintamaximal mixing", which has more complicated predictions: $\sin^2\theta_{12} = (3+\sqrt{2})/(10+4\sqrt{2}) \simeq 0.282$, $|U_{e3}|^2 = (3-2\sqrt{2})/8 \simeq 0.021$, $\sin^2\theta_{23} = \frac{1}{2}$ and $J_{CP} = (3\sqrt{2}-2)/256 \simeq 0.0088$. Here $J_{CP} = {\rm Im}\{U_{e1}\,U_{\mu 2}\,U_{e2}^*\,U_{\mu 1}^*\}$ is the usual measure for CP violation.

generators of the group are chosen such that one is diagonal and the other one leaves $m_\nu^{\rm BM}$ invariant, where $m_\nu^{\rm BM}$ is the most general mass matrix leading to bimaximal mixing, which is obtained from eqn. (2.7) by removing B. Bimaximal mixing can be corrected by charged lepton corrections, leading to QLC scenarios (see below).

Another possibility proposed here is "hexagonal mixing" (HM), where $\theta_{12} = \pi/6$, or $\sin^2\theta_{12} = 1/4$. In this case, again with maximal atmospheric and vanishing reactor neutrino mixings, the mixing matrix is given by

$$U_{\rm HM} = \begin{pmatrix} \frac{\sqrt{3}}{2} & \frac{1}{2} & 0 \\ -\frac{1}{2\sqrt{2}} & \frac{\sqrt{3}}{2\sqrt{2}} & -\frac{1}{\sqrt{2}} \\ -\frac{1}{2\sqrt{2}} & \frac{\sqrt{3}}{2\sqrt{2}} & \frac{1}{\sqrt{2}} \end{pmatrix} . \tag{2.29}$$

Here D_{12} is an appropriate discrete flavor symmetry. The angle $\theta_{12} = \pi/6$ is obviously the external angle of the dodecagon, whose symmetry group is D_{12}. One can also use D_6, where the external angle is $\pi/3$. Both BM and HM require corrections to bring them into agreement with current global fits. A strategy to do this is given in sec. 2.3. Note that this requires a larger correction for bimaximal mixing than for hexagonal mixing, where the necessary correction is moderate.

There are two proposals which link solar neutrino mixing with the golden ratio angle $\varphi = (1+\sqrt{5})/2$:

$$\varphi_1 : \quad \cot\theta_{12} = \ \varphi \Rightarrow \sin^2\theta_{12} = \frac{1}{1+\varphi^2} \simeq 0.276\,, \tag{2.30}$$

$$\varphi_2 : \quad \cos\theta_{12} = \ \frac{\varphi}{2} \Rightarrow \sin^2\theta_{12} = \frac{1}{4}\,(3-\varphi) \simeq 0.345\,. \tag{2.31}$$

The observation that the first relation is allowed has been made in refs. [69, 70]. Interestingly, the first relation may be obtained with the choice of A_5 as the flavor symmetry group, as noted in ref. [71]. This follows since A_5 is isomorphic to the symmetry group of the icosahedron whose 12 vertices separated by edge-length 2 have Cartesian coordinates specified by $(0, \pm 1, \pm\varphi)$, $(\pm 1, \pm\varphi, 0)$ and $(\pm\varphi, 0, \pm 1)$. Indeed, one can write the generators of one of the three-dimensional IRs of A_5 in terms of φ [71]. One could in principle assign the values $\sin^2\theta_{23} = \frac{1}{2}$ and $U_{e3} = 0$ to the two golden ratio relations.

The second golden ratio relation was proposed first in [72]. In ref. [73] a model based on the discrete flavor symmetry D_{10} has been applied to obtain this angle. Believe it or not, $\cos\theta_{12} = \frac{\varphi}{2}$ implies nothing other than $\theta_{12} = \pi/5$, and therefore arguments similar to those given above for hexagonal mixing apply: the angle $\pi/5$ is the external angle of a decagon and D_{10} is its rotational symmetry group.

The final class of alternative mixing scenarios we consider deals with Quark-Lepton Complementarity (QLC), which can be used to relate the quark and lepton mixing matrices. The most naive form relates the solar neutrino mixing angle, θ_{12}, to the quark Cabibbo angle, θ_{12}^q, by [74, 75]

$$\mathrm{QLC}_0 : \ \theta_{12} = \frac{\pi}{4} - \theta_{12}^q \Rightarrow \sin^2\theta_{12} \simeq 0.280\,. \tag{2.32}$$

One may assume a similar relation for the 23-sector, $\theta_{23} = \frac{\pi}{4} - \theta_{23}^q$, leading to $\sin^2\theta_{23} \simeq 0.459$.

These QLC relations can be approximately obtained by multiplying a bimaximal matrix, see eqn. (2.28), with the CKM (or a CKM-like) matrix. For definiteness, we stick to the CKM matrix in what follows. It is given in the Wolfenstein parametrization [76] by

$$V = \begin{pmatrix} 1-\frac{1}{2}\lambda^2 & \lambda & A\lambda^3(\rho - i\eta) \\ -\lambda & 1-\frac{1}{2}\lambda^2 & A\lambda^2 \\ A\lambda^3(1-\rho+i\eta) & -A\lambda^2 & 1 \end{pmatrix} + \mathcal{O}(\lambda^4). \tag{2.33}$$

In analogy to the PMNS matrix it is a product of two unitary matrices, $V = V_{\rm up}^\dagger V_{\rm down}$, where $V_{\rm up}$ ($V_{\rm down}$) is associated with the diagonalization of the up- (down-) quark mass matrix. As reported in [77, 78] the best-fit values and the 1σ, 2σ and 3σ ranges of the parameters $\lambda, A, \bar\rho, \bar\eta$ are

$$\lambda = \sin\theta_C = 0.2272^{+0.0010,\,0.0020,\,0.0030}_{-0.0010,\,0.0020,\,0.0030}\,, \tag{2.34}$$

$$A = 0.809^{+0.014,\,0.029,\,0.044}_{-0.014,\,0.028,\,0.042}\,, \tag{2.35}$$

$$\bar\rho = 0.197^{+0.026,\,0.050,\,0.074}_{-0.030,\,0.087,\,0.133}\,, \tag{2.36}$$

$$\bar\eta = 0.339^{+0.019,\,0.047,\,0.075}_{-0.018,\,0.037,\,0.057}\,, \tag{2.37}$$

where $\bar\rho = \rho(1-\lambda^2/2)$ and $\bar\eta = \eta(1-\lambda^2/2)$. From the relation $U = V^\dagger U_{\rm BM}$ one finds[5]

$$\text{QLC}_1: \quad \sin^2\theta_{12} \simeq \frac{1}{2} - \frac{\lambda}{\sqrt{2}}\cos\phi + \mathcal{O}(\lambda^3)\,, \quad |U_{e3}| \simeq \frac{\lambda}{\sqrt{2}} + \mathcal{O}(\lambda^3)\,, \tag{2.38}$$

$$\sin^2\theta_{23} \simeq \frac{1}{2} - \frac{\lambda^2}{4}(1 + 4A\cos(\phi-\omega)) + \mathcal{O}(\lambda^4)\,, \tag{2.39}$$

$$\tag{2.40}$$

where λ is the sine of the leading 12-entry in V, i.e., the sine of the Cabibbo angle. The phases ϕ and ω are not related to the phase in the CKM matrix but are relative phases [79] between $U_\ell = V$ and $U_{\rm BM}$, with ϕ corresponding to the Dirac phase in neutrino oscillations. With the Jarlskog invariant serving as the measure of leptonic CP violation,

$$J_{CP} = \text{Im}\{U_{e1}\,U_{\mu 2}\,U_{e2}^*\,U_{\mu 1}^*\} \simeq \frac{\lambda}{4\sqrt{2}}\sin\phi + \mathcal{O}(\lambda^3)\,, \tag{2.41}$$

numerically one finds $|U_{e3}| \simeq 0.160$, $\sin^2\theta_{12} \gtrsim 0.339$, and $|J_{CP}| \lesssim 0.0274$, since $\phi \lesssim \pi/4.25$ for $\sin^2\theta_{12}$ to be in its allowed 3σ range.

[5] Sometimes a Georgi-Jarlskog factor of $\frac{1}{3}$ appears in model realizations of QLC, in which case the results to be presented can be obtained approximately by replacing λ with $\lambda/3$.

Scenario	$\sin^2\theta_{12}$		$\sin^2\theta_{23}$		$\sin^2\theta_{13}$	
	min	max	min	max	min	max
TBM	0.333		0.500		0.000	
$\boldsymbol{\mu-\tau}$	–		0.500		0.000	
$\mathbf{TM_1}$	0.296	0.333	**		–	
$\mathbf{TM_2}$	0.333	0.352	**		–	
$\mathbf{TM_3}$	–		0.500		0.000	
$\mathbf{TM^1}$	0.333		–		0.000	
$\mathbf{TM^2}$	**		0.500	0.528	–	
$\mathbf{TM^3}$	**		0.472	0.500	–	
$\mathbf{T^4M}$	0.255		0.500		0.021	
$\mathbf{U{=}U^T}$	0.000	0.389	0.000	0.504	0.0343	0.053
BM	0.500		0.500		0.000	
HM	0.250		0.500		0.000	
$\boldsymbol{\varphi_1}$	0.276		0.500		0.000	
$\boldsymbol{\varphi_2}$	0.345		0.500		0.000	
$\mathbf{QLC_0}$	0.280		0.459		–	
$\mathbf{QLC_1}$	0.331	0.670	0.442	0.534	0.023	0.029
$\mathbf{QLC_2}$	0.276	0.726	0.462	0.540	0.0005	0.0016

Table 2.2: Predictions for $\sin^2\theta_{12}$, $\sin^2\theta_{23}$, and $\sin^2\theta_{13} = |U_{e3}|^2$ for the different mixing scenarios considered. The appearance of the symbol – indicates a free parameter of the model, while the symbol ** indicates a prediction which depends upon the unknown phase δ. The min and max values listed are determined from the presently allowed $3\,\sigma$ range for $|U_{e3}|$.

To obtain this scenario in a seesaw framework[6], an approach somewhat similar to that for Quark-Lepton Universality discussed above is possible [74, 75]: diagonalization of m_ν is achieved via $m_\nu = U^*_{\rm BM}\, m_\nu^{\rm diag}\, U^\dagger_{\rm BM}$ and produces exact bimaximal mixing. The U_ℓ matrix diagonalizing the charged lepton mass matrix m_ℓ corresponds to the CKM matrix V. With $m_\ell = m^T_{\rm down}$, where $m_{\rm down}$ is the down-quark mass matrix, it follows that the up-quark mass matrix $m_{\rm up}$ is real and diagonal. It is assumed to correspond to the Dirac mass matrix in the type I seesaw formula, and this in turn fixes M_R.

Then there is the second QLC scenario, in which the PMNS matrix is given by $U^*_{\rm BM}\, V^\dagger$. One finds

$$\mathrm{QLC}_2: \quad \sin^2\theta_{12} \simeq \frac{1}{2} - \lambda\,\cos\phi + \mathcal{O}(\lambda^3)\;, \quad |U_{e3}| \simeq \frac{A\,\lambda^2}{\sqrt{2}} + \mathcal{O}(\lambda^3)\;, \tag{2.42}$$

$$\sin^2\theta_{23} \simeq \frac{1}{2} + \frac{A\,\lambda^2}{\sqrt{2}}\,\cos\phi' + \mathcal{O}(\lambda^3)\,, \tag{2.43}$$

[6]Seesaw realizations of QLC scenarios are studied in detail in [80–83].

where λ is the 12-entry, and $A\,\lambda^2$ the 23-entry of V. Again the phases ϕ and ϕ' are unrelated to the phase in the CKM matrix. Note that there is now a correlation between leptonic CP violation and quark CKM mixing:

$$J_{CP} \simeq \frac{A\,\lambda^2}{4\sqrt{2}}\,\sin\phi' + \mathcal{O}(\lambda^4)\,. \tag{2.44}$$

Here the type I seesaw realization goes as follows [75]: diagonalization of m_ν is achieved via $m_\nu = U_\nu^*\, m_\nu^{\rm diag}\, U_\nu^\dagger$ and U_ν is related to V (in the sense that $U_\nu = V^\dagger$). The charged leptons are diagonalized by $U_\ell = U_{\rm BM}^T$. This in turn can be achieved when $V_{\rm up} = V^\dagger$, therefore $V_{\rm down}$ must be the unit matrix. With the definition of $M_R = V_R^*\, M_R^{\rm diag}\, V_R^\dagger$, where $V_R = V_{\rm up}^*$, we have $m_{\rm up} = m_D = V_{\rm up}\, m_{\rm up}^{\rm diag}\, V$, and since $V_{\rm up} = V^\dagger$ the neutrino mass matrix $m_\nu = -m_D^T\, M_R^{-1}\, m_D$ is diagonalized by the CKM matrix. Note that QLC1, QLC2 and Quark-Lepton Universality require that the eigenvalues of the fermion mass matrices differ even though some of the mixing angles are the same. Such mass matrices may, e.g., be "form diagonalizable" ones [84], which means that the mixing matrix which diagonalizes the mass matrix is independent of the values of the eigenvalues (such as for bimaximal or TBM).

We summarize the numerical values of all scenarios considered here in tbl. 2.2. For some of the scenarios, all three mixing angles are predicted, while in others one or two of the mixing parameters remain free parameters (indicated by the symbol —) and are not determined by the models in question. Where possible, minimum and maximum values of the mixing parameters are determined by adopting the present experimental 3σ range for the mixing element $|U_{e3}|$, and in the cases of the QLC_1 and QLC_2 models, also for the Wolfenstein parameters. For four of the models, one of the mixing angles is constrained by the other mixing parameters, cf. eqns. (2.12), (2.15), (2.20), and (2.23), but the actual numerical value relies on one knowing the presently unconstrained phase δ. Such constrained predictions are indicated by the symbol ** in tbl. 2.2.

In figs. 2.1, 2.2 and 2.3 we plot the ranges or values of the three mixing variables, $\sin^2\theta_{12}$, $\sin^2\theta_{23}$, and $|U_{e3}|$, respectively that can be obtained for each of the scenarios by varying, if necessary, the other variables over their present 3σ experimental range. The experimentally allowed best-fit values, 1σ and 3σ ranges of the variables are indicated by solid or broken horizontal lines as shown in the figures. Two-dimensional plots are given in figs. 2.4, 2.5, and 2.6 as functions of $\sin^2\theta_{12}$ vs. $|U_{e3}|$, $\sin^2\theta_{23}$ vs. $|U_{e3}|$, and $\sin^2\theta_{23}$ vs. $\sin^2\theta_{12}$, respectively. The correlations between those observables can be crucial to distinguish scenarios with similar predictions.

When we performed this analysis for the first time [13] most of the models covered the then allowed ranges of the mixing angles, with the notable exceptions of the bimaximal and hexagonal mixing models, BM and HM. For these models, one needs to make perturbations on the zeroth order results given in tbl. 2.2. We present in sec. 2.3 a simple procedure to perturb the hexagonal and bimaximal mixing matrices, as well as the relevant procedure for the quark-lepton complementarity models, in order to bring their results into better agreement with the data. With the very precise measurement [15–17] of the then unknown

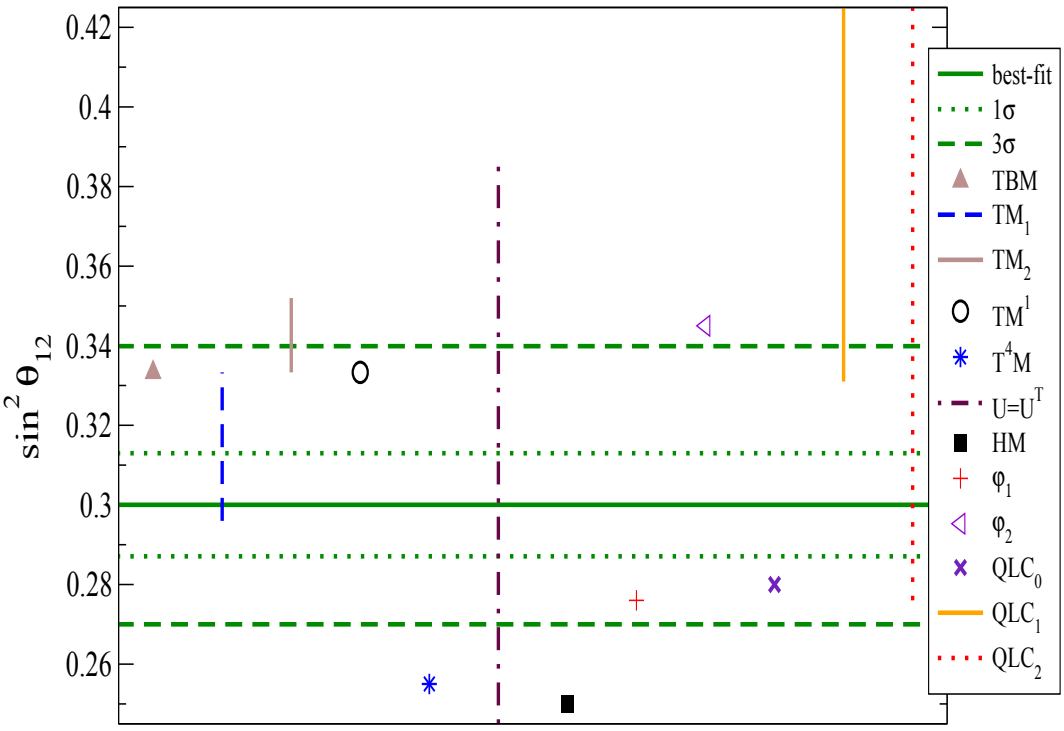

Figure 2.1: Predictions for $\sin^2\theta_{12}$ of the mixing scenarios discussed in the text. For some of the scenarios $\sin^2\theta_{12}$ depends on the other mixing parameters. Varying them in their experimentally allowed 3σ ranges gives the plotted ranges of $\sin^2\theta_{12}$.

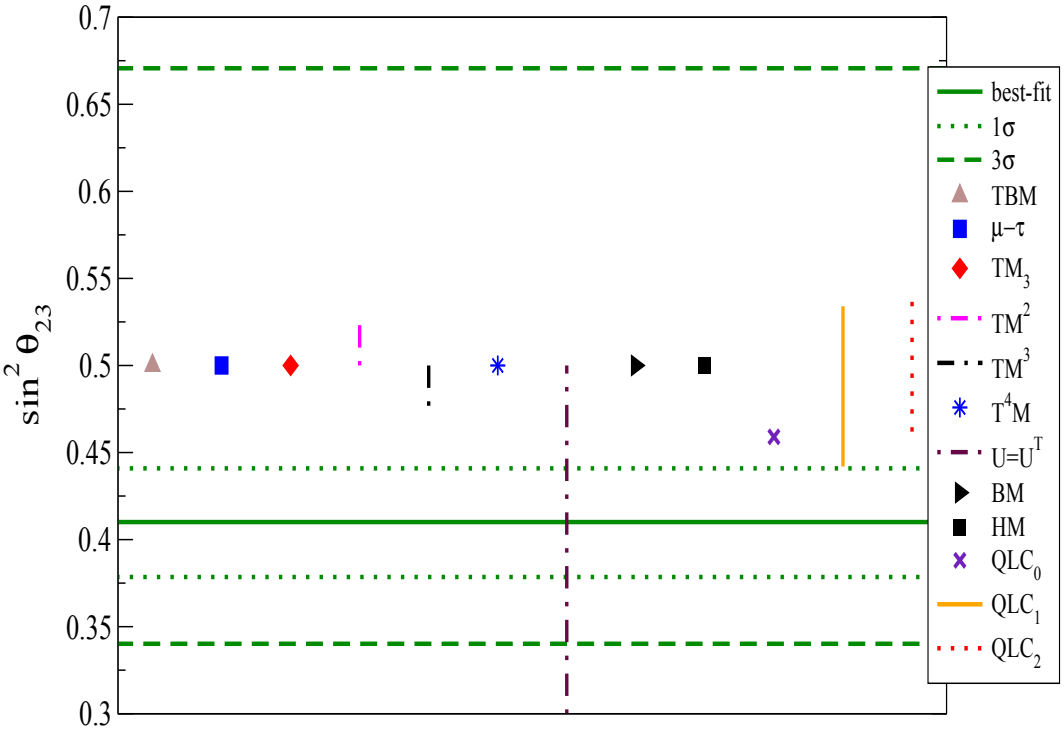

Figure 2.2: Same as fig. 2.1, but now for $\sin^2\theta_{23}$.

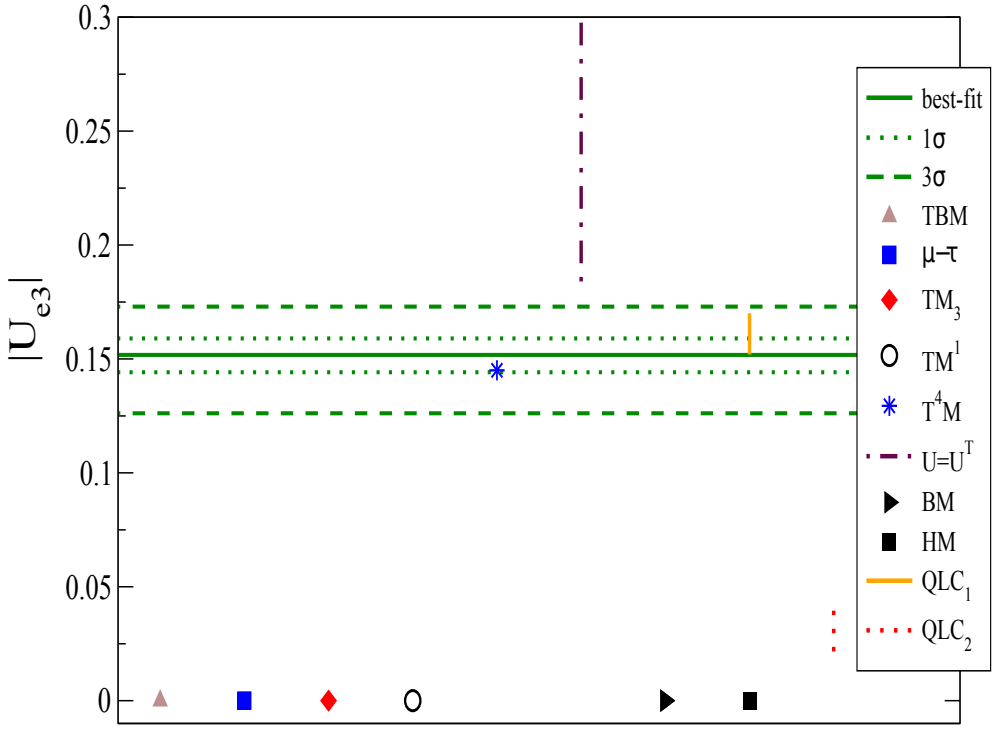

Figure 2.3: Same as fig. 2.1, but now for $|U_{e3}|$.

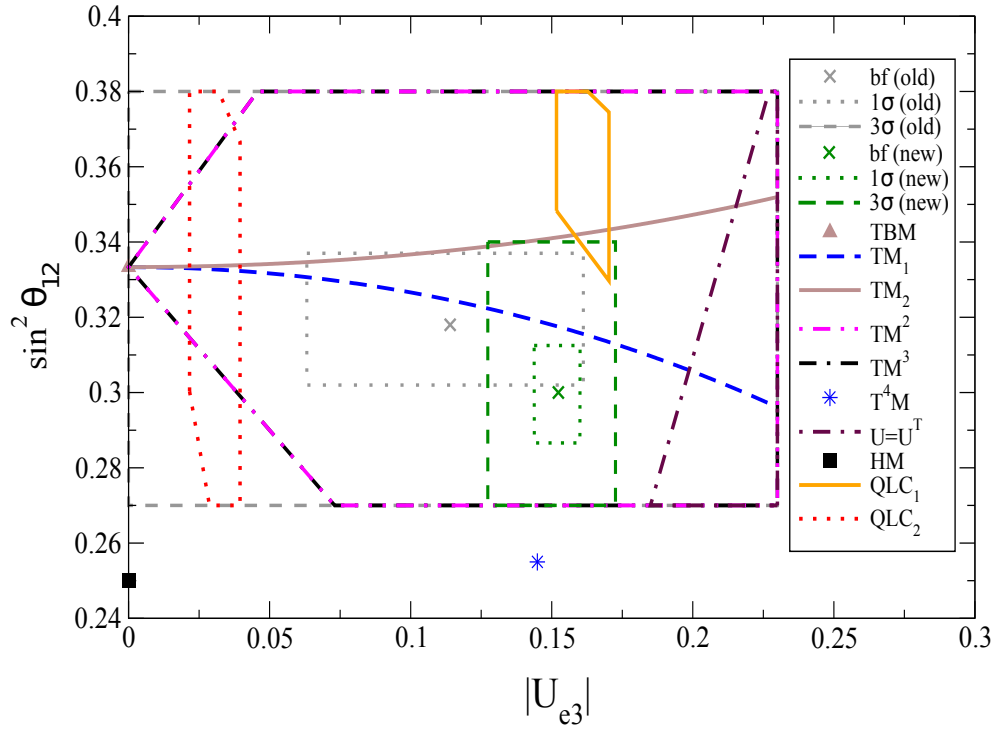

Figure 2.4: Correlations between $\sin^2\theta_{12}$ and $|U_{e3}|$ constrained by the experimental 3σ ranges of the mixing parameters. For scenarios where $\sin^2\theta_{12}$ depends also on the unknown Dirac phase δ the whole area inside the corresponding lines is possible, while in the case of $TM_{1,2}$ only parameter combinations lying on the dashed (blue) and continuous (brown) lines, respectively, are allowed. TM^2 and TM^3 are here indistinguishable. We show the experimental ranges that were allowed when we performed this analysis for the first time [13] (denoted by "old") as well as the currently allowed ranges.

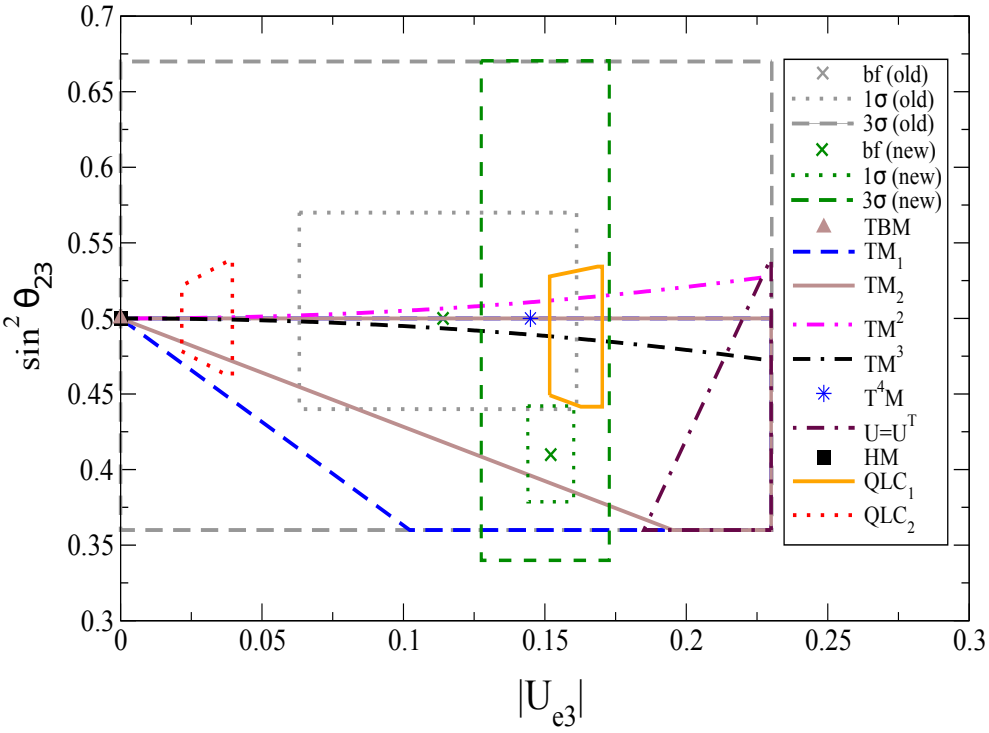

Figure 2.5: Same as fig. 2.4, but now for $\sin^2\theta_{23}$. Like $\sin^2\theta_{12}$ in the $\mathrm{TM}_{1,2}$ scenarios, in the $\mathrm{TM}^{2,3}$ scenarios (magenta and black line, respectively) $\sin^2\theta_{23}$ depends only on $|U_{e3}|$ and not on the Dirac phase δ.

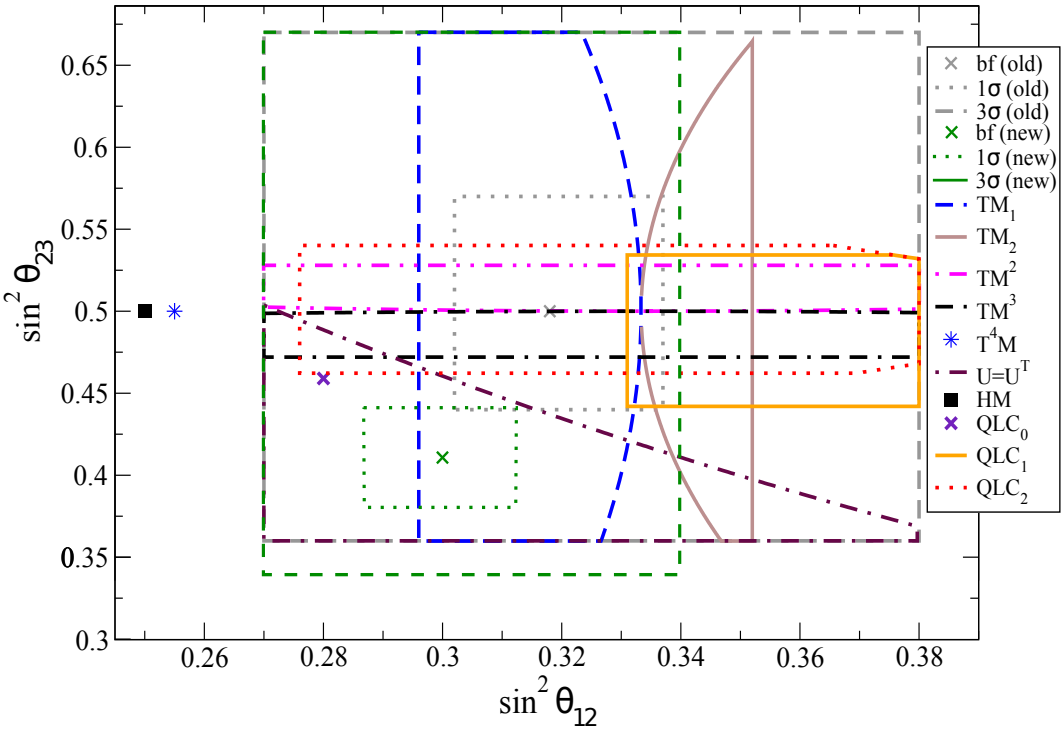

Figure 2.6: Same as figs. 2.4 and 2.5, but now the correlations between $\sin^2\theta_{23}$ and $\sin^2\theta_{12}$ are plotted.

reactor mixing angle, θ_{13}, most scenarios are in trouble, with the notable exceptions of QLC_1, TM^2, and TM^3, albeit one can hold up that $\text{TM}^{2,3}$ profit from not making any prediction on θ_{13}. T^4M, in excellent agreement with the recent determination of θ_{13}, suffers from deviations of its prediction on θ_{12} by more than $3\,\sigma$. For models not in agreement with data one can adobt the procedure of perturbing their leading order mixing matrices, as done for models HM and BM in sec. 2.3.

2.3 Perturbing Hexagonal and Bimaximal Mixing

We begin by discussing the hexagonal mixing Ansatz, defined by

$$\theta_{12}^{\ell} = \frac{\pi}{6} = 30^{\circ} \Rightarrow \sin^2\theta_{12}^{\ell} = \frac{1}{4}\,, \tag{2.45}$$

together with maximal θ_{23}^{ℓ} and $\theta_{13}^{\ell} = 0$. From now on we denote lepton (quark) mixing angles with a superscript ℓ (q). For this scenario the unperturbed mixing matrix in the lepton mass basis reads

$$U_{\text{HM}} = \begin{pmatrix} \sqrt{\frac{3}{4}} & \frac{1}{2} & 0 \\ -\frac{1}{2\sqrt{2}} & \sqrt{\frac{3}{8}} & -\sqrt{\frac{1}{2}} \\ -\frac{1}{2\sqrt{2}} & \sqrt{\frac{3}{8}} & \sqrt{\frac{1}{2}} \end{pmatrix} P\,, \tag{2.46}$$

where the Majorana phases are contained in $P = \text{diag}(1, e^{i\alpha}, e^{i\beta})$. The mass matrix in the charged lepton basis is given by $m_\nu^0 = U^*\, m_\nu^{\text{diag}}\, U^\dagger$ and has the texture

$$m_\nu^0 = \begin{pmatrix} A & B & B \\ \cdot & \frac{1}{2}(A + \sqrt{\frac{8}{3}}\,B + D) & \frac{1}{2}(A + \sqrt{\frac{8}{3}}\,B - D) \\ \cdot & \cdot & \frac{1}{2}(A + \sqrt{\frac{8}{3}}\,B + D) \end{pmatrix}\,, \tag{2.47}$$

where the masses and Majorana phases are contained in

$$A - \sqrt{\frac{2}{3}}\,B = m_1\ ,\quad A + \sqrt{6}\,B = m_2\, e^{-2i\alpha}\ ,\quad D = m_3\, e^{-2i\beta}\,. \tag{2.48}$$

We can also write

$$m_\nu^0 = \frac{m_1}{4}\begin{pmatrix} 3 & -\sqrt{\frac{3}{2}} & -\sqrt{\frac{3}{2}} \\ \cdot & \frac{1}{2} & \frac{1}{2} \\ \cdot & \cdot & \frac{1}{2} \end{pmatrix} + \frac{m_2\, e^{-2i\alpha}}{4}\begin{pmatrix} 1 & \sqrt{\frac{3}{2}} & \sqrt{\frac{3}{2}} \\ \cdot & \frac{3}{2} & \frac{3}{2} \\ \cdot & \cdot & \frac{3}{2} \end{pmatrix} + \frac{m_3\, e^{-2i\beta}}{2}\begin{pmatrix} 0 & 0 & 0 \\ \cdot & 1 & -1 \\ \cdot & \cdot & 1 \end{pmatrix} \tag{2.49}$$

$$= m_1\,\Phi_1\,\Phi_1^T + m_2\, e^{-2i\alpha}\,\Phi_2\,\Phi_2^T + m_3\, e^{-2i\beta}\,\Phi_3\,\Phi_3^T \tag{2.50}$$

where $\Phi_{1,2,3}$ are the columns of the mixing matrix. In this limit the ee element of m_ν^0, whose magnitude governs the rate of neutrinoless double beta decay vanishes when the Majorana phase is such that $e^{-2i\alpha} = -1$ and in addition the relation $m_1 = \frac{1}{3}\, m_2$, or $m_1^2 = \Delta m^2_\odot/8$ holds.

Independent of the source of perturbation, the most general way to describe deviations from hexagonal mixing is [85] (see also [86, 87])

$$U = R_{23}(-\pi/4)\, U_\epsilon\, R_{12}(\pi/6)\,, \text{ where } U_\epsilon = R_{23}(\epsilon^\ell_{23})\, \tilde{R}_{13}(\epsilon^\ell_{13}; \delta^\ell)\, R_{12}(\epsilon^\ell_{12})\,. \tag{2.51}$$

Note that the order of the small rotations in U_ϵ is chosen such that it corresponds to the order of rotations in the usual description of a mixing matrix. This "triminimal" [85] parametrization implies that each small parameter is responsible for only one observable[7]. The observables are obtained from eqn. (2.51) as follows:

$$\sin^2\theta^\ell_{12} = \frac{1}{4}\left(\cos\epsilon^\ell_{12} + \sqrt{3}\,\sin\epsilon^\ell_{12}\right)^2 \simeq \frac{1}{4}\left(1 + 2\sqrt{3}\,\epsilon^\ell_{12} + 3\,(\epsilon^\ell_{12})^2\right), \tag{2.52}$$

$$\sin^2\theta^\ell_{23} = \frac{1}{2} - \cos\epsilon^\ell_{23}\,\sin\epsilon^\ell_{23} \simeq \frac{1}{2} - \epsilon^\ell_{23}\,, \tag{2.53}$$

$$U_{e3} = \sin\epsilon^\ell_{13}\, e^{-i\delta^\ell}\,. \tag{2.54}$$

Note that U_{e3} agrees with its form in the usual parametrization and that the deviation from maximal atmospheric mixing is to very good precision given by ϵ^ℓ_{23}. Regarding solar neutrino mixing, the values $\sin^2\theta^\ell_{12}$ of 0.318, 0.302, 0.337, 0.27, 0.38 and $\frac{1}{3}$ are obtained for $\epsilon^\ell_{12} = 0.076$, 0.058, 0.096, 0.023, 0.141, and 0.092.

In the same way we can perturb the bimaximal mixing matrix, given by eqn. (2.28). The triminimally perturbed bimaximal mixing matrix can be written as

$$U = R_{23}(-\pi/4)\, U_\epsilon\, R_{12}(\pi/4)\,, \tag{2.55}$$

with U_ϵ the same as in eqn. (2.51). The observables are obtained as

$$\sin^2\theta^\ell_{12} = \left(\frac{1}{2} + \sin\epsilon^\ell_{12}\cos\epsilon^\ell_{12}\right) \simeq \frac{1}{2} + \epsilon^\ell_{12}\,, \tag{2.56}$$

$$\sin^2\theta^\ell_{23} = \left(\frac{1}{2} - \sin\epsilon^\ell_{23}\cos\epsilon^\ell_{23}\right) \simeq \frac{1}{2} - \epsilon^\ell_{23}\,, \tag{2.57}$$

$$U_{e3} = \sin\epsilon^\ell_{13}\, e^{-i\delta^\ell}\,. \tag{2.58}$$

$$\tag{2.59}$$

Compared to the hexagonal mixing scenario, the values $\sin^2\theta^\ell_{12}$ of 0.318, 0.302, 0.337, 0.27, 0.38 and $\frac{1}{3}$ are obtained for $\epsilon^\ell_{12} = -0.186$, -0.204, -0.166, -0.239, -0.121, and -0.170.

[7] A similar strategy may be applied to tetra-maximal mixing, where θ_{12} lies slightly below the current 3σ range.

Returning to hexagonal mixing, one may discuss a related parametrization for the CKM matrix in the spirit of QLC. Namely, with the requirement that the 12-mixing angles of the quark and lepton sector add up to 45 degrees, it follows automatically that

$$(\theta_{12}^q)^0 = 15^\circ = \frac{\pi}{12} \Rightarrow \sin(\theta_{12}^q)^0 = \frac{\sqrt{3}-1}{2\sqrt{2}} = 0.2588\,, \tag{2.60}$$

Note that at zeroth order $\theta_{12}^\ell = 2\theta_{12}^q$. There are models in the literature leading to this angle $(\theta_{12}^q)^0$ [88, 89]. In the spirit of triminimality, we can describe the necessary but small deviations of this scheme with

$$V = R_{23}(\epsilon_{23}^q)\, \tilde{R}_{13}(\epsilon_{13}^q; \delta^q)\, R_{12}(\epsilon_{12}^q)\, R_{12}(\pi/12)\,. \tag{2.61}$$

The sine of the 12-mixing angle is given by

$$\sin\theta_{12}^q = \frac{1}{2}\sqrt{2 - \sqrt{3}\,\cos 2\epsilon_{12}^q + \sin 2\epsilon_{12}^q} \simeq \frac{\sqrt{3}-1}{2\sqrt{2}}\left(1 + (2+\sqrt{3})\,\epsilon_{12}^q\right). \tag{2.62}$$

Note that the last expression is equivalent to $\sin\theta_{12}^q \simeq \sin(\theta_{12}^q)^0 + \epsilon_{12}^q\,\cos(\theta_{12}^q)^0$. Numerically we have $\sin\theta_{12}^q \simeq 0.2588 + 0.9659\,\epsilon_{12}^q$, so that ϵ_{12}^q can be almost directly identified with the deviation of the sine of Cabibbo angle from $\frac{\sqrt{3}-1}{2\sqrt{2}}$. In order to bring $\sin\theta_{12}^q$ into the observed 1σ or 3σ range given in eqn. (2.34) one requires

$$\epsilon_{12}^q = -0.0326^{+0.00102,0.00308}_{-0.00102,0.00308}\,. \tag{2.63}$$

Note that here ϵ_{12}^q is negative, while ϵ_{12}^ℓ (see eqn. (2.52)) is positive. Choosing the tempting value $\epsilon_{12}^\ell = -\epsilon_{12}^q$ gives $\sin^2\theta_{12}^\ell \simeq 0.279$.

We finish by noting an interesting observation made in ref. [90]: taking the golden ratio relation φ_1 $(\tan\theta_{12}^\ell = 1/\varphi)$ at face value, and assuming QLC $(\theta_{12}^\ell + \theta_{12}^q = \pi/4)$ gives

$$\tan\theta_{12}^q = \tan(\pi/4 - \theta_{12}^\ell) = \frac{1-1/\varphi}{1+1/\varphi} = \frac{1}{\varphi^3}\,, \tag{2.64}$$

or $\sin\theta_{12}^q \simeq 0.2298$. Hence, the golden ratio may appear in the quark sector as well.

2.4 Conclusions

With more refined neutrino mixing data available, it is clear that TBM gives a reasonably accurate lowest order approximation to the PMNS mixing matrix. With this in mind, many authors have constructed top-down models based on some discrete flavor symmetry group which yield TBM mixing as a natural consequence. Of the possible choices, the A_4 group appears to be the most favored choice based on its simplicity.

We have argued in this chapter, however, that other possible approximations to the mixing matrix exist such as trimaximal mixing or its variants, tetramaximal mixing, a

symmetric mixing matrix, bimaximal and hexagonal mixings, and mixings based on the golden ratio angle or quark-lepton complementarity. Many of these scenarios have already been discussed in the literature, but we have compiled this list in order to make easy comparisons of their predictions. For those requiring perturbations to bring them into better agreement with the data, we have illustrated how triminimal perturbations of the bimaximal, and hexagonal mixings or quark-lepton complementarity, for example, can accomplish this. For each one of the starting mixing matrix assumptions, one can then use a bottom-up approach to determine the appropriate neutrino mass matrix from which a suitable discrete flavor symmetry will presumably reproduce the observed mixing matrix.

The theoretical literature focusses heavily on TBM, and it would be dangerous to avoid looking for and studying alternatives. We hope that the analysis performed in this chapter contributes to the required attention on alternatives.

Chapter 3

Neutrinoless Double Beta Decay, the Inverted Hierarchy and Precision Determination of θ_{12}

3.1 Introduction

The text in this chapter corresponds in large parts to the one in ref. [14] that has been published together with coauthors as A. Dueck, W. Rodejohann, and K. Zuber, *"Neutrinoless Double Beta Decay, the Inverted Hierarchy and Precision Determination of theta(12)"*, Phys. Rev. D 83 (2011) 113010. It is updated here due to more precise data on neutrino mixing angles and new limits on neutrinoless double beta decay available now.

Neutrinoless double beta decay ($0\nu\beta\beta$) is a (as yet unobserved) process of fundamental importance for particle physics [5, 91–94]. In $0\nu\beta\beta$ decay a nucleus with mass number A and atomic number Z decays into a nucleus of mass number A and atomic number $Z+2$ thereby emitting two electrons [93, 95]:

$$(A, Z) \to (A, Z+2) + 2e^- \,. \tag{3.1}$$

The initial state has lepton number $L = 0$ and baryon number $B = A$, whereas the final state has lepton number $L = 2$ and baryon number $B = A$. Hence, this process violates lepton number, an accidental symmetry in the Standard Model (SM), by two units. While lepton and baryon number are not conserved at the quantum level even within the SM [93], $B-L$ is a conserved quantity in the SM also at the quantum level. In many Grand Unified Theories (GUTs) [10] $B-L$ is part of the gauge symmetry and broken spontaneously at some energy scale. Hence, with $0\nu\beta\beta$ decay experiments one also probes fundamental theories at very high energies. We will investigate several GUTs based on $SO(10)$ in part II of this thesis.

Let us now discuss phenomenological aspects of $0\nu\beta\beta$ decay. In the best motivated interpretation [96] of this process, light Majorana neutrinos, whose mixing is observed in neutrino oscillation experiments, are exchanged in the process, while all other mechanisms

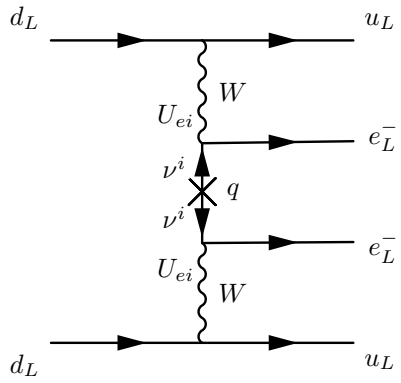

Figure 3.1: Feynman diagram for neutrinoless double beta decay in the standard interpretation [93].

which can lead to $0\nu\beta\beta$ decay play a negligible role. The corresponding Feynman diagram at the quark level is shown in fig. 3.1. In this chapter we will stick to this interpretation of $0\nu\beta\beta$ decay (for other potential mechanisms, see ref. [93] and references therein). In this interpretation the particle physics quantity which is probed is the "effective mass"

$$\langle m_\nu \rangle = \left| U_{e1}^2 \, m_1 + U_{e2}^2 \, m_2 \, e^{i\alpha} + U_{e3}^2 \, m_3 \, e^{i\beta} \right| . \tag{3.2}$$

Here $U_{e1} = \cos\theta_{12} \cos\theta_{13}$, $U_{e2} = \sin\theta_{12} \cos\theta_{13}$ and $U_{e3}^2 = 1 - U_{e1}^2 - U_{e2}^2$. The current knowledge of these mixing angles is given in tbl. 3.1. The lifetime of $0\nu\beta\beta$ decay is inversely proportional to the effective mass-squared.

Apart from verifying the Majorana nature of neutrinos, the effective mass depends on a number of known and unknown neutrino parameters, and testing or cross-checking the values of these parameters is obviously an immensely important task. Among the unknown neutrino parameters the neutrino mass ordering (the sign of the atmospheric mass-squared difference) is of particular interest. It is indeed an exciting possibility to rule out the inverted ordering (IH) with $0\nu\beta\beta$. This is possible because the lower limit of the effective mass is non-zero in this case [97, 98]. Actually, if at the time when the inverted hierarchy regime is under test at double beta decay experiments the mass ordering is known to be inverted (by an oscillation experiment [99–102] or by a galactic supernova explosion), then testing the inverted hierarchy means testing directly the Majorana nature of neutrinos. If the mass ordering is not known, the experiments can rule out the inverted hierarchy if in addition the Majorana nature of neutrinos is assumed. However, this happens in the vast majority of models and scenarios leading to neutrino mass, and is also natural from an effective field theory point of view.

In any case, a natural scale for the effective mass provided by particle physics is the minimal value of the effective mass in the inverted hierarchy, and should be the intermediate- or long-term aim of double beta experiments.

We stress in this chapter that the lower limit of the effective mass is a sensitive function of the solar neutrino mixing angle θ_{12}. When we first performed our analysis [14] the then

Parameter	Best-fit$^{+1\sigma}_{-1\sigma}$	3σ
$\sin^2\theta_{12}$	0.30 ± 0.013	0.27-0.34
$\sin^2\theta_{13}$	0.023 ± 0.0023	$0.016 \rightarrow 0.030$
$\Delta m^2_{\rm A}$ [10^{-3} eV^2]	$2.47^{+0.069}_{-0.067}$	2.27-2.69
$\Delta m^2_{\odot}$ [10^{-5} eV^2]	7.50±0.185	7.00-8.09

Table 3.1: Neutrino mixing parameters: best-fit values as well as $1\,\sigma$ and $3\,\sigma$ ranges [44].

allowed 3σ range of θ_{12} introduced an uncertainty of a factor of 2 on the lower limit of $\langle m_\nu \rangle$. With now more precise data available (see tbl. 3.1), this impact has reduced to a factor of 1.43, but our arguments pointed out at earlier time still apply. In realistic, i.e., background dominated, experiments the achievable half-life reach is proportional to

$$T^{0\nu}_{1/2} \propto a \times \epsilon \times \sqrt{\frac{M \times t}{B \times \Delta E}}, \tag{3.3}$$

where a is the isotopical abundance of the double beta emitter, M the used mass, t the measuring time, ϵ the detection efficiency, ΔE the energy resolution at the peak position and B the background index typically given in counts/keV/kg/yr. Hence, an uncertainty of 1.43 (2) in the effective mass corresponds to a factor of $1.43^2 \simeq 2$ (4) in terms of lifetime reach and a factor of $1.43^4 \simeq 4.2$ (16) uncertainty in the above combination of experimental parameters. We stated in brackets the impact of uncertainty in θ_{12} as it was when we first pointed out this issue, although even a factor of 4.2 is still a rather high uncertainty when it comes to evaluating the physics potential of $0\nu\beta\beta$ decay experiments.

In this chapter we aim to stress this fact and to illustrate its consequences. We quantify the requirements to test the inverted hierarchy in terms of necessary half-life reach. We consider all $0\nu\beta\beta$-isotopes with a Q-value above 2 MeV and compile the nuclear matrix element calculations from six different groups. That is, we study the isotopes ^{48}Ca, ^{76}Ge, ^{82}Se, ^{96}Zr, ^{100}Mo, ^{110}Pd, ^{116}Cd, ^{124}Sn, ^{130}Te, ^{136}Xe, and ^{150}Nd, as well as nuclear matrix element calculations applying QRPA [103, 104], Nuclear Shell Model [105], the Interacting Boson Model [106], the Generating Coordinate Method [107], and the projected-Hartree-Fock-Bogoliubov model [108]. Particular care is taken to put the calculations on equal footing in what regards various convention issues, such as the axial vector coupling g_A and the nuclear radius appearing in the phase space factor. We present the results for different values of θ_{12}, in order to show its impact.

We are taking the point of view that the spread of nuclear matrix elements and lifetimes obtained in our analysis is a fair estimate of the true allowed range. Though experimental approaches to reduce the uncertainty [109], and statistical approaches to better estimate the theoretical uncertainties (see, e.g., ref. [110]), have started, at the current stage the collection of available results and the use of their spread is the most pragmatic procedure.

Nevertheless, our main conclusions are independent of this and quite straightforward: a precision determination of the solar neutrino mixing angle is crucial to determine the physics potential of, and requirements for, neutrinoless double beta decay experiments. Some proposals for solar neutrino experiments which can pin down θ_{12} more precisely can be found in the literature [111–114]. Large-scale long baseline reactor neutrino experiments have also been proposed [115–118], but to our knowledge still await detailed study by experimentalists. The main focus of future precision neutrino oscillation physics is put on mass ordering, the other mixing angles and CP violation in facilities such as super-, beta-beams or neutrino factories. Recently, with the discovery of θ_{13} being relatively large [15–17], there is also increased interest in using reactor neutrinos at intermediate baselines [99–101] or accelerator neutrinos at long baselines [102] to determine the mass hierarchy and CP violating phase. Given the impact of θ_{12} on neutrinoless double beta decay that we discuss here, we hope to provide additional motivation for studies and proposals in order to determine θ_{12} as precisely as possible[1]. At least we encourage to seriously determine and optimize the potential of future experiments in what regards the achievable precision of θ_{12}.

Using our compilation of matrix element calculations, we also present results for the necessary half-life in order to touch the inverted hierarchy regime. Finally, we investigate which limits on the effective mass can be achieved for a given half-life, and what the current limits are. These points are independent of the value of θ_{12}.

We find that the isotope ^{100}Mo tends to be interesting, in the sense that with the same lifetime it can slightly more easily rule out the inverted hierarchy, or achieve the better limit on the effective mass. This may be helpful for experiments considering various alternative isotopes to study.

3.2 Effective Neutrino Mass and Experimental Values of Neutrino Oscillation Parameters

In general, the decay rate of $0\nu\beta\beta$ decay factorizes in a kinematical, nuclear physics and particle physics part:

$$\Gamma^{0\nu} = G_{\rm kin}\,|M_{\rm nucl}|^2\,X_{\rm part}\,. \tag{3.4}$$

The observation of the decay would establish the nature of the neutrino as a Majorana particle [9], independent on whether indeed light Majorana neutrinos are exchanged in the diagram leading to $0\nu\beta\beta$. However, the most natural interpretation is indeed that this is the case, because we know that neutrinos have a non-vanishing rest mass, and in the vast majority of models they are Majorana particles. The particle physics parameter in

[1]The additional physics potential of precision solar neutrino or θ_{12} experiments is, e.g., solving the metallicity problem of the Sun [119], probing the transition region of the electron neutrino survival probability in the Sun's interior [120], or distinguishing theoretical approaches to lepton mixing such as tri-bimaximal mixing from alternative models [13], e.g., as treated in chapter 2.

	$\langle m_\nu \rangle^{\rm IH}_{\rm min}$ [eV]	
$\sin^2\theta_{12}$	minimal	maximal
0.270	0.0196	0.0240
0.318	0.0154	0.0189
0.380	0.0100	0.0123

Table 3.2: Lower limit of the effective electron neutrino mass in the case of an inverted hierarchy for different values of $\sin^2\theta_{12}$. The minimal and maximal values are obtained by varying $\Delta m^2_{\rm A}$, $\Delta m^2_\odot$ and $\sin^2\theta_{13}$ in their allowed 3σ ranges.

the decay width eqn. (3.4) is therefore $X_{\rm part} \propto \langle m_\nu \rangle^2$, where $\langle m_\nu \rangle$ is the effective electron neutrino mass defined as

$$\langle m_\nu \rangle = \left| c^2_{12}\, c^2_{13}\, m_1 + s^2_{12}\, c^2_{13}\, m_2\, e^{i\alpha} + s^2_{13}\, m_3\, e^{i\beta} \right| , \tag{3.5}$$

where $c_{ij} = \cos\theta_{ij}$, $s_{ij} = \sin\theta_{ij}$, and α, β are the two Majorana phases. It depends on the three neutrino mass eigenstates m_i and the first row of the Pontecorvo-Maki-Nakagawa-Sakata (PMNS) mixing matrix. The effective mass, $\langle m_\nu \rangle$, can span a wide range due to the unknown Majorana phases, the unknown total neutrino mass scale, and the unknown mass ordering. We are interested here mostly in the case of the inverted hierarchy (IH), which corresponds to $m_2 > m_1 > m_3$. In this case the maximum and minimum values of $\langle m_\nu \rangle$ are given by (see, e.g., refs. [97, 98, 121])

$$\langle m_\nu \rangle^{\rm IH}_{\rm max} = \sqrt{m^2_3 + \Delta m^2_{\rm A}}\, c^2_{12} c^2_{13} + \sqrt{m^2_3 + \Delta m^2_\odot + \Delta m^2_{\rm A}}\, s^2_{12} c^2_{13} + m_3 s^2_{13} , \tag{3.6}$$

and

$$\langle m_\nu \rangle^{\rm IH}_{\rm min} = \sqrt{m^2_3 + \Delta m^2_{\rm A}}\, c^2_{12} c^2_{13} - \sqrt{m^2_3 + \Delta m^2_\odot + \Delta m^2_{\rm A}}\, s^2_{12} c^2_{13} - m_3 s^2_{13} , \tag{3.7}$$

respectively. Here, $\Delta m^2_\odot = m^2_2 - m^2_1$ is the solar and $\Delta m^2_{\rm A} = |m^2_3 - m^2_1|$ the atmospheric mass-squared difference. The values we use for the mixing parameters are shown in tbl. 3.1.

Unless the smallest mass m_3 is larger than about 0.05 eV, the effective mass does basically not depend on its value, and increases linearly with m_3 afterwards. In the case of $m_3 \lesssim 0.05$ eV, one finds

$$\langle m_\nu \rangle^{\rm IH}_{\rm max} \simeq c^2_{13} \sqrt{\Delta m^2_{\rm A}} , \tag{3.8}$$

and

$$\langle m_\nu \rangle^{\rm IH}_{\rm min} \simeq c^2_{13} \sqrt{\Delta m^2_{\rm A}}\, \cos 2\theta_{12} = \left(1 - |U_{e3}|^2\right) \sqrt{\Delta m^2_{\rm A}}\, \left(1 - 2\, \sin^2\theta_{12}\right) , \tag{3.9}$$

respectively. The maximal value is obtained for $\alpha = 0$ and the minimal value for $\alpha = \pi/2$. Since θ_{12} is non-maximal, the minimal value of $\langle m_\nu \rangle$ is non-zero, which is in contrast to the normal mass ordering, in which the effective mass can vanish. By obtaining experimentally an upper limit on the effective mass below $\langle m_\nu \rangle^{\rm IH}_{\rm min}$, we can rule out the inverted ordering. If we would know by independent evidence that the ordering is inverted (i.e., from a long

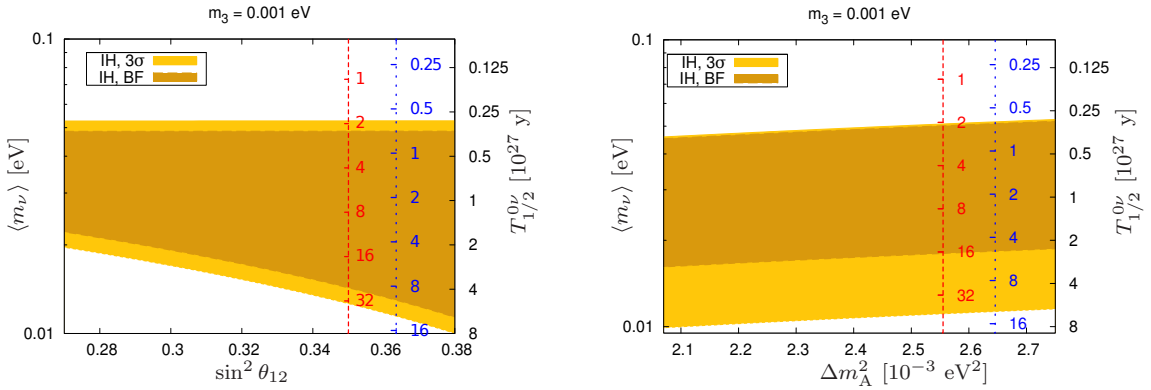

Figure 3.2: The effective electron neutrino mass in the case of an inverted hierarchy is shown as a function of (a) $\sin^2\theta_{12}$ and (b) $\Delta m^2_{\rm A}$ with best-fit values and $3\,\sigma$ ranges for the other oscillation parameters. On the right side of the plots the corresponding half-life for ^{76}Ge is shown assuming three different nuclear matrix elements: $M'^{0\nu} = 2.81$ (red dashed axis), $M'^{0\nu} = 5$ (blue dotted axis), and $M'^{0\nu} = 7.24$ (black solid axis).

baseline experiment, or observation of a galactic supernova), then obtaining such an upper limit would even mean that the Majorana nature of neutrinos would have been ruled out.

From a more pragmatic point of view, particle physics provides a scale for limits on the effective mass, which should be the sensitivity goals of the experimental program. These values are $\langle m_\nu\rangle^{\rm IH}_{\rm max}$ and $\langle m_\nu\rangle^{\rm IH}_{\rm min}$ given in eqn. (3.8) and (3.9), respectively. In fig. 3.2 we show the effective mass for the best-fit and the 3σ ranges of the oscillation parameters as a function of $\sin^2\theta_{12}$ and $\Delta m^2_{\rm A}$. It is clear that the dependence of the lower limit on $\sin^2\theta_{12}$ is very strong. In the currently allowed 3σ range the range of θ_{12} quantifies to a factor of 2 uncertainty for $\langle m_\nu\rangle^{\rm IH}_{\rm min}$, which translates into a factor $2^2 = 4$ in lifetime reach for an experiment. We illustrate this in the plots by translating $\langle m_\nu\rangle$ into the half-life for ^{76}Ge for three representative values of the nuclear matrix elements (see sec. 3.3.1). Tbl. 3.2 shows the numerical values of the effective electron neutrino mass in the case of an inverted hierarchy for different values of the solar neutrino parameter $\sin^2\theta_{12}$. The uncertainty in the other parameters $|U_{e3}|$ and $\Delta m^2_{\rm A}$ is by far not as significant, it amounts in total to a factor less than 25 %. An extensive program to test $\Delta m^2_{\rm A}$ and $|U_{e3}|$ is underway (see, e.g., ref. [122]) and will have decreased this uncertainty considerably by the time the $0\nu\beta\beta$-experiments of the required sensitivity are running. The maximal value of the effective mass does not depend on θ_{12}, and hence its value is uncertain by less than 25 %.

3.3 Half-life Sensitivities and the Inverted Hierarchy

We have seen above that in order to rule out the inverted ordering, and to evaluate the physics potential of future experiments, the value of θ_{12} is of crucial importance. We will now attempt to quantify the impact of θ_{12} in terms of experimentally required half-life.

Isotope	$G^{0\nu}$ [10^{-14} yrs^{-1}]	Q [keV]	nat. abund. [%]
^{48}Ca	6.35	4273.7	0.187
^{76}Ge	0.623	2039.1	7.8
^{82}Se	2.70	2995.5	9.2
^{96}Zr	5.63	3347.7	2.8
^{100}Mo	4.36	3035.0	9.6
^{110}Pd	1.40	2004.0	11.8
^{116}Cd	4.62	2809.1	7.6
^{124}Sn	2.55	2287.7	5.6
^{130}Te	4.09	2530.3	34.5
^{136}Xe	4.31	2461.9	8.9
^{150}Nd	19.2	3367.3	5.6

Table 3.3: $G^{0\nu}$ for different isotopes using $r_0 = 1.2$ fm. Values taken from tbl. 6 of ref. [104] ($G_1^{0\nu}$ in their notation) and scaled to $g_A = 1.25$ ($G^{0\nu}$ of ^{110}Pd taken from tbl. IV of ref. [108]). Also shown is the Q-value for the ground-state-to-ground-state transition which is calculated using isotope masses from ref. [123] and the natural abundance in percent. Note that there is a misprint in ref. [104], which quotes $G^{0\nu}$ for ^{100}Mo as 11.3×10^{-14} yrs^{-1}.

Towards this end, we will have to care with the available calculations of the nuclear matrix elements (NMEs). We have scanned the literature and extracted the NME values for five different calculational approaches of six different groups. If given by the respective authors, we include the error estimates in the calculations for our results. In order to compare them in a proper way, we carefully try to put the NMEs on equal footing, because details of conventions are often different in different publications. We then consider all 11 potential $0\nu\beta\beta$-isotopes with a Q-value above 2 MeV. We discuss the necessary half-lifes to rule out and to touch the inverted hierarchy, putting particular emphasis on the θ_{12}-dependence if necessary. Finally, using our compilation we also give the limits on $\langle m_\nu \rangle$ as a function of future half-life limits for the 11 interesting isotopes. Using the published half-life limits of different isotopes, we also give the current limits on the effective mass.

3.3.1 Nuclear Matrix Elements and the Half-life

The $0\nu\beta\beta$ decay half-life is given according to eqn. (3.4) by[2] [124]

$$(T_{1/2}^{0\nu})^{-1} = G^{0\nu} \left| M^{0\nu} \right|^2 \left(\frac{\langle m_\nu \rangle}{m_e} \right)^2 , \tag{3.10}$$

where $G^{0\nu}$ is the phase space factor, $M^{0\nu}$ the NME, m_e the electron mass, and the effective electron neutrino mass $\langle m_\nu \rangle$ as given in eqn. (3.5). It is known that the conversion of a lifetime into an effective mass, in particular when different NMEs are compared, should

[2]Note that sometimes the factor $1/m_e^2$ is carried into the definition of $G^{0\nu}$.

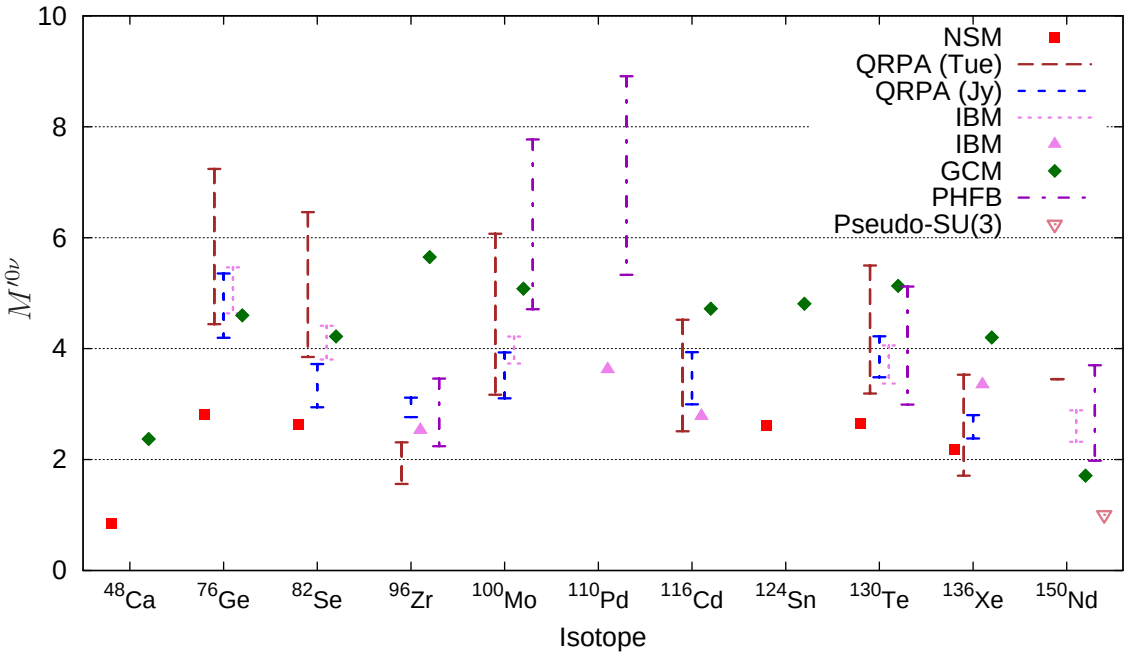

Figure 3.3: NMEs calculated in different frameworks. We have scaled the cited values to $r_0 = 1.2$ fm and $g_A = 1.25$ (see eqn. (3.12)) to make them directly comparable. The exact values are given in tbl. 3.4.

be performed carefully [125, 126]. The nuclear physics parameters, for instance the axial-vector coupling g_A lying in the range $1 \lesssim g_A \lesssim 1.25$, should strictly speaking introduce an uncertainty in the value of $M^{0\nu}$ only. However, it is convention to include g_A in the phase space factor as well. In addition, the nuclear radius $R_A = r_0 A^{1/3}$ (A being the atomic number) appears in $G^{0\nu}$, and there are differences in the normalization of R_A with r_0, which should be taken into account. This leads to the small complication that NMEs calculated with different values for g_A and r_0 cannot be directly compared with each other, since they have different phase space factors and hence seemingly equal (by their value) matrix elements will lead to different decay half-lifes [125] (see also the appendix of [127]). We will outline these issues in more detail in what follows.

The phase space factor is through convention proportional to g_A^4/R_A^2 [104],

$$G^{0\nu} \propto \frac{g_A^4}{R_A^2}, \tag{3.11}$$

with $R_A = r_0 A^{1/3}$ being the nuclear radius and $1 \lesssim g_A \lesssim 1.25$ the axial-vector coupling. The dependence on R_A stems from the desire to make the NMEs dimensionless. Therefore in the definition of the NMEs there is a factor of R_A which is compensated for by the factor $1/R_A^2$ in $G^{0\nu}$. To resolve the issue of comparing matrix elements calculated using different

Isotope	NSM [105] (UCOM)	Tü [128, 129] (CCM)	Jy [130] (UCOM)	IBM [106] (Jastrow)	GCM [107] (UCOM)	PHFB [108] (mixed)
^{48}Ca	0.85	-	-	-	2.37	-
^{76}Ge	2.81	4.44 - 7.24	4.195 - 5.355	4.636 - 5.465	4.6	-
^{82}Se	2.64	3.85 - 6.46	2.942 - 3.722	3.805 - 4.412	4.22	-
^{96}Zr	-	1.56 - 2.31	2.764 - 3.117	2.530	5.65	2.24 - 3.46
^{100}Mo	-	3.17 - 6.07	3.103 - 3.931	3.732 - 4.217	5.08	4.71 - 7.77
^{110}Pd	-	-	-	3.623	-	5.33 - 8.91
^{116}Cd	-	2.51 - 4.52	2.996 - 3.935	2.782	4.72	-
^{124}Sn	2.62	-	-	-	4.81	-
^{130}Te	2.65	3.19 - 5.50	3.483 - 4.221	3.372 - 4.059	5.13	2.99 - 5.12
^{136}Xe	2.19	1.71 - 3.53	2.38 - 2.802	3.352	4.2	-
^{150}Nd	-	3.45	-	2.321 - 2.888	1.71	1.98 - 3.7

Table 3.4: NMEs calculated in different frameworks. The method used to take into account short-range correlations is indicated in brackets. We have scaled the cited values to $r_0 = 1.2$ fm and $g_A = 1.25$ (see eqn. (3.12)) to make them directly comparable. If ranges instead of single NME values are given then they arise due to intrinsic model details varied in the respective publications. This table is graphically represented in fig. 3.3, the pseudo-SU(3) NME for ^{150}Nd plotted there is 1.00 [131].

values of g_A, some – but not all – authors define

$$M'^{0\nu} = \left(\frac{g_A}{1.25}\right)^2 M^{0\nu}, \tag{3.12}$$

thereby carrying the g_A dependence from $G^{0\nu}$ to $M'^{0\nu}$, i.e.,

$$G^{0\nu}(M^{0\nu})^2 = G^{0\nu}_{1.25}(M'^{0\nu})^2, \tag{3.13}$$

with $G^{0\nu}_{1.25} = G^{0\nu}(g_A = 1.25)$. This means that these NMEs share a common $G^{0\nu}$ factor – that of $g_A = 1.25$. Still one has to be careful when comparing NMEs from different groups, since different authors take different values for r_0, usually $r_0 = 1.1$ fm (e.g., refs. [128, 129]) or $r_0 = 1.2$ fm (e.g., refs. [105, 106, 130]). The NMEs are proportional to r_0 and therefore when comparing two different matrix elements $M^{0\nu}_1$, $M^{0\nu}_2$, which have been calculated using $r_{0,1}$ and $r_{0,2}$, respectively, one has to rescale $M^{0\nu}_2$ by $r_{0,1}/r_{0,2}$ or $M^{0\nu}_1$ by $r_{0,2}/r_{0,1}$. Otherwise one introduces an error of $(r_{0,1}/r_{0,2})^2 \simeq 1.19$ in terms of half-life (see eqn. (3.10)). A compilation of g_A, r_0 and $G^{0\nu}$ values used in different works can be found in ref. [126].

In addition, it is often overlooked that there are differences between independent phase space factor calculations, which can be as high as ∼13% (see the appendix of [127]). For instance, ref. [128] uses phase space factors from [132], while ref. [130] uses the ones from [104]. There, $G^{0\nu}$ for the isotope ^{136}Xe is given as 49.7×10^{-15} yrs^{-1} and 43.1×10^{-15} yrs^{-1}, respectively (we scaled them to $g_A = 1.25$ and $r_0 = 1.2$ fm to make them directly comparable). To perform a consistent comparison between different NME calculations we

will take the numerical values for the phase space factors from ref. [104] when calculating the necessary half-life sensitivities and take carefully into account all of the above mentioned difficulties[3]. Tbl. 3.3 shows the phase space factors used in our calculations. All $0\nu\beta\beta$-isotopes with a Q-value above 2 MeV are given. We have chosen the value $r_0 = 1.2$ fm throughout our analysis. Also given in the table is the natural abundance of the isotope in percent.

The convention issues mentioned so far are of course different from the intrinsic uncertainty stemming from the nuclear physics itself. We will not get into detail here, and refer to existing reviews available in the literature [5, 104]. A program to reduce the uncertainty by independent experimental cross checks has been launched [109], but it is unclear whether the results will be available and conclusive for all interesting isotopes at the time when the decisions on the experimental parameters have to be taken.

An important point here are short-range correlations (SRC) since the contribution to NMEs stems mainly from physics of internucleon distances $r \leq (2-3)$ fm [133]. There are different proposals how to treat SRC, namely via a Jastrow-like function [5, 134], Unitary Correlation Operator Method (UCOM) [135], or Coupled Cluster Method (CCM) [128, 136–138]. For instance, the authors of ref. [130] argue that UCOM should be preferred over Jastrow while the authors of [128] prefer CCM.

In this thesis we use the NME values calculated with UCOM or CCM SRC in the NSM, QRPA, and GCM frameworks; the NME values in the IBM framework are calculated with Jastrow SRC. In the case of the PHFB model the authors used a statistical estimate of the theoretical uncertainty by calculating NMEs with three different types of SRC, four different parametrizations of the effective two-body interaction and taking the mean and the standard deviation. We used the NMEs derived in this manner and therefore no particular SRC method can be assigned to them.

With a chosen SRC method, some groups discuss additional sources of error which arise, such as the set of single-particle states, the number of possible wave function configurations, or other model details. These errors are given in some publications, and we include them in our analysis. The NME values and ranges which we have compiled and which will be used in this chapter are tabulated in tbl. 3.4 and plotted in fig. 3.3. The values are scaled to $r_0 = 1.2$ fm and $g_A = 1.25$ so that they are directly comparable. The original NME values can be found in column 3 of tbl. 8 of ref. [105] (NSM), column 6 of tbl. III of ref. [128] and column 4 of tbl. II of ref. [129] (QRPA, Tübingen group), column 6 of tbl. 1 of ref. [130] (QRPA, Jyväskylä group), columns 2 and 3 of tbl. VI of ref. [106] (IBM), column 5 of tbl. I of ref. [107] (GCM), and column 3 of tbl. IV of ref. [108] (PHFB). Regarding IBM, the isotopes for which a range is given are calculated in ref. [106] with two sets of single-particle energies, one extracted from experiment ("experimental"), the other from a specific model ("theoretical"). Their span defines the given range. The IBM values without a range are unpublished "experimental" NMEs kindly provided by Francesco Iachello. As only few calculations for ^{150}Nd are available, we also include the result from ref. [131], which applied the pseudo-SU(3) Ansatz for the calculation, which is suitable for deformed nuclei such as

[3]Note that there is a misprint for the phase space factor of ^{100}Mo in ref. [104].

^{150}Nd. It gives by far the lowest NME.

3.3.2 Ruling out the Inverted Hierarchy

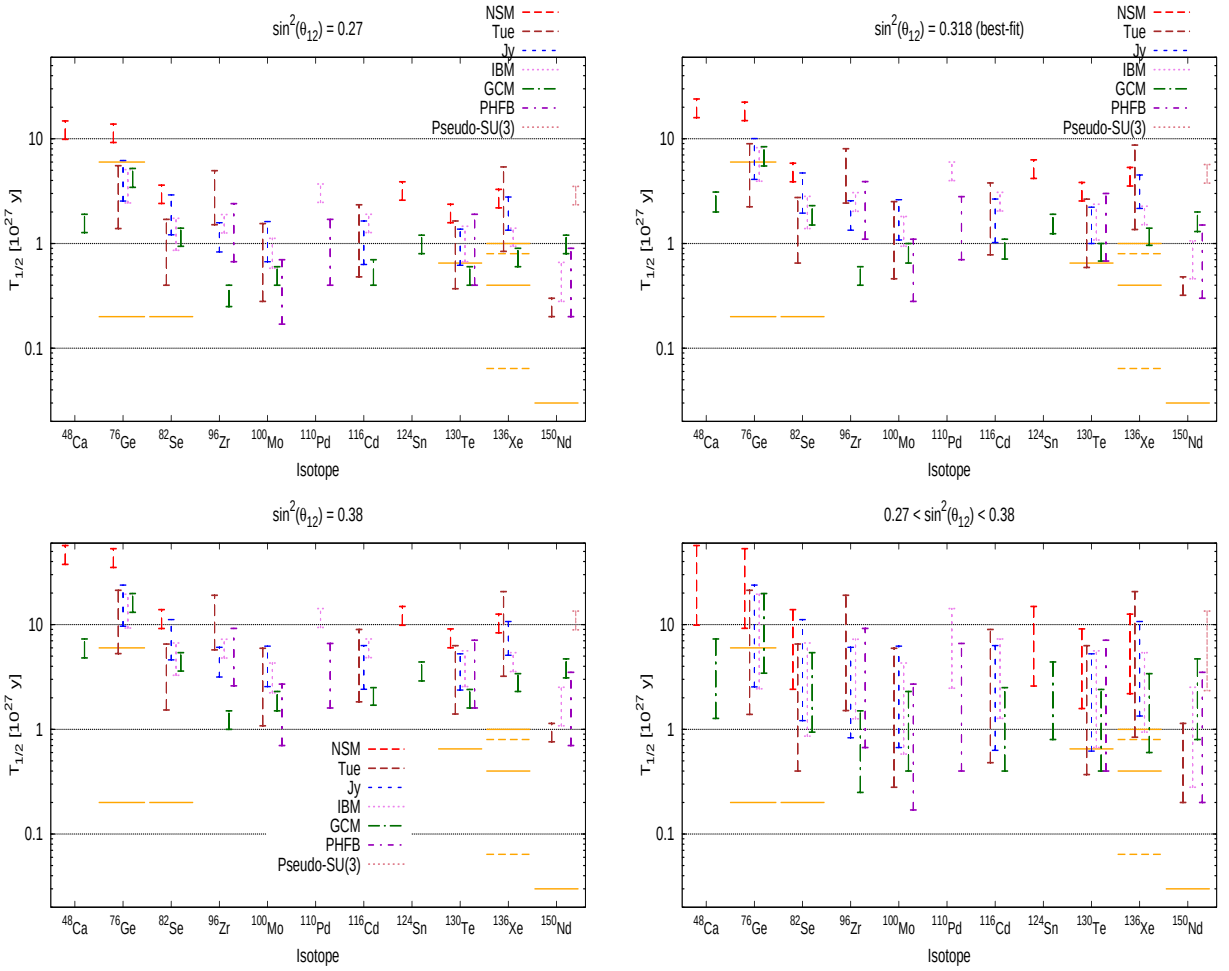

Figure 3.4: Required half-life sensitivities to exclude the inverted hierarchy for different values of θ_{12}. For each value of $\sin^2\theta_{12}$ the other parameters (Δm^2_{A}, $\Delta m^2_{\odot}$, $\sin^2\theta_{13}$) are varied in their 3σ ranges. The lower right plot tries to combine the other three: the lines correspond to the combined uncertainties of the nuclear physics and the oscillation parameters. The small horizontal lines show expected half-life sensitivities at 90% C.L. of running and planned $0\nu\beta\beta$ experiments. The expected limits are from the following experiments: GERDA and MAJORANA (^{76}Ge, equal sensitivity expectations for both experiments); SuperNEMO (^{82}Se), CUORE (^{130}Te); EXO (^{136}Xe, dashed lines); KamLAND (^{136}Xe, solid lines); SNO+ (^{150}Nd). When two sensitivity expectations are given for one experiment they correspond to near and far time goals.

Isotope	Experiment	$T^{0\nu}_{1/2}$/yrs
^{76}Ge	GERDA	2.0×10^{26}
	(+MAJORANA)	6.0×10^{27}
^{82}Se	SuperNEMO	2.0×10^{26}
^{130}Te	CUORE	6.5×10^{26}
^{136}Xe	EXO	6.4×10^{25}
		8.0×10^{26}
^{136}Xe	KamLAND	4.0×10^{26}
		1.0×10^{27}
^{150}Nd	SNO+	4.5×10^{24}
		3.0×10^{25}

Table 3.5: Expected half-life sensitivities for some $0\nu\beta\beta$ experiments [139]. When two values are given they correspond to near and far time expectations with different detector masses.

Having compiled the NMEs in a form which makes it possible to compare them with each other, we can now give the necessary half-lifes in order to rule out the inverted hierarchy. Recall that the value $\langle m_\nu \rangle^{\rm IH}_{\rm min}$ given in eqn. (3.9) has to be reached for this, and that a strong dependence on θ_{12} is present.

In fig. 3.4 we plot the necessary half-lifes to rule out the inverted hierarchy for all 11 isotopes with Q-value above 2 MeV. We display the situation for different values of θ_{12}. The full range, leaving θ_{12} free within the range $0.27 \leq \sin^2\theta_{12} \leq 0.38$, is also displayed. For convenience, we give the numerical values for necessary $T^{0\nu}_{1/2}$ in tbl. A.1, which can be found in appendix A. For each value of $\sin^2\theta_{12}$ the other parameters ($\Delta m^2_{\rm A}$, $\Delta m^2_\odot$, $\sin^2\theta_{13}$) are varied in their 3σ ranges such that in Table A.1 one has a somewhat more optimistic and more pessimistic prediction for the $0\nu\beta\beta$ decay half-life. Recall that the dependence on the oscillation parameters other than θ_{12} is rather weak (less than 25 %) and will be strongly reduced in the future.

One can compare the necessary half-lifes with the foreseen sensitivities of up-coming experiments. We refer here to the compilation from ref. [139], which listed confirmed sensitivities of the currently "most developed" experiments. Table 3.5 gives the numbers, staged experiments have two values. We have included those sensitivities in our plots. To give an example on the interpretation of the plots, with the final sensitivity GERDA and Majorana (6×10^{27} yrs) could rule out the inverted hierarchy if $\sin^2\theta_{12} = 0.27$ for all NMEs except for the NSM. Several experiments are currently taking data and EXO and KamLAND have already their first publications [18, 19] (see tbl. 3.6 for their current half-life limits).

Another way to display the interplay of nuclear physics, θ_{12} and $0\nu\beta\beta$ is shown in fig. 3.5: assuming for four interesting isotopes a certain half-life limit, we show for which NME values the inverted hierarchy is ruled out. For instance, for ^{76}Ge and a half-life of 5×10^{27}

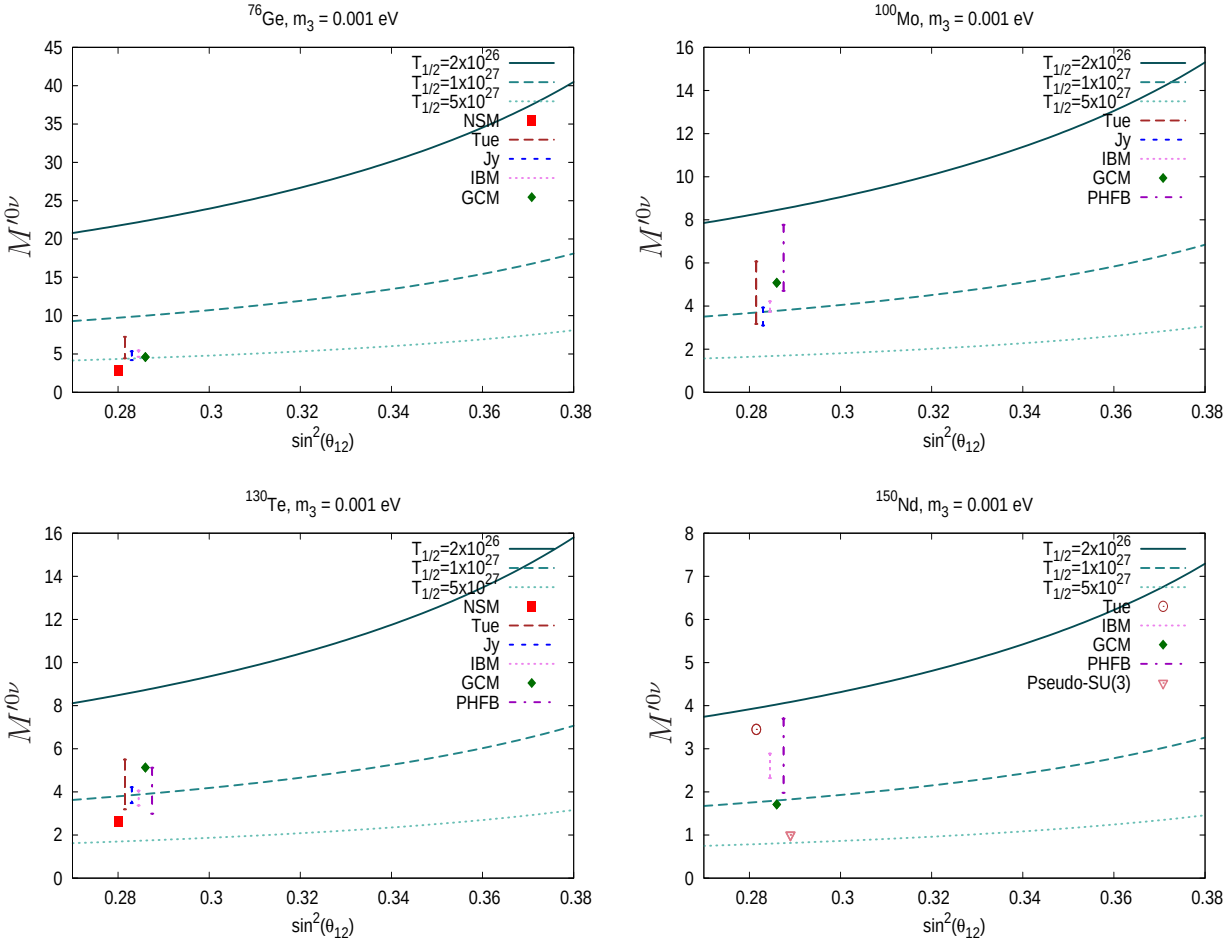

Figure 3.5: Assuming the case of an inverted neutrino mass hierarchy and a measurement of a $0\nu\beta\beta$ decay signal, this plot shows the minimal NMEs for which the inverted hierarchy can be ruled out. For the mixing parameters Δm^2_{A}, $\Delta m^2_{\odot}$, and $\sin^2\theta_{13}$ best-fit values are taken. The ranges of the NME calculations are also displayed in the figures.

yrs, we can rule out the inverted hierarchy if the matrix element is larger than about 5 if $\sin^2\theta_{12} = 0.32$. For a half-life of 1×10^{27} yrs, the NME has to be larger than about 12, hence not too realistic. Nevertheless, the ranges of the NME calculations are also displayed in the figures.

Fig. 3.6 shows the required half-life to touch the inverted hierarchy. This half-life (corresponding to the value $\langle m_\nu \rangle^{\mathrm{IH}}_{\mathrm{max}}$ given in eqn. (3.8)) does not depend on θ_{12}. The other parameters, Δm^2_{A}, $\Delta m^2_{\odot}$ and θ_{13} are varied in their current 3σ range. The numerical values are given in tbl. A.2 in the appendix. For instance, the combined GERDA and Majorana results, as well as CUORE, could touch the inverted hierarchy for all available NMEs.

From the figures and tables presented in this section, one identifies ^{100}Mo as the somewhat

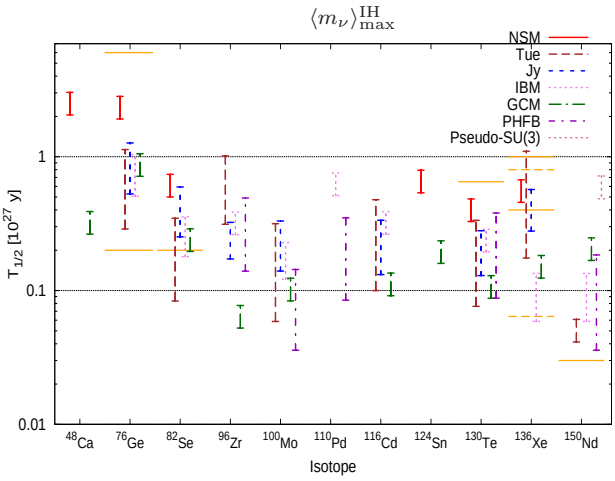

Figure 3.6: Required half-life sensitivities to touch the inverted hierarchy. The mixing parameters are varied in their 3σ ranges. The small horizontal lines show expected half-life sensitivities as in fig. 3.4.

most interesting isotope. With our compilation of NMEs, the required lifetimes to reach and/or exclude the inverted hierarchy tends to be generally lowest for this $0\nu\beta\beta$-candidate. If the very low pseudo-SU(3) NME for ^{150}Nd would be omitted, then this isotope would even more favorable than ^{100}Mo. These tentative conclusions may be helpful for experiments which have alternatives in the isotopes to investigate, such as LUCIFER [140] (currently considering ^{82}Se or ^{100}Mo or ^{116}Cd), MOON [141] (^{82}Se or ^{100}Mo), or SuperNEMO [142] (^{82}Se, ^{150}Nd or others).

3.3.3 Current and Future Limits on the Effective Mass

In tbl. 3.6 we show the current limits on the half-life of $0\nu\beta\beta$, obtained in a variety of experiments[4]. Using the largest and smallest NME from our compilation, we give the range of the current limit of $\langle m_\nu \rangle$ for the particular isotope.

Finally, we give the limit on the effective mass as a function of achieved half-life for the 11 isotopes under investigation. This is shown in fig. 3.7. We have given four different half-life values. With a half-life sensitivities of about 5×10^{25} yrs the first isotopes start to touch the inverted hierarchy. Without specifying the value of θ_{12}, no isotope can rule out the inverted hierarchy unless sensitivities above 10^{27} yrs are reached. Entering the inverted hierarchy regime requires sensitivities above 10^{26} yrs.

[4]Part of the Heidelberg-Moscow collaboration has claimed observation [152] of $0\nu\beta\beta$ corresponding to a half-life of 2.23×10^{25} yrs, and a 95% C.L. range of $(0.8 - 18.3) \times 10^{25}$ yrs. This would correspond to a range of the effective mass of $(0.19 - 0.49)$ eV, and $(0.066 - 0.82)$ eV, respectively.

Isotope	$T^{0\nu}_{1/2}$/yrs	Experiment	$M'^{0\nu}$ min	$M'^{0\nu}$ max	$\langle m_\nu \rangle$ [eV] min	$\langle m_\nu \rangle$ [eV] max
^{48}Ca	5.8×10^{22}	CANDLES [143]	0.85	2.37	3.55	9.91
^{76}Ge	1.9×10^{25}	HDM [144]	2.81	7.24	0.21	0.53
^{82}Se	3.2×10^{23}	NEMO-3 [145]	2.64	6.46	0.85	2.08
^{96}Zr	9.2×10^{21}	NEMO-3 [146]	1.56	5.65	3.97	14.39
^{100}Mo	1.0×10^{24}	NEMO-3 [145]	3.10	7.77	0.31	0.79
^{116}Cd	1.7×10^{23}	SOLOTVINO [147]	2.51	4.72	1.22	2.30
^{130}Te	2.8×10^{24}	CUORICINO [148]	2.65	5.50	0.27	0.57
^{136}Xe	5.0×10^{23}	DAMA [149]	1.71	4.20	0.83	2.04
^{136}Xe	1.6×10^{25}	EXO-200 [19]	1.71	4.20	0.15	0.36
^{136}Xe	1.9×10^{25}	KamLAND-Zen [18]	1.71	4.20	0.13	0.33
^{136}Xe	3.4×10^{25}	KamLAND-Zen + EXO-200 [18]	1.71	4.20	0.10	0.25
^{150}Nd	1.8×10^{22}	NEMO-3 [150]	1.71	3.70	2.35	8.65

Table 3.6: Experimental $0\nu\beta\beta$ decay half-life limits at 90 % C.L. Columns 4 and 5 show the minimal and maximal NMEs from our compilation (see tbl. 3.4), and columns 6 and 7 the corresponding upper limits on the effective electron neutrino mass $\langle m_\nu \rangle$. Similar limits on ^{76}Ge to the ones in [144] have been obtained by the IGEX experiment [151].

3.4 Experimental Aspects

A large variety of different upcoming experiments exists in various stages of realization. They are in order of increasing isotope mass CANDLES [153] (^{48}Ca), GERDA [154] and MAJORANA [155] (^{76}Ge), LUCIFER [140] (^{82}Se or ^{100}Mo or ^{116}Cd), SuperNEMO [142] (^{82}Se or ^{150}Nd), MOON [141] (^{82}Se or ^{100}Mo), COBRA [156] (^{116}Cd) , CUORE [157] (^{130}Te), EXO [158], XMASS [159], KamLAND-Zen [160] and NEXT [161] (^{136}Xe), DCBA [162] and SNO+ [163] (^{150}Nd).

As discussed before not for all proposals the final decision on the selected isotope is already made. From the discussion of the previous sections it would of course be desirable to rule out the inverted scenario and thus tune the experimental parameters and hence the sensitivity to do so. The obtainable half-life can be estimated to be

$$T^{0\nu}_{1/2} = \frac{N_A \ln 2}{n_\sigma} \left(\frac{a \times \epsilon}{W} \right) M \times t \tag{3.14}$$

in a background-free scenario and

$$T^{0\nu}_{1/2} = \frac{N_A \ln 2}{n_\sigma} \left(\frac{a \times \epsilon}{W} \right) \sqrt{\frac{M \times t}{B \times \Delta E}} \tag{3.15}$$

in case of a background limited search [92], where n_σ is the number of standard deviations corresponding to the desired confidence level, W the molecular weight of the source material, and the other parameters as in eqn. (3.3). Notice, only in the background-free scenario

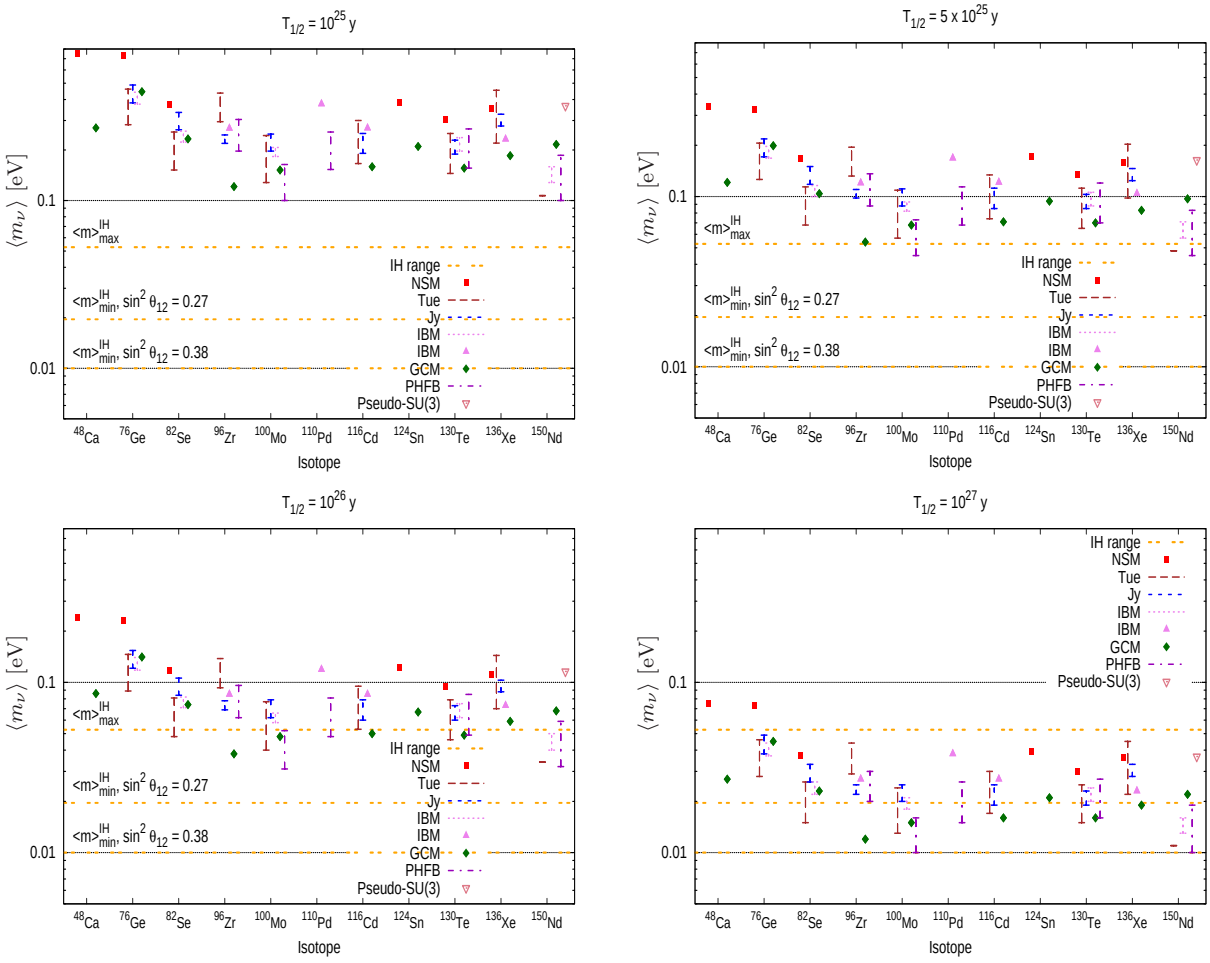

Figure 3.7: Limits on the effective mass which can be set assuming different half-lifes for the 11 isotopes under investigation. The orange double-dashed horizontal lines show the upper and lower lines of the inverted hierarchy when the mixing parameters are varied in their 3σ range (see fig. 3.2). Thereby the horizontal line at 0.02 eV (0.01 eV) corresponds to the lower line of the IH for $\sin^2\theta_{12} = 0.27$ ($\sin^2\theta_{12} = 0.38$).

the half-life sensitivity scales linearly with the measuring time. To be more conservative and realistic we assume a background limited case.

As shown in fig. 3.2a, the minimal effective Majorana mass which has to be explored shows a factor of 1.43[5] difference due to the current uncertainty in the mixing angle θ_{12}, depending on whether the actual value of θ_{12} comes off at the high or low end of its currently allowed range. Thus, this implies a factor of 4.2 difference in the combination of measuring time, energy resolution, background index and detector mass. From the experimental point of view such a big potential factor causes a significant challenge and work, as half-

[5]Note that the range of $\sin^2\theta_{12}$ in fig. 3.2a is larger than the currently allowed $3\,\sigma$ range.

life measurements well beyond 10^{26} yrs itself are already non-trivial. Therefore it would be extremely desirable to reduce the uncertainty on θ_{12} in future solar experiments like SNO+ [111].

As an example consider a 1 ton Ge-experiment, enriched to 90 % in ^{76}Ge. Furthermore, consider a full detection efficiency, an energy resolution (FWHM) of 3 keV at peak position, the best one of all considered double beta experiments, and 10 years of running time. For an optimistic combination of the other mixing parameters (upper rows in tbls. A.1 and A.2) such an experiment could touch the IH at 2σ C.L. even using the less favorable NME if a background level of 5.5×10^{-3} counts/keV/kg/yr could be achieved. This should be feasible as already for GERDA phase II the aim is to achieve 10^{-3} counts/keV/kg/yr. Ruling out the complete IH for small θ_{12} would require 2.4×10^{-4} counts/keV/kg/yr. For large θ_{12} it is not possible to exclude the IH (assuming the smallest NME) with the considered experimental parameters. Excluding the IH would require a half-life sensitivity of 3.5×10^{28} yrs (Tab. A.1). But even considering a background-free case and therefore using eqn. (3.14), one obtains a 2σ half-life limit of only 2.47×10^{28} yrs. By using eqn. (3.15) one could formally calculate a necessary background of 1.6×10^{-5} counts/keV/kg/yr to exclude a half-life of 3.5×10^{28} yrs with the stated experimental set-up. But this background corresponds to only about 0.5 total background counts during the whole operational period of 10 years which has to be compared to 1.4 expected counts from the $0\nu\beta\beta$ decay with a half-life of 3.5×10^{28} yrs. Hence, the experiment cannot be considered to be background dominated and thus eqn. (3.15) is not applicable.

As another example, consider a large scale experiment like SNO+ using ^{150}Nd, enriched to 60%. With a total mass of 760 kg of natural Nd, 10 years of running time and an energy resolution of about 300 keV (the resolution depends on the percentage of Nd-loading of the scintillator, here a resolution of $3.5\%/\sqrt{E}$ was assumed) it would require a background of 6.1×10^{-4} counts/keV/kg/yr to touch the IH at 2σ C.L. To exclude IH a background as small as 2.7×10^{-5} counts/keV/kg/yr (for small θ_{12}) or 1.9×10^{-6} counts/keV/kg/yr (for large θ_{12}) would be required (note that due to the presence of the $2\nu\beta\beta$ mode in conjunction with the energy resolution of only 300 keV this low background is very hard to reach and one has to scale up the other parameters of the experiment to fully cover the IH). Nevertheless, one can check that the background levels we have estimated here still correspond to a background dominated case.

3.5 Conclusions

The main focus of the present chapter was put on testing the inverted neutrino mass hierarchy with neutrinoless double beta decay experiments. The maximal and (non-zero) minimal values of the effective mass are natural sensitivity goals for the experimental program.

We have stressed that the mixing parameter θ_{12}, the solar neutrino mixing angle, introduces an uncertainty of a factor of 1.43 on the minimal value of the effective mass. This implies an uncertainty of a factor of $1.43^2 \simeq 2$ on the lifetime and $1.43^4 \simeq 4.2$ on the com-

bination of isotope mass, background level, energy resolution and measuring time. Given the long-standing problem of nuclear matrix element calculations we have taken a pragmatic point of view: to quantify the necessary half-lifes to test and/or rule out the inverted hierarchy we have attempted to collect as many theoretical calculations as possible, and included their errors if available. The nuclear matrix elements we have compiled have been put on equal footing in what regards convention issues. We have used our compilation of NMEs to give the current limits on the effective mass of different isotopes, and to give the limits on the effective mass as a function of reached half-life. The isotope ^{100}Mo tends to look interesting, in the sense that with the same lifetime limit stronger constraints on the effective mass than for the other isotopes can be reached, an observation potentially interesting for upcoming experiments without a final decision on which isotope to use.

We finish by stressing once more that a precision determination of the solar neutrino mixing angle θ_{12} is of crucial importance to evaluate the physics potential of neutrinoless double beta decay experiments. A better knowledge of this parameter is desirable, and we hope to provide here additional motivation for further studies.

Part II

SO(10) Origin of Fermion Masses and Mixings

Chapter 4

Introduction to Fermion Masses in $SO(10)$ Models

The origin of fermion masses and mixings is a long-standing question in elementary particle physics. Among different frameworks to address this problem, theories unifying strong and electroweak interactions as well as – partly or completely – quarks and leptons offer very attractive solutions. Particularly intriguing are models based on $SO(10)$ symmetry.

In $SO(10)$ all SM particles of one generation plus a right-handed neutrino are assigned to a single 16-dimensional representation. The masses of the particles arise from Yukawa interactions of two 16s with suitable Higgs fields when the Higgs develops a vacuum expectation value (VEV). Since [10, 164]

$$16 \otimes 16 = 10_{\mathrm{S}} \oplus \overline{126}_{\mathrm{S}} \oplus 120_{\mathrm{A}}, \tag{4.1}$$

the Higgs fields of renormalizable $SO(10)$ models can belong to 10, 126, or 120 dimensional representations (denoted henceforth by 10_H, $\overline{126}_H$, and 120_H, respectively) yielding the Yukawa part of the Lagrangian,

$$\mathcal{L}_Y = 16\,(Y_{10}10_H + Y_{126}\overline{126}_H + Y_{120}120_H)\,16. \tag{4.2}$$

After spontaneous symmetry breaking the fermions obtain the masses [10, 165]

$$\begin{aligned}
M_u &= v_{10}^u Y_{10} + v_{126}^u Y_{126} + v_{120}^u Y_{120}\,, \\
M_d &= v_{10}^d Y_{10} + v_{126}^d Y_{126} + v_{120}^d Y_{120}\,, \\
M_D &= v_{10}^u Y_{10} - 3v_{126}^u Y_{126} + v_{120}^D Y_{120}\,, \\
M_l &= v_{10}^d Y_{10} - 3v_{126}^d Y_{126} + v_{120}^l Y_{120}\,, \\
M_R &= v_{126}^R Y_{126}\,, \\
M_L &= v_{126}^L Y_{126}\,,
\end{aligned} \tag{4.3}$$

where $M_u, M_d, M_D, M_l, M_R, M_L$ are the up-quark, down-quark, Dirac neutrino, charged lepton, right-handed Majorana neutrino (type I seesaw), and left-handed Majorana neutrino (type II seesaw) mass matrices, and Y_{10}, Y_{126}, and Y_{120} are the Yukawa coupling

matrices between the 16 fermions and the Higgs in the **10**, $\overline{\mathbf{126}}$, and **120** representations, respectively. Y_{10} and Y_{126} are symmetric whereas Y_{120} is anti-symmetric. $v_{10/126/120}^{u/d/D/l/R/L}$ represents the part of the VEV (or combination of VEVs) of the Higgs fields that is important for the respective particle. Eqn. (4.3) holds at the scale of $SO(10)$ symmetry breakdown, henceforth referred to as $M_{\rm GUT}$. We will consider supersymmetric (SUSY) as well as non-supersymmetric $SO(10)$ models. In non-SUSY $SO(10)$ the 10_H can be chosen real, but one can argue that this will not lead to a viable particle spectrum [166]. Taking the 10_H to be complex, its real and imaginary parts can couple separately to the fermionic 16 and will lead to two independent Yukawa matrices. To avoid this complication in the case of non-SUSY $SO(10)$ we impose an additional Peccei–Quinn $U(1)$ symmetry [167] as described in refs. [166, 168]. Then eqn. (4.3) is valid both in the case of non-SUSY as well as SUSY $SO(10)$.

The effective mass matrix of light neutrinos is given by [11]

$$m_\nu = M_L - M_D^T M_R^{-1} M_D = m_\nu^{\rm II} + m_\nu^{\rm I}, \tag{4.4}$$

with type I & II seesaw contributions as indicated in above equation.

As obvious from eqn. (4.3) in $SO(10)$ all fermion mass matrices are related since they are all combinations of the same Yukawa matrices. Albeit a nice feature, there are still lots of parameters in the Yukawas making the models not very predictive and the process of fermion mass generation somewhat arbitrary and messy.

Another possibility to constrain fermion mass matrices is to make additional assumptions, e.g., one can impose texture zeros [169–176], zero determinant [177, 178], vanishing minors [179–182], vanishing trace [183–185], and many more, see, e.g., ref. [186]. One can also make assumptions on the mixing matrices, e.g., tri-bimaximal mixing [6], or other relations as reviewed in chapter 2 (ref. [13]).

Combining flavor symmetries with GUTs leads to too many constraints and phenomenologically not viable models. In order to increase predictivity, a promising way is to combine above mentioned two possibilities, namely using a GUT framework like $SO(10)$ and applying additional constraints to the Yukawa matrices. In refs. [187–189] texture zeros on fermion mass matrices are imposed using the framework of $SO(10)$. While an interesting option, from the viewpoint of $SO(10)$ it appears unlikely to find symmetries in the mass matrices. After all they receive contributions from different Yukawa matrices weighted by *a priori* undetermined VEVs. More natural from the $SO(10)$ perspective would be to find symmetries in the Yukawa matrices [191]. Hence, in addition to fitting the "naked" $SO(10)$ models, we also want to analyze the possibility of different texture zeros in Y_{10}, Y_{126}, and Y_{120} and check the textures for phenomenological viability.

We fit fermion masses and mixings at low energy (M_Z) as well as the baryon asymmetry of the universe subject to constraints from $SO(10)$ (eqn. (4.3)). In this regard we consider several classes of $SO(10)$ models, differing in the choice of Higgs representations. A minimal model with only one Higgs field is phenomenologically not viable since all fermions are then proportional to the same Yukawa matrix and are hence diagonal in the same basis, resulting in no mixing between up- and down-quarks or between charged leptons and neutrinos. A

$\overline{126}_H$ field is required for neutrino mass generation. We consider models that additionally contain either a 10_H, or a 120_H, or both a 10_H and a 120_H. Further we analyse both supersymmetric versions of the models as well as models without SUSY.

The $SO(10)$ relations in eqn. (4.3) as well as the additionally imposed texture zeros are valid at $M_{\text{GUT}} = 2 \times 10^{16}$ GeV. Fermion masses and mixings are measured at much lower energies, e.g., at $M_Z \approx 91.19$ GeV. To fit the parameters of a model to the data at M_{GUT}, one has to use renormalization group evolution (RGE) to obtain the values of the observables at M_{GUT}. Therefore one necessarily needs certain model details as input, such as the as yet undetermined lightest neutrino mass and the masses M_i of the right-handed neutrinos, which in general are free parameters of a model and start to contribute to the β-functions for energies above M_i (see the appendix). Earlier studies either did not include renormalization effects at all [187,189], or faced this issue by evolving experimental values to M_{GUT} while neglecting model details (either themselves or by using published data at various energy scales [192–194]). They then fitted the data at the energy scale $\mu = M_{\text{GUT}}$ [168,188,191,195], without being concerned with RGE anymore. Other studies used charged lepton masses evolved to M_{GUT}, while at the same time using low-energy values for neutrino parameters for their fits at M_{GUT} [168,191,195].

When using observables evolved to M_{GUT} to make a fit using relations from eqn. (4.3) one runs into the following problem: on the one hand, to evolve observables from M_Z to M_{GUT} certain high-energy model details (such as the seesaw scale) have to be known, since they have an impact on the running of observables (this has been demonstrated long ago, e.g., for the m_b/m_τ ratio [196]). On the other hand, exactly these model details are varied while the fit is performed.

An additional issue which is commonly neglected are effects coming from non-degenerate seesaw scales (i.e., non-degenerate right-handed neutrinos, ν_{R_i}). Treating non-degenerate ν_{R_i} correctly, i.e. integrating them out during RG evolution one by one at $\mu = M_i(M_i)$ (as opposed to integrating out all at once at a common seesaw scale), can have sizable effects on neutrino parameters as has been demonstrated in ref. [197]. For our analysis we apply the method described in ref. [197] and integrate out ν_{R_i} at appropriate energies. This produces several effective field theories (EFT) during RGE – one EFT per heavy degree of freedom which is integrated out.

Besides yielding more trustworthy results, a more precise analysis that takes into account RGE also leads to more reliable predictions of experimentally undetermined observables like the effective neutrino mass governing neutrinoless double beta decay (see chapter 3) or the leptonic CP violating phase δ^l_{CP}.

Furthermore, our analysis differs from previous studies in that we also consider the baryon asymmetry Y_B, which is usually not done within the context of $SO(10)$. We assume that the baryon asymmetry is generated through thermal leptogenesis and also include flavor effects in our analysis (see sec. 6.4 for details). Ref. [198] checks an $SO(10)$ inspired model for compatibility with the experimentally measured value of Y_B, assuming it is generated through thermal leptogenesis. Furthermore, in ref. [198] RGE is only accounted for using a generic multiplicative factor. In contrast, we will include Y_B as an observable in our fits of real $SO(10)$ models including full RGE, which to the best of our knowledge has not

been done before. Since thermal leptogenesis takes place at temperatures corresponding to the mass of the lightest right-handed neutrino, one needs to know the value of the relevant parameters at this energy scale to make accurate statements. Finally, the correct treatment of RGE allows us to consider the Higgs mass in the analysis of non-SUSY models, as will be described in sec. 6.2.

Chapter 5

Model Details and Previous Work

We now simplify the notation and rewrite eqn. (4.3) [168, 195]:

$$\begin{aligned} Y_u &= r(H + sF + it_u G)\,, \\ Y_d &= H + F + iG\,, \\ Y_D &= r(H - 3sF + it_D G)\,, \\ Y_l &= H - 3F + it_l G\,, \\ M_R &= r_R^{-1} F\,, \end{aligned} \tag{5.1}$$

where Y_i are the mass matrices M_i from eqn. (4.3) divided by the VEVs v or $v_{u/d}$ of the Standard Model (SM) or Minimal Supersymmetric Standard Model (MSSM), respectively. H, F, G correspond to Y_{10}, Y_{126}, and Y_{120}, respectively, i.e., H and F are symmetric and G is anti-symmetric. s, t_u, t_D, t_l are complex parameters, whereas r, r_R can be chosen real without loss of generality [168]. We have omitted the type II seesaw term (compare to eqn. (4.3)) since we assume that the type I seesaw term dominates.

We now define the different models which we want to test for viability using experimental data on fermion masses and mixings. The first differentiation between the models concerns their Higgs content. We consider two minimal setups with $10_H + \overline{126}_H$ or $120_H + \overline{126}_H$ and a setup with $10_H + \overline{126}_H + 120_H$. We refer to the $10_H + \overline{126}_H$ setup as "M1" ("MS") and to the $10_H + \overline{126}_H + 120_H$ setup as "F1" ("FS") in case we consider the non-SUSY (SUSY) versions of the models (M stands for "minimal", F for "full"). The non-SUSY $120_H + \overline{126}_H$ setup was argued based on an analytical two generation approximation to be an attractive minimal model to describe fermion masses and mixings [166]. We analyze this non-SUSY setup numerically in the full three generation case and will refer to this model as "M2". A further model corresponds to model M1 with an imposed texture. We denote this model by MT. The models we considered are summarized in tbl. 5.1. More details on the models is given in the following sections.

The Higgs representations mentioned above are not enough to break $SO(10)$ down to the SM. Therefore further Higgs representations are necessary. In case of non-SUSY models a minimal choice would be to add one 45_H [199] and in case of SUSY models one 210_H [200, 201]. Furthermore, in SUSY models one needs additionally a 126_H which keeps SUSY

Higgs content	SUSY	non-SUSY	free parameters
one of 10_H, 120_H, or $\overline{126}_H$	no mixing		–
$10_H + 120_H$	no type I seesaw		–
$10_H + \overline{126}_H$	MS	M1	19
$10_H + \overline{126}_H$ + texture	–	MT	15
$120_H + \overline{126}_H$	–	M2	19
$10_H + 120_H + \overline{126}_H$	FS	F1	18

Table 5.1: Brief overview of models we considered, names given to them in the text and the number of free parameters in the models. Models with only one Higgs representation cannot produce mixing and models without $\overline{126}_H$ do not have type I seesaw.

from being broken by D terms [201]. We will not analyze the details of different viable breaking chains. In principle one would have to use appropriate RGEs between the scales of intermediate symmetries and the $SO(10)$ breaking scale $M_{\rm GUT}$. Instead we assume that intermediate symmetries are close to $M_{\rm GUT}$ and the running of parameters between these scales and $M_{\rm GUT}$ is not affected sizably. Hence, the relevant information for our analysis is the Higgs content given in tbl. 5.1 and eqns. (4.3) or (5.1) together with the beta-functions of the SM or MSSM as given in the appendix.

Gauge coupling unification crucially depends on the breaking chain and the values of intermediate scales. E.g., in the minimal non-SUSY model based on $10_H + \overline{126}_H$, it has been shown [199,202] that with Higgs VEVs of 45_H and $\overline{126}_H$ of $\sim 10^{11}$ GeV gauge coupling unification can be achieved. In contrast, for the SUSY version of the minimal model it has been shown [203] that reproducing known values of neutrino mass squared differences requires intermediate scales, which in case of supersymmetric theories is excluded by gauge coupling unification constraints. Nevertheless we will also do a fit of the minimal SUSY $SO(10)$ GUT to have the possibility to compare the results of the program we developed with results obtained by other authors.

Since we do not analyze the details of $SO(10)$ breaking we will not check the unification of gauge couplings but will set the values of SM gauge couplings at $M_{\rm GUT}$ to such values that they coincide with the experimental values at M_Z after renormalization group evolution.

5.1 Minimal Model with $10_H + \overline{126}_H$ (M1, MS)

In this model we do not have a 120_H, hence $Y_{120} = 0$ in eqn. (4.3). To count the number of free parameters we use a basis in which H is real and diagonal, which leaves us with 19 real parameters: 3 in H, 12 in F (complex symmetric), and 4 in r (real), s (complex), and r_R (real) (assuming type I seesaw dominance).

There is a plethora of literature about the supersymmetric version of this model [168,203–

220], which is often referred to as the "Minimal Supersymmetric Grand Unified Theory" (MSGUT). A limited amount of literature analyzing the non-supersymmetric version also exists [166, 168, 198, 199, 202, 221]. All authors analyzing the fermion spectrum neglect details of the RGE which affect the running of observables between M_Z and $M_{\rm GUT}$, as described in chapter 4.

5.2 Alternative Minimal (non-SUSY) Model with $120_H + \overline{126}_H$ (M2)

Due to absence of 10_H we have $H = 0$ in this model. Going to a basis with real diagonal F (3 parameters), we have 6 real parameters in G and 10 in r, s, t_u, t_l, t_D, r_R, altogether 19 parameters (neglecting type II seesaw).

This model is analytically analyzed in ref. [166] in the case of only two fermion generations (second and third) and argued to be viable and predictive. A numerical three generation analysis finds the model to be unable to fit fermion masses and mixings [168]. To provide further evidence for this result we perform a fit of this model. In addition to the normal neutrino mass hierarchy considered in ref. [168] we also try to fit the inverted hierarchy. Further, we include full RGE into our analysis, which has not been done in the previous study.

5.3 Model with "full" Higgs Content $10_H + \overline{126}_H + 120_H$ (F1, FS)

Without additional constraints, we would have the maximal number of parameters in this model. One can considerably reduce the number of parameters by assuming all parameters to be real. This can be motivated or derived from an underlying parity symmetry [222] or spontaneous CP violation [223]. If CP is violated spontaneously solely by purely imaginary VEVs of the 120_H this corresponds to taking all parameters in eqn. (5.1) to be real. We will use the model with this reduced number of parameters and refer to it as "F1" in the non-supersymmetric case and as "FS" in the supersymmetric case. In a basis with real diagonal H (3 parameters) we count 6 parameters in F, 3 in G, and 6 in r, s, t_u, t_l, t_D, r_R, altogether 18 parameters. So in spite of introducing 120_H in addition to 10_H and $\overline{126}_H$, through the additional constraints this model has one parameter less than the "minimal" one. Therefore some authors refer to the SUSY version of this model as the "New Minimal Supersymmetric GUT" (NMSGUT) [224].

As in the minimal model there is a large amount of literature coping with the ability of the SUSY version of this model to reproduce the fermion spectrum and mixing [168, 191, 195, 212, 217, 222–232]. Without invoking supersymmetry, this model is analyzed only in ref. [168].

5.4 Models with Imposed Textures

As outlined in the introduction, one can reduce the number of free parameters within a model by making additional assumptions on the form of the $SO(10)$ Yukawa coupling matrices. We want to briefly demonstrate here the effect of applying texture zeros. To be definite, let us consider a texture with zeros in the (1,1) and (1,3) elements and apply this texture to H and F in eqn. (5.1), i.e.,

$$H, F \sim \begin{pmatrix} 0 & \cdot & 0 \\ \cdot & \cdot & \cdot \\ 0 & \cdot & \cdot \end{pmatrix} \tag{5.2}$$

Since H and F are symmetric, the zero in the (1,3) element implies a zero in the (3,1) element as well. This texture imposes four real constraints on each of the matrices H and F. In case of model M1 from sec. 5.1, where the elements of H and F are complex, the (1,1) element and the (1,3) element each have two real parameters. Since we can choose a basis where, e.g., H, is diagonal, only the constraints imposed on F reduce the number of parameters. Hence, imposing the texture in eqn. (5.2) on model M1 reduces the number of parameters of the model from 19 to 15.

Chapter 6

Details of the Fitting Procedure

We fit the models to experimental values of the masses of quarks and charged leptons, mass-squared differences of neutrinos, and mixing angles of quarks (including δ_{CKM}) and leptons, as well as the baryon asymmetry of the universe Y_B (see sec. 6.4). The quark and charged lepton masses are taken at M_Z from ref. [193]. Since the masses of charged leptons are measured with a very high accuracy which goes beyond our 1-loop RGE analysis and since furthermore such precise values make a numerical fit very challenging we assume an uncertainty of 5 % for these observables when fitting the models to the data. Only in case of the minimal non-SUSY model without RG evolution where we can do the fit in the charged lepton basis we take the best-fit values of the charged leptons as direct input for the fit. For the neutrino observables we neglect the running below M_Z and take the values from ref. [44][1].

To check our numerical algorithm we also make fits without RGE as in ref. [168]. Therefore we take their experimental values of observables at $\mu = M_{\mathrm{GUT}}$, but update the neutrino observables to which the models are fitted. We also include the leptonic mixing angle θ_{13}^l in our analysis, for which only an upper bound existed when the results of ref. [168] were published. Note that we symmetrized the error bars whenever they were not symmetric around the best-fit value to simplify the fitting procedure. This will not have a large effect on the fits, since strongly non-symmetric errors are present only for the light quark masses where the uncertainty is large anyway. Finally, we try separate fits for both a normal hierarchy (NH) and an inverted hierarchy (IH) of the neutrino masses (see sec. 6.1). We collect the values of observables underlying our analysis in tbls. 6.1, 6.2 and 6.3. To fit the model parameters to the observables we minimize

$$\chi^2 = \sum_{i=1}^{n} \left(\frac{y_i^{theo}(x) - y_i^{exp}}{\sigma_i^{exp}} \right)^2 \tag{6.1}$$

numerically with respect to $x = (x_1, ..., x_m)$, where y_i^{exp} are observables measured experimentally with uncertainty σ_i^{exp}, and $y_i^{theo}(x)$ is the corresponding theoretical prediction given the vector x of model parameters. We will later also look at χ^2 as a function of the

[1] See also refs. [45] and [46].

Observable	Exp. value	Observable	Exp. value
m_d [GeV]	0.0029 ± 0.001215	$\Delta m^2_{\odot}$ [GeV^2]	$(7.5 \pm 0.185) \times 10^{-23}$
m_s [GeV]	0.055 ± 0.0155	Δm^2_{31} (NH) [GeV^2]	$(2.47 \pm 0.0685) \times 10^{-21}$
m_b [GeV]	2.89 ± 0.09	Δm^2_{31} (IH) [GeV^2]	$(-2.355 \pm 0.0540) \times 10^{-21}$
m_u [GeV]	0.00127 ± 0.00046	$\sin^2\theta^l_{12}$	0.30 ± 0.013
m_c [GeV]	0.619 ± 0.084	$\sin^2\theta^{l,(\text{NH \& IH1})}_{23}$	0.41 ± 0.031
m_t [GeV]	171.7 ± 3.0	$\sin^2\theta^{l,(\text{IH2})}_{23}$	0.59 ± 0.022
$\sin\theta^q_{12}$	0.2246 ± 0.0011	$\sin^2\theta^l_{13}$	0.023 ± 0.0023
$\sin\theta^q_{23}$	0.042 ± 0.0013	m_e [MeV]	0.48657 ± 0.02433
$\sin\theta^q_{13}$	0.0035 ± 0.0003	m_μ [GeV]	0.10272 ± 0.00514
δ_{CKM}	1.2153 ± 0.0576	m_τ [GeV]	1.74624 ± 0.08731
λ	0.521 ± 0.01	Y_B	$8.75 \times 10^{-11} \pm 2.3 \times 10^{-12}$

Table 6.1: Experimental values of observables at $\mu = M_Z$ used for our fits. The quark and charged lepton masses are taken from ref. [193], quark mixing parameters from ref. [168], neutrino mixing parameters from ref. [44] (table 1, second column), the baryon asymmetry from ref. [233]. A 5 % uncertainty is assumed fot the charged leptons, as explained in the text. The value of the Higgs quartic coupling λ is derived from the measurements of ATLAS [21] and CMS [22] as explained in sec. 6.2. Note that in our convention the Higgs self-interaction term in the Lagrangian is $-\frac{\lambda}{4}(\phi^\dagger\phi)^2$.

leptonic Dirac-like CP violating phase, δ^l_{CP}, or the atmospheric mixing angle, $\sin^2\theta_{23}$. To derive such a function, one can add a term $(O^{theo}(x) - O^*)^2/(0.01O^*)^2$ to the definition of χ^2, where O^* is the desired value of the observable O, e.g., δ^l_{CP}, and the denominator is a very small artificial uncertainty to let the minimization algorithm converge to a minimum with the desired value of O. If O itself was part of the definition of χ^2 in eqn. (6.1), than its term with the experimental uncertainty is removed from there. After performing the minimization of the so defined $\chi^2(O)$ function, one evaluates with the parameters obtained from that fit, χ^2 as given in eqn. (6.1), i.e. without the contribution of the artificial error, but including the contribution of the real experimental uncertainty. This method was previously used in refs. [168, 203, 223].

For the minimization we use the downhill simplex algorithm [234, 235]. We use its implementation from the GNU Scientific Library [236], which also provides useful functions for numerical matrix diagonalization and for solving differential equations numerically.

Let us stress a general caveat of numerical minimization. The problem at hand is nonlinear and multidimensional – therefore many local minima exist. With numerical algorithms it is impossible to determine whether a minimum is a global minimum of the function under consideration. A standard procedure to increase the confidence that a global minimum out of the many local ones has been found is to start the minimization many times with different initial parameters and to choose the lowest out of the many local minima that will be found. Furthermore one can perturb a minimum and restart the minimization

Obs.	Value [GeV]	Obs.	Value [GeV]	Obs.	Value [GeV]
m_d	0.00114 ± 0.000495	m_u	0.00048 ± 0.000185	$m_e \times 10^3$	0.46965 ± 0.02348
m_s	0.022 ± 0.0065	m_c	0.235 ± 0.0345	m_μ	0.09915 ± 0.00496
m_b	1.0 ± 0.04	m_t	74.0 ± 3.85	m_τ	1.68558 ± 0.08428

Table 6.2: Experimental values of observables at $\mu = M_{\text{GUT}}$ [168] used for non-SUSY fits without RGE. For mixing parameters as well as neutrino mass squared differences the same values as in tbl. 6.1 are used.

from the perturbed point [235, 236]. These steps can be repeated many times until no improvement of the minimum is found any more. Still, this gives no guarantee that the absolute minimum has been found and lower minima might exist in the parameter space. This is a generic property of numerical minimization.

6.1 Normal vs. Inverted Neutrino Mass Hierarchy

In the neutrino sector the absolute mass scale is experimentally not yet determined. At present, only the solar mass-squared difference Δm^2_{21} and the absolute value of the atmospheric mass-squared difference $|\Delta m^2_{31}|$ are known [44],

$$\begin{aligned}
\Delta m^2_{21} &= 7.5 \pm 0.185 \times 10^{-5}\ \text{eV}^2 \\
\Delta m^2_{31} &= 2.47 \pm 0.0685 \times 10^{-3}\ \text{eV}^2\ \text{(NH)} \\
\Delta m^2_{31} &= -2.355 \pm 0.0540 \times 10^{-3}\ \text{eV}^2\ \text{(IH)}\,,
\end{aligned}$$

where NH (normal hierarchy) and IH (inverted hierarchy) refer to two currently viable situations with $m_1 < m_2 \ll m_3$ and $m_3 \ll m_2 < m_1$, respectively. Note that for the IH case we derived Δm^2_{31} from the values of Δm^2_{32} and Δm^2_{21} given in ref. [44]. We do this conversion because our program always calculates Δm^2_{31}, no matter which hierarchy is fitted. Further we symmetrized the uncertainties, as explained before.

Besides the different signs and values of Δm^2_{31}, also the neutrino mixing parameters have different preferred values depending on which mass hierarchy is assumed [44–46]. This hierarchy dependence is mostly pronounced for $\sin^2\theta_{23}$. Here, the best-fit value of $\sin^2\theta_{23}$ depends on further aspects of the analysis, including the experiments that were considered. Comparing refs. [44–46] we notice that there currently exist two different equally valid best-fit values and corresponding $1\,\sigma$ regions for $\sin^2\theta_{23}$. We take the values to which the models will be fitted from ref. [44] and distinguish the following cases in our analysis:

$$\begin{aligned}
\sin^2\theta_{23} &= 0.41 \pm 0.031 \quad \text{NH} \\
\sin^2\theta_{23} &= 0.41 \pm 0.031 \quad \text{IH1} \\
\sin^2\theta_{23} &= 0.59 \pm 0.022 \quad \text{IH2}\,.
\end{aligned} \tag{6.2}$$

Observable	$\tan\beta = 50$	$\tan\beta = 38$	$\tan\beta = 10$
m_u/m_c	0.0027 ± 0.0006	0.0027 ± 0.0006	0.0027 ± 0.0006
m_d/m_s	0.051 ± 0.007	0.051 ± 0.007	0.051 ± 0.007
m_c/m_t	0.0023 ± 0.0002	0.0024 ± 0.0002	0.0025 ± 0.0002
m_s/m_b	0.016 ± 0.002	0.017 ± 0.002	0.019 ± 0.002
m_e/m_μ	0.0048 ± 0.0002	0.0048 ± 0.0002	0.0048 ± 0.0002
m_μ/m_τ	0.05 ± 0.002	0.054 ± 0.002	0.059 ± 0.002
m_b/m_τ	0.73 ± 0.04	0.73 ± 0.04	0.73 ± 0.03
$\sin\theta^q_{12}$	0.227 ± 0.001	0.227 ± 0.001	0.227 ± 0.001
$\sin\theta^q_{23}$	0.0371 ± 0.0013	0.0386 ± 0.0014	0.04 ± 0.0014
$\sin\theta^q_{13}$	0.0033 ± 0.0007	0.0035 ± 0.0007	0.0036 ± 0.0007
$\delta_{\rm CKM}$	0.9828 ± 0.1784	0.9828 ± 0.1784	0.9828 ± 0.1787
$\Delta m^2_\odot/\Delta m^2_{\rm A}$	0.03036 ± 0.0011	0.03036 ± 0.0011	0.03036 ± 0.0011
m_t	94.7 ± 9.4	94.7 ± 9.4	92.2 ± 8.7

Table 6.3: Experimental values of observables at $\mu = M_{\rm GUT}$ [168] used for SUSY fits without RGE. The ratio of solar to atmospheric neutrino mass-squared difference is calculated from their values at $\mu = M_Z$ as given in tbl. 6.1. The top quark mass m_t at $\mu = M_{\rm GUT}$ is taken from ref. [193]. For the neutrino mixing angles as well as Δm^2_{31} the values at $\mu = M_Z$ as given in tbl. 6.1 are used.

The quality of fits with the inverted neutrino mass hierarchy had the same quality for both IH1 and IH2. Hence, we will stick in our discussion of results in chapter 8 to the case IH2.

6.2 Higgs Mass and Quartic Coupling

Although the Higgs boson mass $m_{\rm H}$ does not enter the $SO(10)$ relations in eqn. (4.3) there is interplay between $m_{\rm H}$ and the fermion observables during renormalization group evolution. In RGE in the non-supersymmetric case the Higgs quartic coupling λ appears which in the SM is related to $m_{\rm H}$ by[2]

$$\lambda = \frac{2}{v^2}\, m_{\rm H}^2 \,. \tag{6.3}$$

Recently, ATLAS and CMS experiments at the Large Hadron Collider (LHC) have observed a new particle which is in good agreement with a Standard Model Higgs boson with the mass [21, 22]

$$\begin{aligned} m_{\rm H} &= 126.0 \pm 0.4\ (\text{stat}) \pm 0.4\ (\text{sys})\ \text{GeV} \qquad (\text{ATLAS}) \\ m_{\rm H} &= 125.3 \pm 0.4\ (\text{stat}) \pm 0.5\ (\text{sys})\ \text{GeV} \qquad (\text{CMS})\ . \end{aligned} \tag{6.4}$$

[2]In our convention the Higgs self-interaction term in the Lagrangian is $-\frac{\lambda}{4}(\phi^\dagger\phi)^2$

For our analysis we take a conservative estimate of the true Higgs mass, since there is no official combined analysis available presently. Our 1 σ interval shall overlap exactly the 1 σ intervals of the ATLAS and CMS experiments and we take the central value of this range as best-fit point, i.e. we take for our fits

$$m_{\mathrm{H}} = 125.6 \pm 1.2 \text{ GeV} . \tag{6.5}$$

The standard error propagation formula applied to eqn. (6.3) then yields

$$\lambda = 0.521 \pm 0.010 . \tag{6.6}$$

Note that for fits at M_{GUT}, i.e. without RG evolution, we do not take into account the Higgs mass, since in that case there is no restriction on λ from the other observables.

Supersymmetric Case

Above the supersymmetry breaking scale M_{SUSY} supersymmetry fixes λ to be[3] [237]

$$\lambda(\mu \geq M_{\mathrm{SUSY}}) = \frac{1}{4}\left(\frac{3}{5}\, g_1^2 + g_2^2\right)(\mu) . \tag{6.7}$$

Below M_{SUSY} the Higgs mass gets radiative corrections, the leading one given in a rough approximation (within the MSSM) by [237]

$$m_{\mathrm{H}}^2 = M_Z^2 + \frac{3\, g_2^2\, m_t^4(\mu_t)}{8\pi^2 M_W^2} \ln\left(\frac{M_{\mathrm{SUSY}}^2}{m_t^2(\mu_t)}\right) , \tag{6.8}$$

with $\mu_t = \sqrt{m_t\, M_{\mathrm{SUSY}}}$ and all SUSY particles are assumed to have masses around M_{SUSY} in this approximation. By varying M_{SUSY} one can reproduce the measured value of m_{H} as given in eqns. (6.4) and (6.5). Solving eqn. (6.8) for M_{SUSY} yields $M_{\mathrm{SUSY}} \approx 1$ TeV. Since our main goal is to fit fermion masses and mixings within the $SO(10)$ framework and not performing a detailed analysis of the MSSM, we do not specify M_{SUSY} or the specific SUSY spectrum. Hence, we will not try to fit m_{H} in the supersymmetric models. For implications of $m_{\mathrm{H}} \approx 125$ GeV and other LHC results for the MSSM we refer to existing literature [238–247].

6.3 Renormalization Group Evolution

The relations in eqn. (5.1) have to be obeyed at M_{GUT}. Therefore, for a given set of $SO(10)$ parameters in order to calculate the model predictions for the observables one has to use RGEs and evolve the parameters down to the energy scale at which the observables are known. In addition one has to integrate out heavy degrees of freedom during this process at their mass scale. In our case this applies to the right-handed neutrinos (ν_R), as their

[3] We apply GUT normalization to the $\mathrm{U}(1)_{\mathrm{Y}}$ charge.

masses usually lie somewhere between 10^{10} GeV and $M_{\rm GUT}$. After integrating out a degree of freedom one ends up with an effective field theory (EFT) and has to match coefficients of effective operators with parameters from the full theory. Since ν_R are not degenerate in general, one has to integrate out several times and thus has to use different EFTs during the evolution from $M_{\rm GUT}$ to M_Z. This formalism is nicely described in refs. [197, 248]. We use the 1-loop β-functions as presented in ref. [248] for the SM and MSSM, respectively (see also [249]). The beta-functions are also presented in appendix C for reference. We shall mention that we do not integrate out the top-quark below $\mu = m_t(m_t)$, since the energy scales m_t and M_Z are quite close. Furthermore we assume $M_{\rm SUSY} = M_Z$, i.e. we use the beta-functions of the MSSM for the evolution of parameters down to M_Z in case of SUSY models, since this is just a small effect as long as the SUSY breaking scale is not too far away from M_Z. We expect models being able to fit experimental data with $M_{\rm SUSY} = M_Z$ to be equally well suited to fit the data with $M_{\rm SUSY} = 500$ GeV or 1 TeV. Finally, since we do not specify the SUSY spectrum, we also do not consider SUSY threshold effects, which can have an impact for large $\tan\beta$ [168, 194, 250–255].

6.4 Baryon Asymmetry Y_B

The aim of this section is to discuss how we calculate the baryon asymmetry Y_B, including RG evolution effects. We assume the baryon asymmetry is produced through thermal leptogenesis. Therefore, we start with a presentation of (flavored) leptogenesis and all relevant formulae that will be needed later based on the presentation given in ref. [233]. We will explain our method to calculate Y_B at the end of this section.

During the evolution of the universe the right-handed neutrinos can decay out of equilibrium and given presence of CP violation produce a lepton asymmetry which is then transferred to a baryon asymmetry through sphaleron processes [256, 257]. For hierarchical masses only the decay of the lightest right-handed neutrino contributes to the asymmetry.

The baryon asymmetry is defined by [233]

$$Y_B = \frac{n_B - n_{\bar{B}}}{s}\,, \tag{6.9}$$

where n_B, $n_{\bar{B}}$, and s are the number densities of baryons, antibaryons, and entropy density, respectively. Experimentally, the baryon asymmetry can be inferred from Big Bang Nucleosynthesis (BBN) [258], Cosmic Microwave Background (CMB) anisotropies [259], and from the Sloan Digital Sky Survey [260]. One finds [233]

$$Y_B = (8.75 \pm 0.23) \times 10^{-11}\,. \tag{6.10}$$

Assuming the reheating temperature $T_{\rm R}$ is smaller than the temperature of electroweak

phase transition $T_{\rm EWPT}$[4], the theoretical prediction gives [233]

$$\begin{aligned} Y_B &= \frac{12}{37}\sum_\alpha Y_\alpha \quad \text{(SM)}\,, \\ Y_B &= \frac{10}{31}\sum_\alpha Y_\alpha \quad \text{(MSSM)}\,, \end{aligned} \tag{6.11}$$

where the prefactors in eqn. (6.11) account for how much of the lepton asymmetry is transferred to a baryon asymmetry through sphaleron processes. The $B/3-L_\alpha$ asymmetries read

$$Y_\alpha = 4\times 10^{-3}\,\epsilon_{\alpha\alpha}\,\eta_\alpha\,, \tag{6.12}$$

with CP asymmetry[5]

$$\begin{aligned} \epsilon_{\alpha\alpha} = &\frac{1}{8\pi\,(Y_\nu Y_\nu^\dagger)_{11}}\sum_j \text{Im}\left\{(Y_\nu Y_\nu^\dagger)_{j1}(Y_\nu)_{j\alpha}(Y_\nu^*)_{1\alpha}\right\} g\,(x_j) \\ &+\ \frac{1}{8\pi\,(Y_\nu Y_\nu^\dagger)_{11}}\sum_j \text{Im}\left\{(Y_\nu Y_\nu^\dagger)_{1j}(Y_\nu)_{j\alpha}(Y_\nu^*)_{1\alpha}\right\}\frac{1}{1-x_j}\,, \end{aligned} \tag{6.13}$$

where

$$x_j \equiv M_j^2/M_1^2\,,$$

M_i the masses of right-handed neutrinos, and, within the SM [261],

$$g(x) = \sqrt{x}\left[\frac{1}{1-x}+1-(1+x)\ln\left(\frac{1+x}{x}\right)\right] \overset{x\gg 1}{\longrightarrow} -\frac{3}{2\sqrt{x}}-\frac{5}{6x^{3/2}}+\ldots\,. \tag{6.14}$$

Note that the second term in eqn. (6.13) is suppressed by a factor $1/\sqrt{x}$ compared to the first factor.

In the MSSM, in addition to decaying to lepton + Higgs, the right-handed neutrinos can also decay to a slepton + Higgsino. To leading order in $1/x$ the sum of the asymmetries to leptons and to sleptons is twice as large as the SM asymmetry [261]:

$$g(x) = -\sqrt{x}\left(\frac{2}{x-1}+\ln\left[1+1/x\right]\right) \overset{x\gg 1}{\longrightarrow} -\frac{3}{\sqrt{x}}-\frac{3}{2x^{3/2}}+\ldots\ . \tag{6.15}$$

In the limit $M_{2,3}\ll M_1$ eqn. (6.13) can also be expressed in terms of the light neutrino mass matrix m_ν [233]:

$$\epsilon_{\alpha\alpha} = -\frac{3M_1}{8\pi v_u^2 (Y_\nu Y_\nu^\dagger)_{11}}\,\text{Im}\left\{(Y_\nu)_{1\alpha}(m_\nu^* Y_\nu^T)_{\alpha 1}\right\}\,. \tag{6.16}$$

[4]In case $T_{\rm R} > T_{\rm EWPT}$, the prefactors in eqn. (6.11) change to $\frac{28}{79}$ (SM) and $\frac{8}{23}$ (MSSM) [233], an effect smaller than 10%.

[5]The relation between our notation and ref. [233] is $Y_\nu = \lambda^{\rm T}$.

This is a convenient expression when treating RGE and non-degenerate right-handed neutrinos correctly. Since $\epsilon_{\alpha\alpha}$ has to be calculated at energies $\mu = M_1$, when both heavier neutrinos have already been integrated out, s.t. their effect is accounted for only through an effective dimension 5 operator leading to the masses of light neutrinos, m_ν. Hence, at $\mu = M_1$ eqn. (6.13) cannot be applied. On the other hand, if $M_1 \lesssim 10 M_2$, eqn. (6.16) is not accurate anymore, since then contributions from the second term in eqn. (6.13) are not generally negligible. In such a case one can evolve to $\mu = M_1$ without integrating out $N_{3,2}$ and apply eqn. (6.13) to calculate the CP asymmetry.

Finally, the washout factor η_α is given by [233]

$$\begin{aligned} \eta_\alpha &= \left[\left(\frac{|A_{\alpha\alpha}|\, \tilde{m}_{\alpha\alpha}}{2.1\, m_*} \right)^{-1} + \left(\frac{m_*}{2\, |A_{\alpha\alpha}|\, \tilde{m}_{\alpha\alpha}} \right)^{-1.16} \right]^{-1} && (\tilde{m} > m_*)\,, \\ \eta_\alpha &= \frac{|A_{\alpha\alpha}|\, \tilde{m}_{\alpha\alpha}}{2.5\, m_*} \frac{\tilde{m}}{m_*} && (\tilde{m} < m_*)\,, \end{aligned} \tag{6.17}$$

with [233, 262][6]

$$\tilde{m} \equiv \sum_\alpha \tilde{m}_{\alpha\alpha} \equiv \sum_\alpha \frac{v_u^2\, (Y_\nu)_{1\alpha}\, (Y_\nu^\dagger)_{\alpha 1}}{2\, M_1} = \frac{v_u^2}{2\, M_1}\, (Y_\nu Y_\nu^\dagger)_{11}\,, \tag{6.18}$$

$$m_* \equiv \frac{8\, \pi^{5/2} \sqrt{g_*}}{3\, \sqrt{5}} \frac{v_u^2}{M_{\rm Pl}} \simeq 1.07 \times 10^{-3}\ {\rm eV}\,, \tag{6.19}$$

and the matrix A given by [233]

$$A = \begin{pmatrix} -151/179 & 20/179 & 20/179 \\ 25/358 & -344/537 & 14/537 \\ 25/358 & 14/537 & -344/537 \end{pmatrix}. \tag{6.20}$$

With the formulae given above we can now calculate the baryon asymmetry Y_B, but first one needs to evolve the GUT scale parameters of the model under consideration to the energy scale M_1 where leptogenesis takes place. During RG evolution, ν_{R_3} and ν_{R_2} are integrated out. Hence, one can only apply eqn. (6.16). On the other hand, if $M_1 \simeq M_2$, eqn. (6.16) is very unprecise, since it neglects the second term in eqn. (6.13), which is not suppressed in this case. To circumvent this issue and still keep the fitting procedure simple, when calculating Y_B we evolve the parameters to M_1 without integrating out right-handed neutrinos and always apply eqn. (6.13). We made a numerical check in the hierarchical case $M_1 \ll M_2 \ll M_3$ and the deviation of the two methods described above turns out to be only 1 %.

[6] In our notation $v = 246$ GeV which amounts to a factor of $\frac{1}{2}$ in eqns. (6.18) and (6.19) for $\tilde{m}$ and m_* in comparison to a notation with $v = \frac{246}{\sqrt{2}}$ GeV $= 174$ GeV. Since the washout factor η_α, eqn. (6.17), depends only on the ratio of $\tilde{m}$ and m_*, its definition is not affected by this convention.

Chapter 7

Numerical Methods

In this section we give some details about the methods employed to find the best-fit parameters. For this purpose we want to first describe the methods and issues in an abstract way and then describe with a more explicit example our implementation.

The program to minimize χ^2 in eqn. (6.1) is written in C++. Within the program GNU Scientific Library (GSL) [236] is used for numerical minimization, matrix diagonalization, numerical solution of differential equations (RGEs), and random number generation. With this functionality GSL provides the basic building blocks needed to a) calculate χ^2 as a function of model parameters $x = (x_1, ..., x_m)$ and b) minimize χ^2 with respect to x. Furthermore, we use the Message Passing Interface (MPI) [263][1] to parallelize computations. The computations are performed on the computer cluster of the Max-Planck-Institut für Kernphysik, Heidelberg, where up to 1700 CPU cores can be used.

Since GSL does not contain an algorithm to diagonalize complex symmetric matrices rather than complex hermitian or real symmetric matrices, we decompose complex symmetric $n \times n$ matrices into real symmetric $2n \times 2n$ matrices as described in [264] and use the GSL function for diagonalization of real symmetric matrices to calculate eigenvalues and eigenvectors of complex symmetric matrices.

As already mentioned in the introduction to chapter 6 our χ^2 function is highly non-linear and thus possesses many local minima. Since there is no way to numerically ascertain that one has found a global minimum, we apply a standard procedure to at least get a high degree of belief that a local minimum that has been found numerically is also the global minimum. Therefore we start the minimization algorithm many times with different (random) initial parameters and choose the lowest out of the many local minima that will be found. Furthermore we perturb a minimum and restart the minimization from the perturbed point [235, 236]. These steps are repeated until no improvement of the minimum is found any more. Still, this gives no guarantee that the absolute minimum has been found and lower minima might exist in the parameter space.

Our implementation of the described procedure for finding the global minimum is such that the program supports different modes. In the "threshold mode" the minimization

[1] A brief introduction to the most relevant MPI functions is "A User's Guide To MPI" by Peter S. Pacheco, available online at ftp://math.usfca.edu/pub/MPI/mpi.guide.ps.

starts from randomly chosen initial parameters. Thereby only such initial parameters are considered as valid ones, which yield a χ^2 value below some specified threshold. In the "pert mode" a previously found local minimum is randomly perturbed (the size of perturbations can be specified) and the resulting parameter vector is taken as the starting point for the next minimization. In this mode it is often useful to take initial parameters from a previous fit with a slightly different setup, if one does not have already parameters corresponding to a good local minimum. E.g., fits including renormalization group evolution can be performed taking the best-fit parameters of the same model without RGE as initial parameters (with maybe random perturbations applied, if one wants to make several fits simultaneously). Those parameters should already be much closer to the minimum than randomly chosen parameters. This speeds up the minimization since RGE slows down the evaluation of χ^2 and hence the whole minimization by a factor of $\sim 10^3$. Therefore looking for the "first local minimum" in the "threshold mode" would be an additional lengthy exercise which can be avoided.

Another mode automatically restarts a fit after a minimum has been found and repeats the fit in "pert mode" several times with perturbations of different magnitude applied to the best parameter vector found so far. This decreases the required manual interaction.

7.1 Choosing the Seed of a Random Number Generator

The initial parameters are generated with the help of a random number generator (RNG) provided by GSL. A random number generator needs an initial input number called seed from which it produces a series of quasi-random numbers [265]. Certainly, if the seed is not random then the produced series will not be random in the sense that two series of quasi-random numbers produced by a RNG initialized with the same seed will be equal to each other.

For many purposes the current timestamp of the system (on UNIX systems the number of seconds passed since Jan 1st, 1970 0:00 UTC) serves as a suitable seed. In our case usually several hundreds of fits are started in a "set" simultaneously. Taking the system timestamp as seed of a RNG would result in all fits which are started at the same second to have the same seed and hence the same series of random numbers and finally the same initial parameters. One way out is to add the job ID of each fit to the timestamp, since the job ID is unique within a set of jobs. On the other hand, sometimes it is necessary to start several sets of jobs simultaneously (due to limitations of the computer cluster). Then, for each job within one set there is another job within all other sets with the same ID, which reintroduces the problem of equal seeds. Even if two sets of jobs are not started within the same second, hence having different timestamps, there still will be some fraction of jobs with overlapping seeds, as long as the time difference between the start of two sets in seconds is not at least as large as the number of jobs within the set with the larger amount of jobs. E.g., let job 2 of set 1 have some seed $s_1 = t + 2$, with t the timestamp, whereas

```
uint32_t hash32shift(uint32_t key){
    key = ~key + (key << 15); // key = (key << 15) - key - 1
    key = key ^ (key >> 12);
    key = key + (key << 2);
    key = key ^ (key >> 4);
    key = key * 2057;         // key = (key + (key << 3)) + (key << 11)
    key = key ^ (key >> 16);
    return key;
}
```

Listing 7.1: Hash function used in random seed generation [266].

job 1 of set 2, started one second later, will have the seed $s_2 = (t + 1) + 1 = t + 2 = s_1$. This illustrates that we shall try to find a method to generate a random seed[2].

In ref. [267] some methods are suggested how to choose a random seed, all of which can be summarized under the title "genuine source of randomness", like radioactive sources, user interactions, or behaviour of changing information on the system like number of virtual memory pages, network status, or timing of hard disk drives. For practical reasons we choose to derive a seed from measuring time differences. It is possible to let the program "sleep" for some milliseconds by invoking a system function (e.g., usleep() on UNIX systems). What helps us here is that the exact timelag between invoking usleep() and continuation of the program is to some extent random, since it depends on what exactly is going on on the system at the time when usleep() is invoked. The randomness is further increased, if one measures the time lag in μs rather than ms. At this point, if two processes measure a time lag with the same argument given to usleep(), their results are likely to be different.

Fits that are started together in a set can communicate using MPI functions. Therefore it is enough for one process in each set to perform the time measurement which is then communicated to the other processes. Every process then adds its unique ID to the time measurement to produce a number unique within the set.

Still, one should further reduce the probabililty of two or several processes getting the same seed, since even if two processes within two different sets measure different time delays, having many processes in each set which add their respective IDs to those time delays can still result in overlapping seeds as explained in the previous paragraph.

Now one could simply repeat this procedure and add up the results. The problem is that two processes having different measurements of the time lag in each single iteration may still have the same sum of time delays ("$5 + 9 = 6 + 8$"). The probability distribution of the sum of many independent identically distributed random variables converges to a Gaussian distribution due to the central limit theorem[3]. The standard deviation of the

[2]Even if one can randomly choose a seed one still needs a RNG since methods to generate random seeds are orders of magnitude more expensive (in terms of computation time) than generating quasi-random numbers from a seed.

[3]See standard textbooks on statistics.

```
unsigned long int calcNewSeed(){
    unsigned long int seed = 0;

    if(myid == 0){
        seed = hash32shift(time(NULL));
        for(int i=0; i<5; i++){
            uint32_t usechash = hash32shift(getUSec());
            seed = hash32shift(seed + usechash);
            usleep(3000); // sleep 3 ms ( 3000 us )
        }
    }

    MPI_Bcast(&seed, 1, MPI_UNSIGNED_LONG, 0, MPI_COMM_WORLD);

    seed = hash32shift(seed + myid);

    return seed;
}
```

Listing 7.2: Seed calculation using time delay measurements and hash function from listing 7.1.

resulting Gaussian distribution scales as the square root of the number of random variables that are summed. Therefore, to avoid a high probability of equal seeds after summation one would need to make many independent time measurements.

Although not a problem as long as one does not need to calculate many seeds, a solution to this issue is provided through the use of hash functions [268]. A hash function maps one number from a set to a number (the "hash") of another set (usually a set of integers). An important requirement to a hash function is that even very similar input numbers (say, 5 and 7) should nevertheless be hashed to very different hashes [266] (e.g., $5 \rightarrow 1679$, $7 \rightarrow 976634$). We exploit this property by hashing each time measurement with a 32 bit hash function provided as 'hash32shift()' in ref. [266] and reprinted in listing 7.1 for reference. Then each 'root-process' can make a second time measurement and hash its result again. Afterwards the two hashes are added. Two sums of hashes calculated by two different processes performing the steps described above will only be equal, if both processes get the same results from every single time measurement performed. With the help of formulae one can express it like that: Even if

$$\Delta t_1 + \Delta t_2 = \Delta t_3 + \Delta t_4 \tag{7.1}$$

we still have

$$h(\Delta t_1) + h(\Delta t_2) \neq h(\Delta t_3) + h(\Delta t_4)\,, \tag{7.2}$$

with a very high probability[4] as long as $\Delta t_1 \neq \Delta t_{3,4}$, with h being the hash function.

[4]The probability of two different numbers having the same hash is $2^{-32} \simeq 2.3 \times 10^{-10}$ if the hash function maps to a 32 bit integer.

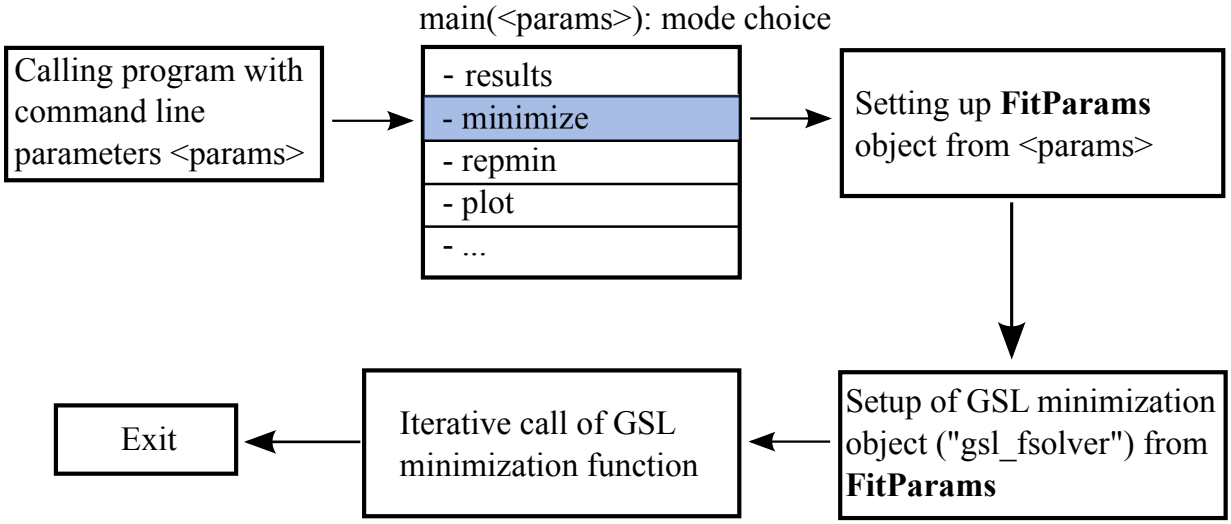

Figure 7.1: Flow chart of our minimization program. A detailed description of each step is given in the text.

Now we can efficiently reduce the probability of two equal seeds by simply adding not only the hashes of two time delay measurements, but some more. After performing n such sums the probability of two equal seeds reduces roughly as p^n (for not too large n), with p being the probability for two processes to measure the same time delay. In our implementation (see listing 7.2) we use 5 iterations, which is certainly enough for our purposes. Furthermore, for $p \sim 0.01$, $p^n \sim 10^{-10}$, which already saturates our 32 bit hash function (see footnote 4).

7.2 Technical Details of the Minimization Program

We now continue to describe the subsequent steps our program performs to get to the solution of the minimization problem. The program flow is illustrated in fig. 7.1. The program is invoked with several command line parameters specifying the model to be fitted and details to be considered in the fit such as fitting an inverted or normal hierarchy for neutrinos, using RGE or not, fitting the baryon asymmetry or not, and in case of IH in the neutrino sector whether the small or the large value of $\sin^2\theta_{23}$ shall be used during the fit, since experimental data currently allows two solutions (see sec. 6.1). Command line parameters also specify details about how to choose initial parameters (e.g., randomly or from a file). From these parameters an object "FitParams" is created which is passed over to several functions initializing a GSL library object (GSL minimizer) in order to perform the minimization. The GSL minimizer contains, among other information, a pointer to the function which is to be minimized (i.e. our χ^2 function, eqn. (6.1)), a pointer to the vector of model parameters (see eqn. (5.1)), and a pointer to further (optional) parameters which are needed by the function that shall be minimized. In the next step a GSL function is

invoked iteratively which upon each iteration tries to find a vector of parameters for which the value of χ^2 is lower than the current one. The GSL minimization function thereby uses the information stored in the GSL minimizer object to calculate χ^2 for different parameter vectors. When the function converges to a (probably local) minimum, the program stores the corresponding parameters and value of χ^2 at that minimum and exits.

Chapter 8

Results

In this section we present and discuss the results of our analysis. We quantify the deviation of model predictions by stating the pulls of all the observables considered. The pull of a model with respect to an observable y_i is defined as

$$\text{pull}(y_i) = \frac{y_i^{theo}(x) - y_i^{exp}}{\sigma_i^{exp}} \,, \tag{8.1}$$

with the variables as defined in eqn. (6.1) on page 53. The pull measures the deviation of theoretical predictions (or best-fit values) from experimentally measured values in units of uncertainty of the observable. Its sign shows whether the theoretical prediction is too small or too large.

Different Sets of Observables

We will present the results of fits including RG evolution where the input values are taken at $\mu = M_Z$ as well as the results of fits made at the GUT scale. Our full set of observables to which the models are fitted are the masses of quarks and charged leptons, mass-squared differences of neutrinos, mixing angles of quarks and leptons, the CP phase δ_{CKM} in the CKM matrix, the baryon asymmetry Y_B and the Higgs quartic coupling λ. The full set of observables is used only in non-SUSY models with full RG analysis. λ is generally not fitted in SUSY models and in non-SUSY models without RG analysis (see sec. 6.2 for details). Fits including Y_B are made only together with full RG evolution. Hence the number of observables taken into account for the fits varies between 18 and 20. Numerical input values can be found in chapter 6. There we also pointed out that in case of the inverted neutrino mass hierarchy currently two numerically different best-fit solutions exist for the value of $\sin^2\theta_{23}$. Since good fits could be achieved for both possibilities, we restrict the discussion of our results to the case where $\sin^2\theta_{23}^{IH} > 0.5$. For the normal hierarchy, the experimental best-fit value is $\sin^2\theta_{23}^{IH} = 0.41 < 0.5$. We now proceed with the discussion of each model.

Model	$\tan\beta$	Comment	χ^2
M1	–	no RGE, no Y_B	1.103
	–	RGE, no Y_B	22.97
	–	RGE, Y_B	23.46
MT	–	no RGE, no Y_B	11.76
	–	RGE, no Y_B	49.55
MS	50	no RGE, no Y_B	9.411
	50	RGE, no Y_B	3.294
	50	RGE, Y_B	3.347
	38	no RGE, no Y_B	9.715
	38	RGE, no Y_B	3.016
	38	RGE, Y_B	3.150
	10	no RGE, no Y_B	10.45
	10	RGE, no Y_B	2.889
	10	RGE, Y_B	3.096

Table 8.1: Fit results for models M1, MT, and MS with normal neutrino mass hierarchy. We differentiate between fits to observables at the GUT scale ("no RGE") which also do not include the baryon asymmetry Y_B as an observable and fits to observables at M_Z ("RGE"). The latter further subdivide into fits with or without Y_B as an observable to which the models are fitted. For the fits of M1 and MT including RGE the Higgs quartic coupling has also been fitted, as described in sec. 6.2.

8.1 Minimal Model with $10_H + \overline{126}_H$

Before making our own analysis we checked the best-fit parameters for the non-SUSY version of this model (M1 in our convention) presented in ref. [168] for the fit at the GUT scale and in case of normal neutrino mass hierarchy. From the best-fit model parameters published in ref. [168] for model M1 we get $\delta_{\text{CKM}} = 1.928$ which is off a lot from the value stated in ref. [168] of $\delta_{\text{CKM}} = 69.5262\,^\circ = 1.213$ rad. We checked this value using the REAP package [248]. Our fit of model M1 gives $\chi^2 = 1.1$, with now $\delta_{\text{CKM}} = 1.219$, in very good agreement with experimental data. The somewhat better fit in ref. [168] with $\chi^2 \approx 0.7$ is due to new and more precise data in the neutrino sector which underlies our analysis and the inclusion of the leptonic mixing angle θ_{13}^l in our fits. The SUSY model MS with normal neutrino mass hierarchy has also been analyzed before (without RG evolution) [168, 203], albeit with older data underlying the analyses. The results lie in the range between $\chi^2 = 3.7$ and $\chi^2 = 5.1$ in case of type I seesaw dominance. Our fits yield $\chi^2 = 9.41$, 9.72, and 10.45 for $\tan\beta = 50$, 38, and 10, respectively. The results are summarized in tbl. 8.1 and the best-fit values of observables and corresponding pulls, to be discussed below, are compiled

	M1, no RGE		M1, no Y_B		M1, Y_B	
Observable	best-fit	pull	best-fit	pull	best-fit	pull
m_d	0.00067	-0.9458	0.00298	0.0621	0.00300	0.0831
m_s	0.02406	0.3172	0.06887	0.8951	0.06970	0.9485
m_b	1.00309	0.0772	2.89370	0.0411	2.90899	0.2110
m_u	0.00048	0.0072	0.00131	0.0977	0.00130	0.0722
m_c	0.24243	0.2153	0.70754	1.0541	0.70401	1.0120
m_t	73.69305	-0.0797	161.41161	-3.4295	161.45551	-3.4148
$\sin\theta^q_{12}$	0.22462	0.0227	0.22476	0.1433	0.22471	0.1012
$\sin\theta^q_{23}$	0.04204	0.0304	0.04170	-0.2291	0.04157	-0.3312
$\sin\theta^q_{13}$	0.00350	0.0091	0.00342	-0.2520	0.00344	-0.1872
δ_{CKM}	1.21930	0.0699	1.25285	0.6525	1.24018	0.4325
$\Delta m^2_{\odot}$	7.5033e-23	0.0180	7.5301e-23	0.1626	7.5377e-23	0.2038
Δm^2_{A}	2.4686e-21	-0.0204	2.4573e-21	-0.1858	2.4534e-21	-0.2419
$\sin^2\theta^l_{12}$	0.30039	0.0303	0.29864	-0.1044	0.30012	0.0090
$\sin^2\theta^l_{23}$	0.40631	-0.1189	0.34571	-2.0739	0.33558	-2.4006
$\sin^2\theta^l_{13}$	0.02262	-0.1652	0.01847	-1.9678	0.01907	-1.7085
m_e	4.697e-4	—	0.00049	0.0704	0.00049	0.0942
m_μ	9.914e-2	—	0.10143	-0.2508	0.10199	-0.1427
m_τ	1.686	—	1.73804	-0.0939	1.69996	-0.5301
Y_B	—	—	—	—	8.7463e-11	-0.0161
λ	—	—	0.52731	0.6307	0.52729	0.6293
χ^2		**1.103**		**22.97**		**23.47**

Table 8.2: Observables and pulls for model M1 (minimial non-SUSY) with and without considering RGE. Note that the fit without RGE was performed in the charged lepton basis, s.t. those observables are input parameters and do not have a pull. Masses are given in GeV, mass-squared differences in GeV^2.

in tbls. 8.2–8.4.

With inverted neutrino mass hierarchy it was impossible to produce a good fit of this model, with $\chi^2 > 200$ (400) in case of SUSY (non-SUSY) models. Within SUSY versions of such models this observation has already been made by other authors [203]. But that work did not include RGE during the fitting procedure and hence neglected running of neutrino parameters which can be sizable in the inverted hierarchy case. Therefore, our conclusion is more stringent. Since with the inverted hierarchy it is impossible to fit the data, we present only results for the normal neutrino mass hierarchy.

For the fits including RG evolution we see that for the minimal models in the non-supersymmetric case including the full RG analysis worsens the fit considerably while doing the same for the SUSY model gives a better result than fitting without RG evolution (tbl. 8.1). In case of non-SUSY models there is a big additional constraint when fitting

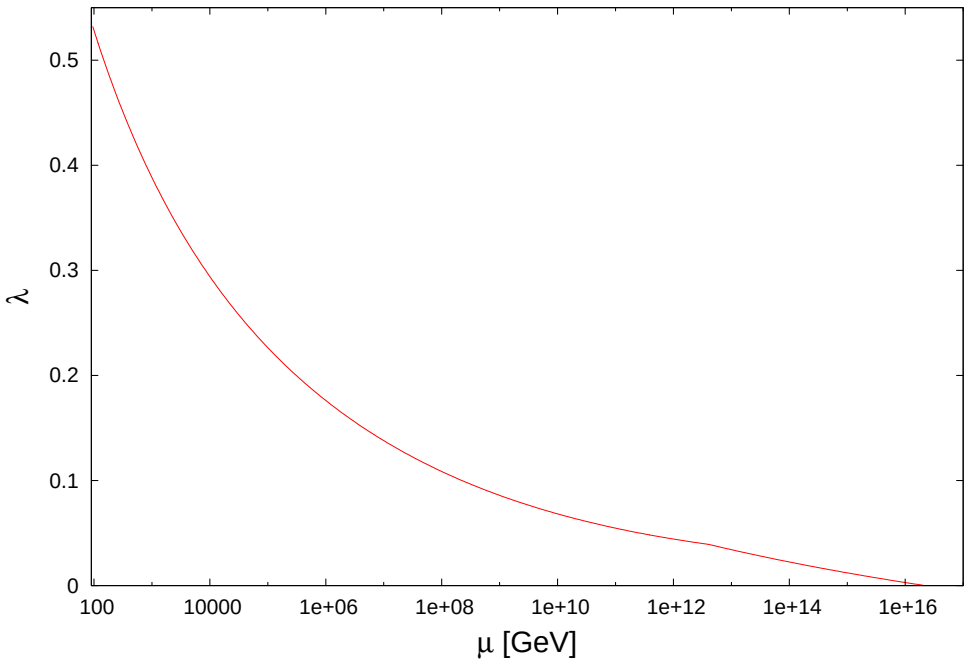

Figure 8.1: Running of λ for the best-fit parameters of model M1 with normal neutrino mass hierarchy, RG evolution and inclusion of Y_B. The kink between $\mu = 10^{12}$ GeV and $\mu = 10^{13}$ GeV results from integrating out the heaviest neutrino. There is no further such kink at energies where the other heavy neutrinos are integrated out, since their contribution to the running of λ is negligible compared to the contribution of the top-quark.

with RG evolution, since in that case we also consider the Higgs mass (see sec. 6.2). We also performed a fit of model M1 without including the Higgs mass. As expected from the pull of the top-quark (see discussion below), the fit improves to $\chi^2 = 13.2(8.3)$ in case Y_B was fitted (not fitted). Still, both non-SUSY and SUSY models can fit the data, the SUSY models being in better agreement. For the SUSY model we see no preferred value of $\tan\beta$ from our fits. Concerning the baryon asymmetry Y_B, the quality of all fits stays the same when Y_B is included in the analysis. Its absolute impact on the value of χ^2 is $\Delta\chi^2_{Y_B} \equiv \chi^2_{Y_B} - \chi^2_{\text{no } Y_B} \sim 0.5$ for the non-SUSY case and $\Delta\chi^2_{Y_B} \sim 0.05, 0.14, 0.2$ for the SUSY case with $\tan\beta = 50, 38, 10$, respectively. There seems to be a tendency of higher impact of Y_B on the fit quality of SUSY fits with lower values of $\tan\beta$.

Let us now discuss the different contributions to χ^2. We show the best-fit values of observables and their corresponding pulls in tbls. 8.2, 8.3 and 8.4. In case of non-SUSY fits without RGE one observes that the dominating contribution to χ^2 is due to the pull of the down-quark's mass. In case of the SUSY fit without RGE we fit mass ratios instead of masses. There the dominating contribution is the m_d/m_s ratio (not shown). In case of non-SUSY fits the main contribution to χ^2 comes from the mass of the top-quark ($\sim 3.4\sigma$) followed by the pulls of $\sin^2\theta^l_{23}$ and $\sin^2\theta^l_{13}$. The tension in the fit of the top-quark mass

MS, no Y_B

	$\tan\beta = 50$		$\tan\beta = 38$		$\tan\beta = 10$	
Observable	best-fit	pull	best-fit	pull	best-fit	pull
m_d	0.00087	-1.6714	0.00090	-1.6449	0.00091	-1.6381
m_s	0.04512	-0.6371	0.04711	-0.5089	0.04870	-0.4063
m_b	2.87626	-0.1526	2.88217	-0.0870	2.88499	-0.0557
m_u	0.00127	0.0018	0.00127	0.0068	0.00127	0.0064
m_c	0.62848	0.1129	0.62738	0.0997	0.62854	0.1135
m_t	171.45308	-0.0823	171.52203	-0.0593	171.53886	-0.0537
$\sin\theta^q_{12}$	0.22460	-0.0040	0.22460	-0.0018	0.22460	-0.0009
$\sin\theta^q_{23}$	0.04191	-0.0675	0.04193	-0.0565	0.04193	-0.0543
$\sin\theta^q_{13}$	0.00351	0.0241	0.00351	0.0322	0.00351	0.0314
$\delta_{\rm CKM}$	1.21318	-0.0364	1.21398	-0.0225	1.21409	-0.0205
$\Delta m^2_\odot$	7.5004e-23	0.0021	7.5002e-23	0.0013	7.5002e-23	0.0009
$\Delta m^2_{\rm A}$	2.4699e-21	-0.0022	2.4699e-21	-0.0013	2.4699e-21	-0.0010
$\sin^2\theta^l_{12}$	0.30015	0.0112	0.30007	0.0053	0.30004	0.0028
$\sin^2\theta^l_{23}$	0.40960	-0.0129	0.40977	-0.0073	0.40987	-0.0043
$\sin^2\theta^l_{13}$	0.02299	-0.0045	0.02297	-0.0138	0.02297	-0.0123
m_e	0.00049	0.0702	0.00049	0.0660	0.00049	0.0605
m_μ	0.10315	0.0839	0.10306	0.0665	0.10298	0.0513
m_τ	1.76204	0.1809	1.75740	0.1278	1.75528	0.1035
χ^2		**3.294**		**3.016**		**2.889**

Table 8.3: Observables and pulls for model MS (minimial SUSY) with RGE, without fitting Y_B, for different values of $\tan\beta$. Masses are given in GeV, mass-squared differences in Gev^2.

is easily understood from the relatively light Higgs mass (and hence low quartic coupling λ). Namely, the beta-function governing the evolution of the Higgs quartic coupling λ, as given in appendix C.1, reads

$$\begin{aligned} 16\pi^2\,\beta_\lambda \;=\; & 6\,\lambda^2 - 3\,\lambda\left(3g_2^2+\frac{3}{5}g_1^2\right) + 3\,g_2^4 + \frac{3}{2}\left(\frac{3}{5}g_1^2+g_2^2\right)^2 \\ & + 4\,\lambda\;\mathrm{Tr}\left[Y_e^\dagger Y_e + Y_\nu^\dagger Y_\nu + 3\,Y_d^\dagger Y_d + 3\,Y_u^\dagger Y_u\right] \\ & - 8\;\mathrm{Tr}\left[Y_e^\dagger Y_e\,Y_e^\dagger Y_e + Y_\nu^\dagger Y_\nu\,Y_\nu^\dagger Y_\nu + 3\,Y_d^\dagger Y_d\,Y_d^\dagger Y_d + 3\,Y_u^\dagger Y_u\,Y_u^\dagger Y_u\right], \end{aligned}$$

where Y_i are the Yukawa matrices of quarks and leptons and g_i the SM gauge couplings.

The dominating contribution here is the top-quark Yukawa coupling y_t within Y_u which is of order one (we neglect Y_ν since it does not change the argument). Therefore, the first trace in this expression evaluates to $\sim 3y_t^2$ and the second to $\sim 3y_t^4$. Then we can identify the three leading terms of β_λ: $6\,\lambda^2$, $12\,\lambda\,y_t^2$, and $-24\,y_t^4$. Hence, setting $y_t \sim 1$, for not too large

λ ($\lambda \lesssim 2$) the second trace in above expression will dominate. Since it has a negative sign it lets λ (and hence m_{H}) decrease with increasing energy. Or, since we evolve from M_{GUT} to M_Z, λ increases for lower energies. I.e., the large top-quark Yukawa coupling needed to get the correct top-quark mass favors a larger Higgs mass than (possibly) experimentally established. Or the other way around, to reproduce m_{H} as stated in sec. 6.2 one needs a smaller top-quark mass. This ultimately results in relatively large pulls for the top-quark mass in fits with RG evolution.

Note, however, that there is no consensus in the community on the measurement of the top-quark mass via kinematic reconstruction [269]. The top-quark mass determination at the Tevatron is based on the final state of the decay products. Another possibility is to reconstruct the top-quark mass from the total cross section in the top-quark pair production. This method is more rigorous from a theoretical perspective and yields a smaller top-quark mass 168.9 ± 3.5 GeV[1] [270] than the world average and it has larger error bars.

The evolution of λ with energy for the best-fit parameters of model M1 with normal neutrino mass hierarchy, RG evolution and inclusion of Y_B is shown in fig. 8.1. Notice the kink between $\mu = 10^{12}$ GeV and $\mu = 10^{13}$ GeV which results from integrating out the heaviest neutrino with a mass of $M_3 = 3.6 \times 10^{12}$ GeV (see sec. 8.4). There is no further such kink at energies where the other heavy neutrinos are integrated out, since their contribution to the running of λ is negligible compared to the contribution of the top-quark.

The results of the minimal model with $10_H + \overline{126}_H$ are summarized in tbl. 8.1 and the corresponding best-fit values and pulls can be found in tbls. 8.2–8.4. We present our parameters corresponding to the best-fit values in appendix B.

In sec. 5.4 we have shown how the number of free parameters can be reduced by imposing textures onto the Yukawa matrices. To illustrate that such a procedure can also produce viable models, we performed a fit to model M1 with the texture imposed as described in sec. 5.4. The results of the fit are contained in tbl. 8.1 together with the results of models M1 and MS and are denoted there by MT. While the fit without RGE is acceptable, including RGE into the fit poses tension to such a model, with now in addition to the top-quark mass also the strange-quark mass and the reactor mixing angle $\sin^2\theta_{13}$ cannot be fitted and have deviations of $3 \div 4\,\sigma$ to their experimental best-fit values. Therefore we will not discuss the model in more detail, but we note that after all this model has 4 parameters less than M1, which by itself does not provide a perfect fit once RGE and the Higgs mass are included into the fit.

8.2 Alternative Minimal Model with $\overline{126}_H + 120_H$

This model was analyzed only in the non-SUSY version (as it was originally proposed to be attractive in that case [166]) and we find that it is unable to reproduce fermion masses and

[1] Note that this is the pole-mass $m_t(m_t)$ while the value given in tbl. 6.1 is the mass at M_Z in the $\overline{MS}$ scheme.

MS, Y_B

	$\tan\beta = 50$		$\tan\beta = 38$		$\tan\beta = 10$	
Observable	best-fit	pull	best-fit	pull	best-fit	pull
m_d	0.00085	-1.6892	0.00082	-1.7093	0.00080	-1.7247
m_s	0.04577	-0.5956	0.05002	-0.3214	0.05281	-0.1414
m_b	2.87840	-0.1289	2.88338	-0.0736	2.88683	-0.0352
m_u	0.00127	0.0104	0.00127	0.0034	0.00127	0.0100
m_c	0.63609	0.2034	0.63954	0.2445	0.63828	0.2295
m_t	171.42259	-0.0925	171.45737	-0.0809	171.52678	-0.0577
$\sin\theta^q_{12}$	0.22459	-0.0123	0.22459	-0.0123	0.22459	-0.0105
$\sin\theta^q_{23}$	0.04181	-0.1462	0.04181	-0.1476	0.04181	-0.1455
$\sin\theta^q_{13}$	0.00351	0.0455	0.00351	0.0291	0.00351	0.0370
$\delta_{\rm CKM}$	1.21008	-0.0901	1.20950	-0.1002	1.21020	-0.0881
$\Delta m^2_{\odot}$	7.5004e-23	0.0020	7.5002e-23	0.0010	7.5005e-23	0.0026
$\Delta m^2_{\rm A}$	2.4698e-21	-0.0025	2.4699e-21	-0.0016	2.4698e-21	-0.0036
$\sin^2\theta^l_{12}$	0.30014	0.0107	0.30006	0.0046	0.30013	0.0097
$\sin^2\theta^l_{23}$	0.40950	-0.0160	0.40963	-0.0120	0.40928	-0.0234
$\sin^2\theta^l_{13}$	0.02297	-0.0142	0.02301	0.0058	0.02296	-0.0194
m_e	0.00049	0.1140	0.00049	0.1098	0.00049	0.1068
m_μ	0.10303	0.0607	0.10285	0.0251	0.10265	-0.0132
m_τ	1.75961	0.1531	1.75372	0.0857	1.74951	0.0375
Y_B	8.7499e-11	-0.0005	8.7498e-11	-0.0009	8.7497e-11	-0.0014
χ^2		**3.347**		**3.150**		**3.096**

Table 8.4: Observables and pulls for model MS (minimial SUSY) with RGE, including Y_B, for different values of $\tan\beta$. Masses are given in GeV, mass-squared differences in Gev^2.

mixings. Although this result has been obtained previously [168], the authors of ref. [168] considered only the normal hierarchy and further did not include a detailed RGE, but fitted some idealized data set at $M_{\rm GUT}$. In this thesis we used full RGE to arrive at our results, thus our conclusion is much stronger. Further, we also checked and excluded the possibility of the inverted hierarchy. Our best-fit result has a χ^2 value of ~ 100 in case of the normal hierarchy. For the inverted hierarchy the fit becomes even worse with $\chi^2 \sim 700$. Therefore we will not present tables with best-fit values or pulls for this model.

8.3 Model with $10_H + \overline{126}_H + 120_H$

This class of models, inspite of having one more Higgs representation, through the additional constraints (see chapter 5) has one parameter less than the minimal models. Nevertheless, it is not only able to fit the data, but reproduces the data even much better

Model	$\tan\beta$	Comment	χ^2 NH	χ^2 IH
F1	–	no RGE, no Y_B	6.6×10^{-5}	2.5×10^{-4}
	–	RGE, no Y_B	11.2	13.3
	–	RGE, Y_B	11.5	13.3
FS	50	no RGE, no Y_B	9.0×10^{-10}	3.9×10^{-8}
	50	RGE, no Y_B	6.9×10^{-6}	0.602
	50	RGE, Y_B	0.220	20.5

Table 8.5: Value of χ^2 at the best-fit position for the model with $10_H + \overline{126}_H + 120_H$ in case of normal (NH) and inverted (IH) neutrino mass hierarchy. For IH we present the solution with $\sin^2\theta_{23} > 0.5$, but both possibilities yield equally good fits. Remarks as in tbl. 8.1 apply analogously.

than the other models. This is especially the case for the SUSY versions of this model. Furthermore, these models are also able to fit the data with inverted neutrino mass hierarchy which differentiates them clearly from the previous models. Since we do not observe a significant difference in the quality of fits of SUSY models with different values of $\tan\beta$ we fitted this model only for $\tan\beta = 50$ and $\tan\beta = 10$, which again yield very similar results, as in the case of the $10_H + \overline{126}_H$ model. Therefore we present here only the results for $\tan\beta = 50$. Our results are tabulated in tbl. 8.5 and the best-fit values of observables and their pulls are compiled in tbls. 8.6 and 8.7.

Let us first discuss the fits with normal hierarchy. This setup has been analyzed without RG evolution in the SUSY case in refs. [168, 195, 223] with χ^2 ranging between 0.01 and 0.33. The non-SUSY case has been fitted to data only in ref. [168] and results in $\chi^2 \sim 10^{-6}$. Again we observe that fitting the non-SUSY version of this model including RG evolution significantly worsens the fit. As in the $10_H + \overline{126}_H$ model this is due to fitting the Higgs mass. Fitting Y_B yields a χ^2 value that is by 0.3 higher than without fitting Y_B. The SUSY fits turn out to be even better than the non-SUSY fits. Here, fits at the GUT scale as well as fits at M_Z (without Y_B) yield χ^2 values that are essentially zero. Including Y_B puts severe constraints on the setup as χ^2 increases to 0.22. We notice that the absolute increase of χ^2 due to inclusion of Y_B (denoted henceforth by $\Delta\chi^2_{Y_B}$) is roughly the same for all setups within the normal neutrino mass hierarchy.

We now turn to the inverted hierarchy. In constrast to the $10_H + \overline{126}_H$ model an inverted neutrino mass hierarchy is viable here. The SUSY case with inverted hierarchy has been fitted to data in ref. [223], but RG evolution was not taken into account, which is especially important for the inverted hierarchy. Their best-fit point has $\chi^2 = 0.011$. We are not aware of any analysis of the non-SUSY case with inverted hierarchy.

In our analysis, in the non-SUSY model the fit quality is approximately the same as in the normal hierarchy. Again, when fitting with RG evolution inclusion of m_{H} severely constrains the model. The value of χ^2 for fits with RG evolution is slightly higher in case

	F1, NH, no Y_B		F1, NH, Y_B		F1, IH, Y_B	
Observable	best-fit	pull	best-fit	pull	best-fit	pull
m_d	0.00295	0.0414	0.00314	0.1978	0.00305	0.1213
m_s	0.06199	0.4512	0.06195	0.4482	0.06651	0.7427
m_b	2.88874	-0.0140	2.89203	0.0225	2.88964	-0.0040
m_u	0.00127	0.0003	0.00127	0.0013	0.00127	0.0008
m_c	0.62395	0.0590	0.62563	0.0789	0.62383	0.0574
m_t	161.94256	-3.2525	161.84354	-3.2855	161.20820	-3.4973
$\Delta m^2_\odot$	7.5003e-23	0.0015	7.501e-23	0.0053	7.5e-23	-0.0001
$\Delta m^2_{\rm A}$	2.4697e-21	-0.0037	2.4694e-21	-0.0089	-2.3549e-21	0.0019
$\sin\theta^q_{12}$	0.22460	-0.0044	0.22459	-0.0115	0.22460	0.0042
$\sin\theta^q_{23}$	0.04192	-0.0646	0.04190	-0.0795	0.04182	-0.1359
$\sin\theta^q_{13}$	0.00350	-0.0031	0.00350	-0.0061	0.00350	-0.0007
δ_{CKM}	1.21402	-0.0217	1.21201	-0.0566	1.21651	0.0215
$\sin^2\theta^l_{12}$	0.30006	0.0048	0.30031	0.0242	0.30000	0.0002
$\sin^2\theta^l_{23}$	0.41029	0.0093	0.41092	0.0295	0.59024	0.0114
$\sin^2\theta^l_{13}$	0.02302	0.0078	0.02300	-0.0021	0.02300	0.0013
m_e	0.00049	0.0001	0.00049	0.0002	0.00049	0.0005
m_μ	0.10232	-0.0777	0.10222	-0.0975	0.10211	-0.1180
m_τ	1.74663	0.0045	1.74145	-0.0548	1.74172	-0.0518
Y_B	—	—	8.7501e-11	0.0002	8.75e-11	0.0000
λ	0.52745	0.6455	0.52749	0.6493	0.52792	0.6916
χ^2		**11.2**		**11.5**		**13.3**

Table 8.6: Observables and pulls for model F1 fitted assuming normal (NH) or inverted (IH) hierarchy. For the NH case results with and without fitting Y_B are shown, for the IH case both fits are indistinguishable at the presented precision and only the results of the fit including Y_B are shown. Masses are given in GeV, mass-squared differences in GeV^2.

of the inverted hierarchy as compared to the normal hierarchy. The constraint through fitting Y_B is nearly vanishing ($\Delta\chi^2_{Y_B} < 0.001$, s.t. it is not seen in tbl. 8.5). For F1 in case of inverted hierarchy we again, as for M1 with normal hierarchy, performed an additional fit without including the Higgs mass. As expected from the discussion in sec. 8.1 the pull of the top-quark diminishes and we get $\chi^2 = 0.67$ (Y_B not fitted; not shown in any table) to be compared to $\chi^2 = 13.3$ in case the Higgs mass is included in the fit.

The situation in the SUSY fits with inverted hierarchy differs more significantly from the corresponding fits with normal hierarchy. While fits without RG evolution give $\chi^2 \sim 0$, turning on RG evolution seriously worsens the fit with now $\chi^2 \sim 0.6$. This difference is not totally surprising, since in case of inverted hierarchy neutrino parameters are known to evolve sizably between $M_{\rm GUT}$ and M_Z and for the fits at $M_{\rm GUT}$ the low-energy values of neutrino parameters were assumed, which only for the normal hierarchy is a good ap-

	FS, NH, Y_B		FS, IH, no Y_B		FS, IH, Y_B	
Observable	best-fit	pull	best-fit	pull	best-fit	pull
m_d	0.00275	-0.1275	0.00305	0.1255	0.00015	-2.2636
m_s	0.06071	0.3682	0.04337	-0.7500	0.00194	-3.4231
m_b	2.88911	-0.0099	2.88344	-0.0729	2.92904	0.4338
m_u	0.00127	0.0007	0.00127	-0.0062	0.00127	0.0007
m_c	0.62172	0.0324	0.61551	-0.0416	0.61485	-0.0494
m_t	171.52330	-0.0589	171.65509	-0.0150	177.30747	1.8692
$\Delta m^2_\odot$	7.4947e-23	-0.0287	7.5e-23	0.0000	7.5e-23	0.0001
$\Delta m^2_{\rm A}$	2.472e-21	0.0285	-2.355e-21	-0.0000	-2.3551e-21	-0.0013
$\sin\theta^q_{12}$	0.22460	-0.0005	0.22460	-0.0012	0.22460	-0.0021
$\sin\theta^q_{23}$	0.04194	-0.0462	0.04201	0.0114	0.04201	0.0068
$\sin\theta^q_{13}$	0.00350	-0.0045	0.00350	-0.0015	0.00350	0.0011
δ_{CKM}	1.21519	-0.0015	1.21507	-0.0035	1.21480	-0.0082
$\sin^2\theta^l_{12}$	0.29899	-0.0773	0.30000	-0.0000	0.30000	0.0001
$\sin^2\theta^l_{23}$	0.41340	0.1097	0.58972	-0.0129	0.58987	-0.0059
$\sin^2\theta^l_{13}$	0.02342	0.1812	0.02300	0.0011	0.02300	-0.0006
m_e	0.00049	0.0020	0.00049	-0.0025	0.00049	0.0197
m_μ	0.10230	-0.0819	0.10320	0.0937	0.10275	0.0062
m_τ	1.75034	0.0470	1.75356	0.0838	1.74032	-0.0678
Y_B	8.7512e-11	0.0053	—	—	8.75e-11	-0.0000
χ^2		**0.220**		**0.602**		**20.5**

Table 8.7: Observables and pulls for model FS fitted assuming normal (NH) or inverted (IH) hierarchy. For the NH case results from fits including Y_B are shown, for the IH case both fit results with and without Y_B are shown. Masses are given in GeV, mass-squared differences in GeV^2.

proximation. What is more surprising is that the quality of the fit diminishes a lot when including Y_B into the fit. The down quark mass is fitted $2.3\,\sigma$ the strange-quark mass $3.4\,\sigma$ too small, while the top-quark mass is fitted $1.9\,\sigma$ too large. In contrast, all other observables are reproduced in perfect agreement with data. One may argue that in terms of complex phases this model is less flexible than the $10_H + \overline{126}_H$ model, since H and F in this model are purely real and the only source of complex phases comes from G, which is purely imaginary (including its prefactor; see eqn. (5.1)) and has only three parameters, since it is anti-symmetric. Still, from the SUSY fits of the normal hierarchy and non-SUSY fits of both hierarchies one would not expect such a dramatic impact of including Y_B into the fit in the inverted hierarchy in the SUSY model.

In what concerns the different contributions to χ^2, in the "no RGE" case and for the SUSY fit of the normal hierarchy also in the "no Y_B" case $\chi^2 \sim 0$. The best-fit values of observables are essentially identical with the experimental values presented in chapter

6. Therefore we do not tabulate these values separately. In the non-SUSY fits including RG evolution (but no Y_B) we have again the dominating contribution from m_t with a pull of ~ -3.25 (NH) or ~ -3.5 (IH) corresponding to $\Delta\chi^2_{m_t} \sim 10.6$ (NH) or $\Delta\chi^2_{m_t} \sim 12.2$ (IH) followed by the pulls of λ and the strange-quark mass m_s, 0.65 and 0.45 (NH) or 0.69 and 0.74 (IH), respectively. When also fitting Y_B, the biggest change in the NH case concerns the pull of the down-quark mass rising from 0.04 (no Y_B) to 0.2 (including Y_B). This amounts only to a small fraction of $\Delta\chi^2_{Y_B}$ and the rest is distributed on basically all observables in such a way, that they all stay essentially at the experimental best-fit position to an accuracy, s.t. all pulls $< 0.1\,\sigma$. For the IH case, as already mentioned, $\Delta\chi^2_{Y_B} \sim 0$ and there are no big changes in the values of the pulls. In the SUSY case with normal hierarchy and Y_B the main contribution to χ^2 is the strange-quark mass with a pull of 0.37 followed by $\sin^2\theta^l_{13}$, m_d, and $\sin^2\theta^l_{23}$. Fitting the inverted hierarchy without Y_B again the pull of the strange-quark mass gives the main contribution to χ^2 with now the pull being -0.75 accounting for nearly the whole value of χ^2. Including Y_B into the fit introduces severe tensions for the validity of the model, as pointed out above. The best-fit values of observables and their pulls for the non-SUSY and SUSY version of this model are summarized in tbls. 8.6 and 8.7, respectively.

8.4 Model Predictions

There are observables which have not yet been measured experimentally but are fixed by the fits we performed, so they can be understood as predictions of the models we analyzed. The observables predicted are effective $0\nu\beta\beta$ mass $\langle m_\nu\rangle$ (eqn. (3.5) on page 29), leptonic CP violation δ^l_{CP} (eqn. (2.2) on page 9), lightest neutrino mass m_0 ($m_0 = m_1$ for NH and $m_0 = m_3$ for IH), and masses of heavy neutrinos M_i. We will discuss the non-SUSY case as well as the SUSY case. In case of SUSY models we will restrict the discussion to models with $\tan\beta = 50$, since the results of models with other values of $\tan\beta$ are very similar and show only small numerical deviations from the models with $\tan\beta = 50$. One common effect is that in case of normal hierarchy the masses generally increase in models with lower values of $\tan\beta$ while in case of inverted hierarchy they decrease. For low-energy observables, such as $\langle m_\nu\rangle$, this is only an effect of a few percent. The numerical values are tabulated in tbl. 8.9 and will be discussed below.

Further, there is the question whether the atmospheric neutrino mixing angle, θ_{23}, deviates from maximal mixing (i.e., $\theta_{23} = 45°$). Its best-fit value already deviates by about $1\,\sigma$ from maximal mixing (see tbl. 6.1) and we want to see whether the models considered here pin down θ_{23} more precisely than experimental limits. Besides the question of whether the atmospheric mixing angle is maximal or not one of the next questions to be answered in neutrino physics is the value of δ^l_{CP}. Therefore, we investigate how stringent the model predictions are for δ^l_{CP}. For both quantities we analyze the behaviour of χ^2 as a function of $\sin^2\theta_{23}$ or δ^l_{CP}, respectively, employing the method described at the beginning of chapter 6. For the still viable models M1, F1, and FS we plot $\Delta\chi^2(\sin^2\theta_{23}) = \chi^2(\sin^2\theta_{23}) - \chi^2|_{min}$ in fig. 8.2. As can be seen from fig. 8.2 neither model F1 nor FS restricts the value of θ_{23}

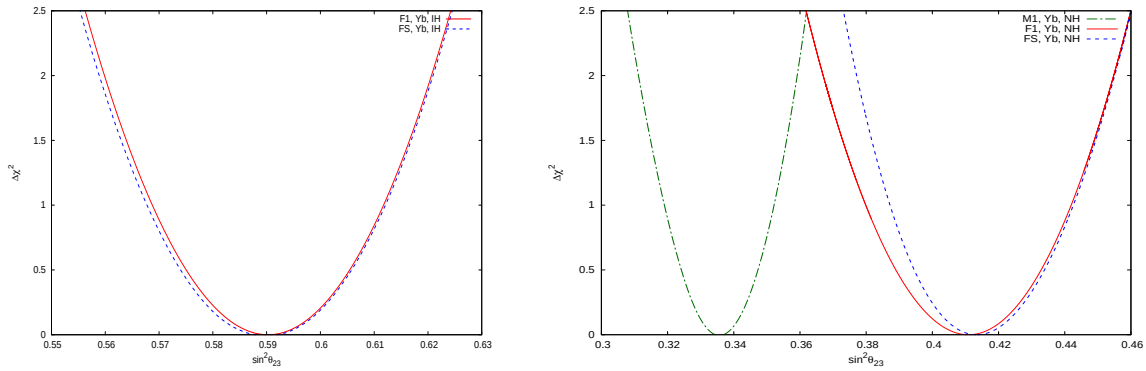

(a) (b)

Figure 8.2: $\Delta\chi^2(\sin^2\theta_{23}) = \chi^2(\sin^2\theta_{23}) - \chi^2|_{min}$ is shown (a) for models F1 and FS in case of an inverted neutrino mass hierarchy and (b) for models M1, F1, and FS in case of a normal hierarchy and the baryon asymmetry Y_B included into the fit.

sizably beyond its experimental boundaries[2], independently of the neutrino mass hierarchy. $\Delta\chi^2(\sin^2\theta_{23})$ simply increases due to the deviation of $\sin^2\theta_{23}$ from the experimental best-fit value, i.e.,

$$\Delta\chi^2(\sin^2\theta_{23}) \simeq \left(\frac{\sin^2\theta_{23} - \sin^2\overline{\theta}_{23}}{\sigma_{23}}\right)^2 ,$$

where $\overline{\theta}_{23}$ is the experimental best-fit value of θ_{23} and σ_{23} the uncertainty on $\sin^2\overline{\theta}_{23}$. Model M1 in case of normal hierarchy, however, strongly favors a rather small value, $\sin^2\theta_{23} = 0.335 \pm 0.015$ at 68 % C.L. (corresponding to $\Delta\chi^2 = 1$), with a much steeper $\Delta\chi^2(\sin^2\theta_{23})$ function. Therefore, if after more precise measurements the value of θ_{23} contracts around its current experimental best-fit value, model M1 will be strongly disfavored. For other cases, not shown in fig. 8.2, especially the fits without RGE, the situation is similar to that of models F1 and FS as presented in fig. 8.2.

A similar analysis was carried out for δ^l_{CP} with models M1, F1, and FS. The 68 % C.L. intervals are summarized for these models in tbl. 8.8 differentiated by neutrino mass hierarchy and by the fitting procedure – without RGE or with RGE, whereas the fits with RGE, again, include the baryon asymmetry Y_B. For a selection of setups we plot $\Delta\chi^2(\delta^l_{CP})$ in fig. 8.3. As can be seen from the ranges presented in tbl. 8.8, first of all there are big differences in the predicted values of δ^l_{CP} for one and the same model, depending on whether RGE and Y_B are taken into account or not. E.g., for model M1, when the analysis is done without RGE and without inclusion of Y_B, within 68 % C.L. δ^l_{CP} is completely unconstrained. In contrast, the investigation including RGE and Y_B yields only certain intervals for δ^l_{CP} which are allowed at the same C.L.. For model F1 in case of inverted neutrino mass hierarchy this contrast is most pronounced, with δ^l_{CP} being unconstrained in the "no RGE" setup, while being locked to a rather small interval, $\delta^l_{CP} \in [4.6; 5.0]$, in the "RGE & Y_B" setup. In the analysis including RGE also Y_B was fitted, which strongly

[2]M1 is not viable in the case of inverted hierarchy, as discussed in sec. 8.1

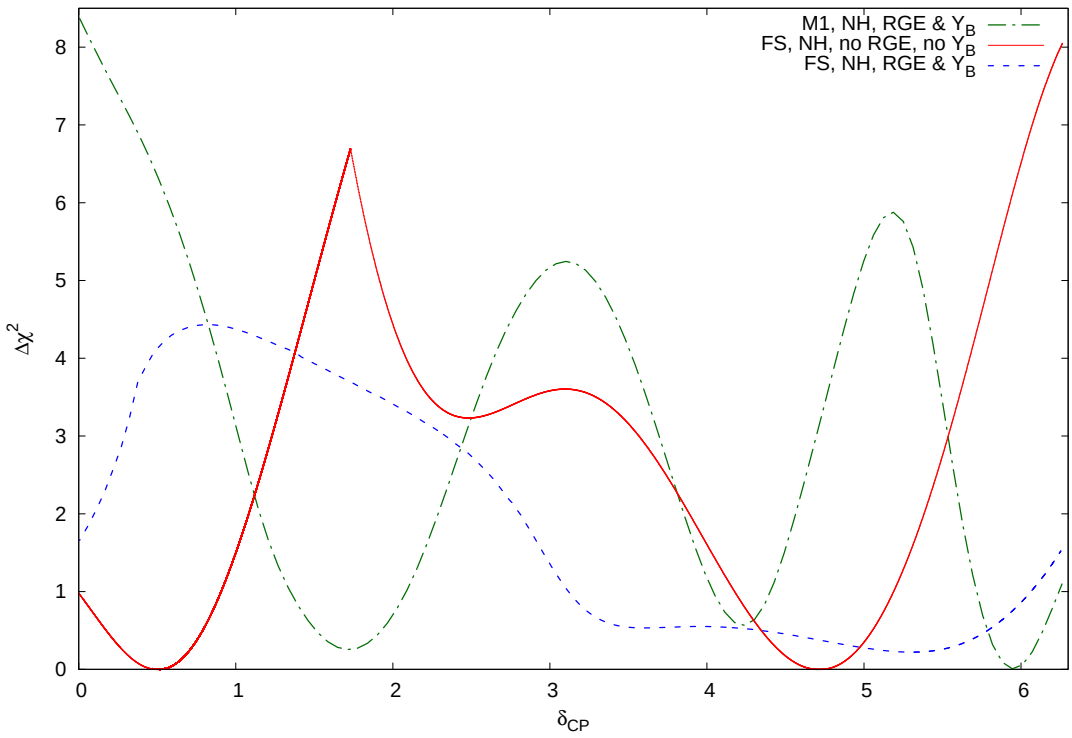

Figure 8.3: $\Delta\chi^2$ as a function of δ^l_{CP} plotted for models M1 & FS (NH, with RGE, Y_B fitted) and model FS (NH, no RGE, Y_B not fitted).

depends on phases in the Yukawa matrix Y_ν (see eqn. (6.13) on page 59), whose phases also influence δ^l_{CP}. So intuitively, one may think that the tighter limits would always arise when Y_B is fitted. But this intuition is proven wrong within model FS with normal hierarchy, where the limits are tighter in the case without RGE than in the case with RGE and Y_B, as can be seen from tbl. 8.8 and fig. 8.3. Still we emphasize the importance of doing a correct RGE analysis, since numerically, the allowed intervals differ vastly and do not even overlap. Finally, we note that different setups have different allowed ranges for δ^l_{CP} and thus can be distinguished experimentally.

Let us now come to a discussion of the other model predictions, as summerized in tbl. 8.9 and start with model M1. The effective $0\nu\beta\beta$ mass at the best-fit position in the minimal model and normal hierarchy is rather small, $\langle m_\nu \rangle \sim (0.4 \pm 0.1)$ meV, to be compared with the generic expectation in case of NH of $1 \div 4$ meV [121]. Such low values are only allowed for a small range of masses of the lightest neutrino of $2 \div 10$ meV and the model predictions of the lightest neutrino mass is consistent with this range, $m_0 \sim 2 \div 7$ meV.

The seesaw scale (M_3) in all versions of the minimal model is a few times 10^{12} GeV and the two lighter of the heavy neutrinos have masses between 10^{10} and 10^{12} GeV. One might wonder why the seesaw scale is so low. Generically, extending the Standard Model by singlet right-handed neutrinos one can include a Dirac mass term M_D coupling left-

		δ^l_{CP}	
Model	Hierarchy	no RGE	RGE & Y_B
M1	NH	$[0; 2\pi]$	$[1.3; 2.1]$, $[4.0; 4.4]$, $[5.7; 6.2]$
F1	NH	$[1.3; 2.6]$, $[3.7; 4.8]$	$[5.6; 5.9]$
F1	IH	$[0; 2\pi]$	$[4.6; 5.0]$
FS	NH	$[0.0; 0.9]$, $[4.1; 5.2]$	$[3.0; 6.1]$
FS	IH	$[0; 2\pi]$	$[0.5; 0.6]$, $[3.1; 3.3]$, $[3.6; 3.7]$

Table 8.8: Allowed ranges for δ^l_{CP} at 68 % C.L. for models M1, F1, and FS. Ranges for normal and inverted neutrino mass hierarchy are shown. Furthermore, we distinguish ranges derived from fits without RGE and fits including RGE, where in the second case also the baryon asymmetry Y_B has been fitted when deriving the ranges. As can be seen, the ranges differ sizably for fits with RGE and without RGE and even do not necessarily overlap.

and right-handed neutrinos and a Majorana mass term M_R for the right-handed neutrinos, which result in the (type I) seesaw formula for the masses of light neutrinos,

$$m_\nu = -M_D^T M_R^{-1} M_D \,. \tag{8.2}$$

In the generic argument one assumes the Dirac mass term to be of the order of the top-quark, $M_D \sim 174$ GeV and derives the scale of M_R from requiring $\sqrt{\Delta m^2_A} \sim m_\nu$. This gives $M_R \sim (174 \text{ GeV})^2/\sqrt{2.5 \times 10^{-21} \text{ GeV}} = 6 \times 10^{14}$ GeV, tantalizingly close to the GUT scale. One would expect this scenario to be realized especially in $SO(10)$ models, since here we have a strong correlation between the up-quark mass matrix and M_D as can be seen from eqns. (4.3) and (5.1). Still, there is a decisive difference between M_u and M_D, since the $\overline{126}_H$ contribution enters into M_R with a relative sign and an additional factor of 3. Hence, through cancellations between Y_{10} and Y_{126} terms the Dirac neutrino mass term M_D can easily be an order of magnitude lighter than M_u requiring a corresponding correction of two orders of magnitude (since M_D enters eqn. (8.2) quadratically) in M_R.

In the $10_H + \overline{126}_H + 120_H$ model with normal hierarchy the predicted value of $\langle m_\nu \rangle$ is sizably higher. Depending on the setup (with/without RGE or Y_B) of the fit, $\langle m_\nu \rangle \sim 0.7 \div 0.9$ meV (SUSY) and $\langle m_\nu \rangle \sim 2.5 \div 5.0$ meV (non-SUSY). Consequently, any value ≤ 1 eV of neutrino masses is allowed in principle and the different fits cover more or less the entire range. The seesaw scale in this scenario can be considerably higher than in the minimal models. In the non-SUSY case with RG evolution it is about 10^{15} GeV, whereas in the fit without RG evolution it is about 10^{13} GeV. In the SUSY case what is remarkable is that including Y_B into the fit the seesaw scale diminishes from $M_3 \sim 4 \times 10^{13}$ to $M_3 \sim 4 \times 10^{12}$.

In the $10_H + \overline{126}_H + 120_H$ model with inverted hierarchy in the non-SUSY case, $\langle m_\nu \rangle \sim 35$ meV, independent of the fit details. In the inverted hierarchy, m_0 is not related to

Model	Comments	$\langle m_\nu \rangle$ [meV]	δ^l_{CP} [rad]	m_0 [meV]	M_3 [GeV]	M_2 [GeV]	M_1 [GeV]
M1	no RGE, NH	0.35	0.7	3.03	5.53e12	7.24e11	1.45e10
M1	RGE, no Y_B, NH	0.49	6.0	2.40	3.57e12	2.02e11	1.17e11
M1	RGE, Y_B, NH	0.52	5.9	2.38	3.62e12	1.97e11	1.39e11
MS	no RGE, NH	0.38	0.3	2.58	4.08e12	7.14e11	1.60e10
MS	RGE, Y_B, NH	0.44	2.8	6.83	1.06e12	5.66e10	1.45e10
MS	RGE, Y_B, NH	0.44	2.5	6.52	1.32e12	2.77e10	2.74e10
F1	no RGE, NH	4.96	1.7	8.8	1.91e13	2.80e12	2.21e10
F1	RGE, no Y_B, NH	2.87	5.0	1.54	9.92e14	7.30e13	1.18e13
F1	RGE, Y_B, NH	2.56	5.8	1.27	8.82e14	1.07e14	7.86e12
FS	no RGE, NH	0.75	0.5	1.16	1.46e13	5.25e11	5.67e10
FS	RGE, no Y_B, NH	0.78	5.4	3.17	4.23e13	4.92e11	4.88e11
FS	RGE, Y_B, NH	0.89	4.0	7.78	3.71e12	1.66e09	5.88e07
F1	no RGE, IH	35.37	5.4	35.85	2.20e13	4.92e12	9.19e11
F1	RGE, no Y_B, IH	35.52	4.7	30.24	1.13e13	3.48e12	5.51e11
F1	RGE, Y_B, IH	35.43	4.8	30.0	1.14e13	3.51e12	5.53e11
FS	no RGE, IH	44.21	0.3	6.27	1.21e13	4.18e11	3.51e07
FS	RGE, no Y_B, IH	24.22	3.6	11.97	1.17e13	3.06e11	1.96e03
FS	RGE, Y_B, IH	45.72	0.6	15.11	1.65e10	1.06e10	1.22e09

Table 8.9: Model predictions for effective $0\nu\beta\beta$ mass $\langle m_\nu \rangle$, leptonic CP violation δ^l_{CP}, lightest neutrino mass m_0 ($m_0 = m_1$ for NH and $m_0 = m_3$ for IH), and masses of heavy neutrinos M_i. For the SUSY models the predictions with $\tan\beta = 50$ are shown which do not differ significantly from predictions with other values of $\tan\beta$.

$\langle m_\nu \rangle$. In the non-SUSY case the prediction is $m_0 \sim 30$ meV. The seesaw scale is roughly 10^{13} GeV. For the SUSY case, $\langle m_\nu \rangle \sim 24 \div 46$ meV and depends on the details of the fit. We notice that even the largest values predicted for $\langle m_\nu \rangle$ are still in agreement with limits derived from most recent data on $0\nu\beta\beta$ decay, which in its most stringent form, i.e., taking the largest matrix element for ^{136}Xe from sec. 3.3 and the 68 % C.L. from ref. [19], is $\langle m_\nu \rangle < 86$ meV. The mass of the lightest neutrino also has a rather wide spread depending on fit details, $m_0 \sim 6 \div 15$ meV. The seesaw scale is roughly 10^{13} GeV for the fits without RGE or including RGE but without Y_B, the same as in the non-SUSY case. For fits including RGE and Y_B the seesaw scale is extraordinary low, $M_3 \sim 10^{10}$ GeV.

8.5 Conclusions

In general Grand Unified Theories and in particular models based on $SO(10)$ offer intriguing frameworks to find an answer to the question of the origin of fermion masses and mixings. In

this chapter we analyzed renormalizable $SO(10)$ models based on $10_H + \overline{126}_H$, $120_H + \overline{126}_H$, and $10_H + 120_H + \overline{126}_H$ Higgs representations, assuming type I seesaw dominance. We looked at non-supersymmetric models as well as supersymmetric models with different values of $\tan\beta$. Besides fitting the different models to fermion masses and mixings we also included the baryon asymmetry Y_B in our analysis. We performed fits including Y_B as well as without Y_B to determine its impact on the quality of the fit. We assumed that the baryon asymmetry is produced through thermal leptogenesis and also included flavor effects, which is a novelty in the context of $SO(10)$ models. In non-SUSY models there is interference between the RGE of fermion parameters and the RGE of the Higgs quartic coupling, which is especially important for the top-quark Yukawa coupling. From the Higgs quartic coupling and the Yukawa couplings of fermions at $M_{\rm GUT}$, the quartic coupling and hence the Higgs mass gets determined at low energies as well. Therefore we included the Higgs mass into our list of observables which constrain non-SUSY models, which has not been done in the literature so far.

Further, we performed a complete 1-loop RGE during the analysis, which has not been done in previous studies. In addition, we treated right-handed neutrinos during RGE correctly and integrated them out one by one at their respective energy scales. Using RGE in our study allowed us to consider setups with an inverted neutrino mass hierarchy in addition to the normal neutrino mass hierarchy, which dominates the literature. This has not been done consistently in previous studies, since in case of the inverted hierarchy the low-energy neutrino mixing parameters are a bad approximation to the values at the GUT scale, where previous studies performed their analysis.

Finally, we gave the model predictions for several as yet unmeasured observables. These are the effective mass $\langle m_\nu \rangle$ relevant for neutrinoless double beta decay, the leptonic CP violating phase, δ^l_{CP}, the mass of the lightest neutrino, and the masses of the heavy neutrinos. For δ^l_{CP} we analyzed the sensitivity of the models to a deviation of δ^l_{CP} from its value at the best-fit point and we derived the allowed ranges corresponding to 67 % C.L. A similar analysis was performed for θ_{23}.

The results of our analysis are as follows. We showed that it is possible to fit the minimal setups M1 and MS[3] (both with $10_H + \overline{126}_H$ Higgs representations responsible for fermion mass generation) in the case of the normal neutrino mass hierarchy, while both the non-SUSY (M1) and the SUSY (MS) cases do not work with the inverted hierarchy. Hence, they will be excluded if the neutrino mass hierarchy is experimentally found to be inverted. The alternative minimal model M2 ($120_H + \overline{126}_H$) was excluded firmly for both possibilities of the neutrino mass hierarchy. In contrast, models F1 and FS ($10_H + 120_H + \overline{126}_H$) have been shown to be able to reproduce both the normal and inverted hierarchy. Model F1 works equally well for both hierarchies, while within model FS the normal hierarchy is preferred when including the baryon asymmetry into the fit.

For the non-SUSY models (M1 and F1) we showed that fitting the Higgs mass leads to severe tensions for the top quark mass, which is more than $3\,\sigma$ smaller than the experi-

[3] We remind the reader that model names containing the letter "S" refer to supersymmetric models, while those without "S" refer to non-supersymmetric models.

mental value[4]. For model F1 this is the only observable that cannot be fitted close to its experimental value, while for model M1 also $\sin^2\theta_{23}^l$ deviates significantly, i.e., it is $2.4\,\sigma$ smaller than its experimental value. Comparing fits with and without baryon asymmetry, we have seen that in case of normal neutrino mass hierarchy the quality of the fit stays approximately the same as those without the inclusion of Y_B – the χ^2 values increase by $0.1 \div 0.6$ – whereas in the case of inverted hierarchy, for model F1 there is essentially no impact on the value of χ^2 while for model FS fitting Y_B results in χ^2 increasing from 0.6 to 20.5.

For the atmospheric mixing angle θ_{23} we have shown that only model M1 in the case of normal neutrino mass hierarchy sensitively depends on the value of $\sin^2\theta_{23}$ and prefers a value below the experimental best-fit value.

Concerning model predictions, we have shown that only certain ranges are allowed for δ_{CP}^l. Further, those ranges are different for different models and thus models can in principle be distinguished by a measurement of leptonic CP violation. An import conclusion in this affair is that predictions of the models depend on whether RGE is included or not. The allowed ranges for δ_{CP}^l derived with and without RGE do not even overlap for the same model. Thus we emphasize again the importance of inclusion of RGE when analyzing models defined at high energy scales.

8.6 Outlook

We want to give a few comments on which questions remain open and could be addressed in the future. First of all, the list of models we considered is not exhaustive, so one could analyze further models and compare analyses done with and without RGE. The models we considered either could or could not fit the data, irrespective of considering RGE or not. However, there may well be models where inclusion of RGE makes a difference between considering a model as viable or not. Since we restricted our analysis to the type I seesaw case it would be interesting to consider models where either type II seesaw dominates or where type I and type II seesaw contributions to neutrino mass are of equal order of magnitude. Further, as we have shown, allowed ranges derived for δ_{CP}^l strongly depend on whether one includes RGE or not. In view of future experiments it is desirable to have reliable predictions of further models for δ_{CP}^l. In addition, the analysis we have done for δ_{CP}^l could also be done for other observables. In particular, for setups with inverted neutrino mass hierarchy the effective mass $\langle m_\nu \rangle$ relevant for neutrinoless double beta decay would be an interesting observable to analyze, since ongoing $0\nu\beta\beta$ decay experiments are probing the inverted hierarchy region while independent experiments in the near future will determine the neutrino mass hierarchy.

Last but not least the Yukawa sector is the most unsatisfactory part of gauge theories, as it comes along with a huge number of arbitrary parameters. Hence, another possible subject of future studies is the possibility to further constrain the Yukawa coupling matrices, e.g., by applying textures, as outlined in chapter 4 and as we have briefly demonstrated in sec. 5.4

[4]Note the remarks in sec. 8.1 on possible issues with experimental determination of the top-quark mass.

and in the current chapter. This will help in unveiling structures in the Yukawa sector and provide hints to possible fundamental mechanisms governing the Yukawa structure of $SO(10)$ gauge theories.

Chapter 9

Conclusions

In this thesis we performed studies concerning the major open questions in the phenomenology of neutrino physics, namely the precision determination of mixing parameters and the determination of the neutrino mass hierarchy. Then, motivated by a conjectured relation between leptons and quarks, we studied several specific $SO(10)$ GUTs, checked their ability to fit fermion masses and mixings, the Higgs mass and the baryon asymmetry, and investigated their implications for as yet undetermined observables.

The first part of this work studied phenomenological aspects of neutrino physics. Since the literature heavily focuses on the tri-bimaximal mixing scheme, we provided an analysis of a variety of alternative lepton mixing schemes that are in good agreement with present data. Especially in light of recent measurements showing that θ_{13} is not only non-zero but even relatively large, the tri-bimaximal mixing pattern, which has $\theta_{13} = 0$ as a first order approximation, loses its attraction. We also suggested a new alternative mixing scheme, "hexagonal mixing", which has later been realized within a flavor symmetry model [12]. Its consequences are not in perfect agreement with experimental data, so that, besides analyzing the leading order predictions of that scenario (and, in addition, of the "bimaximal" mixing scenario), we showed various possibilities to perturb the leading order and quantified necessary perturbations. We emphasized that it is dangerous to focus only on tri-bimaximal mixing and ignore alternatives.

Furthermore, we examined the prospects of testing and possibly excluding the inverted neutirno mass hierarchy with neutrinoless double beta decay experiments. In this context we found that within its current $3\,\sigma$ range the solar neutrino mixing angle, θ_{12}, introduces an uncertainty of a factor of 1.43 on the minimal value of the effective mass, $\langle m_\nu \rangle$, relevant for $0\nu\beta\beta$ decay. We pointed out that this implies an uncertainty of a factor of $1.43^2 \simeq 2$ on the lifetime needed to experimentally exclude the inverted hierarchy. This then leads, in a background dominated experiment, to an uncertainty of a factor of $1.43^4 \simeq 4.2$ on the combination of isotope mass, background level, energy resolution and measuring time, which together determine the achievable lifetime limit. Since this is a huge factor, we stressed that a precision determination of θ_{12} is of crucial importance to evaluate the physics potential of $0\nu\beta\beta$ decay experiments. The relation between experimentally determined lifetime limits and $\langle m_\nu \rangle$ depends on Nuclear Matrix Elements, which cannot be measured experimentally

and have a large theoretical uncertainty. Therefore, we have taken a pragmatic approach in considering NMEs. We have resolved various convention issues with NME calculations and compiled a list of calculations performed by six different groups for eleven candidate isotopes. We used this compilation (*i*) to give the current limits on the effective mass from different experiments, (*ii*) the necessary half-life sensitivities of experiments using one of those isotopes to test and/or exclude the inverted hierarchy, and (*iii*) to give limits on $\langle m_\nu \rangle$ as a function of reached half-life. In that regard we gave both limits from the largest calculated NME for the particular isotope as well as for the smallest. We found that the isotope ^{100}Mo sets the strongest limits on $\langle m_\nu \rangle$ with the same lifetime limits, which is a potentially interesting observation for upcoming experiments that have not finally decided on which isotope to use.

Then, in the second part of the thesis, we conducted an analysis of different Grand Unified Theories based on $SO(10)$ symmetry. We considered renormalizable $SO(10)$ models based on $10_H + \overline{126}_H$, $120_H + \overline{126}_H$, and $10_H + 120_H + \overline{126}_H$ Higgs representations, assuming type I seesaw dominance. The model with $10_H + 120_H + \overline{126}_H$ Higgs representations was additionally constrained by assuming that parity is violated spontaneously by the vacuum expectation value of 120_H. We performed an analysis of non-supersymmetric models as well as supersymmetric models with different values of $\tan\beta$, and fitted the models to fermion masses and mixings. In addition we included the baryon asymmetry of the universe, assuming its production through thermal leptogenesis and including flavor effects, which is a new aspect of our analysis in the context of $SO(10)$ models. We demonstrated that thermal leptogenesis including matter effects is a viable explanation for the origin of the baryon asymmetry.

In contrast to previous work we performed our fits at M_Z, the mass of the Z boson, performing renormalization group evolution of all parameters during the fitting procedure, and integrating out heavy neutrinos at their respective energy scale. This elaborate and computationally expensive procedure allowed us to study the inverted neutrino mass hierarchy, for which RGE effects are sizable, in addition to the normal hierarchy, which dominates the literature. For comparison, we also performed fits at the GUT scale using parameters evolved to $M_{\rm GUT}$.

In non-SUSY models the RGE of the Higgs quartic coupling, which is related to the Higgs mass, is influenced by the fermion parameters. From the Higgs quartic coupling and the Yukawa couplings of fermions at $M_{\rm GUT}$ the quartic coupling and hence the Higgs mass gets determined at low energies as well. Therefore we included the Higgs mass into our list of observables that constrain non-SUSY models, which has not been done in the literature so far. We showed that this constitutes a strong constraint for the non-SUSY models leading to severe tensions for the top quark mass, which is fitted more than $3\,\sigma$ below the experimental value.

Models based on $10_H + \overline{126}_H$ (M1 and MS[1]) could be fitted to data assuming normal neutrino mass hierarchy, while both models failed to reproduce the data with the inverted

[1]Model names containing the letter "S" refer to supersymmetric models, while those without "S" refer to non-supersymmetric models.

hierarchy and therefore will be excluded if the neutrino mass hierarchy is experimentally determined to be inverted. The alternative model with only two Higgs representations ($120_H + \overline{126}_H$), M2, was excluded firmly for both possibilities of the neutrino mass hierarchy.

Finally, we gave predictions for as yet unmeasured observables. These are the effective mass $\langle m_\nu \rangle$ relevant for neutrinoless double beta decay, the leptonic CP violating phase, δ^l_{CP}, the mass of the lightest neutrino, and for completeness also the masses of the heavy neutrinos. For δ^l_{CP} we analyzed the sensitivity of the models to a deviation of δ^l_{CP} from its value at the best-fit point and we derived the allowed ranges corresponding to 67 % C.L. A similar analysis was performed for θ_{23}. Our analysis yields that model M1 sensitively depends on the value of $\sin^2\theta_{23}$ and prefers a value below the experimental best-fit value, while the other models are not very sensitive to the value of this observable.

For the as yet unmeasured quantity δ^l_{CP} the allowed ranges derived from the fits of the models to data strongly depend on whether one includes RGE or not. At 67 % C.L. the ranges do not even overlap for the same model. Therefore it is fair to stress the importance of including RGE when analyzing model predictions. Another important outcome of our analysis in view of upcoming experiments aiming to measure δ^l_{CP} is that different models are distinguishable by their preferred values for δ^l_{CP}.

Acknowledgments

I would like to thank everyone without whom the completion of this thesis would have been much more difficult.

First of all, I thank my supervisor Werner Rodejohann, for introducing me to the intriguing subject of particle physics, especially to the many fascinating phenomena in neutrino physics, for giving me the opportunity to work on exciting projects and for always taking the time to discuss problems and explain things. Moreover, I would like to thank Werner for letting me attend the SSI summer school. I have learned a lot and spent a great time there. Further, I thank Manfred Lindner for providing an inspiring scientific atmosphere in our division and for giving me the chance to participate in the organization of the ISAPP summer school. I am also thankful to Tilman Plehn for agreeing immediately to be the second referee of my thesis. Thanks as well to Thomas Schwetz for being a delightful office mate and for giving me many advice in statistics and numerics. Thanks a lot to Michael Duerr and James Barry for proof-reading part of this thesis. Another big thank you goes to all the current and former division members who contributed to the great atmosphere and with whom I had a wonderful time and spent many nice hours with coffee and discussions on the roof-deck of our neighboring institute. Anja Berneiser and Britta Schwarz deserve my gratitude for doing all the administrative work in our division without which many things would not go along so smoothly. I owe a lot to my parents, for lots of helpful advice in all circumstances, for your support, and especially for assisting my wife and myself in raising our daughter. It was an incredible aid at any time. Also to my parents-in-law I am very thankful for visiting and supporting my wife and myself in different ways and for helping us to raise our daughter. Last but not least, I thank my beloved wife Evgenia for enriching my life and being such a wonderful woman and my daughter Lisa for amazing me time and again. I know the last weeks (or even months) were not easy for you, but you shall know, I am very happy to have you two.

Appendix A

Nuclear Matrix Elements

Table A.1: Required $0\nu\beta\beta$ decay half-life sensitivity (in 10^{27} yrs) in order to *exclude* the inverted hierarchy for different values of $\sin^2\theta_{12}$. For each value of $\sin^2\theta_{12}$ we present two values/ranges by varying the other parameters which determine the effective mass ($\Delta m^2_{\rm A}$, $\Delta m^2_{\odot}$, $\sin^2\theta_{13}$) in their currently allowed 3σ region. Thereby, for each value of $\sin^2\theta_{12}$, the numbers in the first row correspond to the smallest possible half-lifes while the numbers in the second row correspond to the largest half-lifes. The values calculated using the pseudo-SU(3) NME for ^{150}Nd from ref. [131] are (in the just described order) 2.34, 3.51, 3.77, 5.68, 8.90, 13.5 ($\times 10^{27}$ yrs).

		half-life sensitivity to exclude IH [10^{27} yrs]					
Isotope	$\sin^2\theta_{12}$	NSM [105]	Tü [128, 129]	Jy [130]	IBM [106]	GCM [107]	PHFB [108]
^{48}Ca	0.270	9.88	-	-	-	1.27	-
		14.82	-	-	-	1.91	-
	0.318	15.93	-	-	-	2.05	-
		24.00	-	-	-	3.09	-
	0.380	37.62	-	-	-	4.84	-
		56.92	-	-	-	7.32	-
^{76}Ge	0.270	9.22	1.39 - 3.69	2.54 - 4.13	2.44 - 3.39	3.44	-
		13.82	2.08 - 5.53	3.80 - 6.20	3.65 - 5.08	5.16	-
	0.318	14.86	2.24 - 5.95	4.09 - 6.67	3.93 - 5.46	5.55	-
		22.38	3.37 - 8.96	6.16 - 10.04	5.92 - 8.22	8.35	-
	0.380	35.09	5.28 - 14.05	9.66 - 15.74	9.28 - 12.89	13.09	-
		53.08	7.99 - 21.26	14.62 - 23.82	14.03 - 19.50	19.81	-

Table A.1: (continued)

Isotope	$\sin^2\theta_{12}$	NSM	Tübingen	Jyväskylä	IBM	GCM	PHFB
^{82}Se	0.270	2.41	0.40 - 1.13	1.21 - 1.94	0.86 - 1.16	0.94	-
		3.61	0.60 - 1.70	1.82 - 2.91	1.29 - 1.74	1.41	-
	0.318	3.88	0.65 - 1.83	1.95 - 3.13	1.39 - 1.87	1.52	-
		5.85	0.98 - 2.75	2.94 - 4.71	2.09 - 2.82	2.29	-
	0.380	9.17	1.53 - 4.31	4.61 - 7.39	3.28 - 4.42	3.59	-
		13.88	2.32 - 6.52	6.98 - 11.17	4.97 - 6.68	5.43	-
^{96}Zr	0.270	-	1.51 - 3.31	0.83 - 1.05	1.26	0.25	0.67 - 1.60
		-	2.26 - 4.96	1.24 - 1.58	1.89	0.38	1.01 - 2.41
	0.318	-	2.43 - 5.34	1.34 - 1.70	2.03	0.41	1.08 - 2.59
		-	3.66 - 8.04	2.01 - 2.56	3.06	0.61	1.63 - 3.90
	0.380	-	5.73 - 12.60	3.16 - 4.01	4.79	0.96	2.56 - 6.11
		-	8.67 - 19.06	4.77 - 6.07	7.25	1.45	3.87 - 9.24
^{100}Mo	0.270	-	0.28 - 1.03	0.67 - 1.08	0.58 - 0.75	0.40	0.17 - 0.47
		-	0.42 - 1.55	1.01 - 1.62	0.88 - 1.12	0.60	0.26 - 0.70
	0.318	-	0.46 - 1.66	1.08 - 1.74	0.94 - 1.20	0.65	0.28 - 0.76
		-	0.69 - 2.51	1.63 - 2.62	1.42 - 1.81	0.98	0.42 - 1.14
	0.380	-	1.08 - 3.93	2.56 - 4.11	2.23 - 2.84	1.53	0.66 - 1.78
		-	1.63 - 5.94	3.88 - 6.22	3.37 - 4.30	2.32	0.99 - 2.70
^{110}Pd	0.270	-	-	-	2.47	-	0.41 - 1.14
		-	-	-	3.70	-	0.61 - 1.71
	0.318	-	-	-	3.98	-	0.66 - 1.84
		-	-	-	5.99	-	0.99 - 2.77
	0.380	-	-	-	9.39	-	1.55 - 4.34
		-	-	-	14.21	-	2.35 - 6.57
^{116}Cd	0.270	-	0.48 - 1.56	0.63 - 1.09	1.27	0.44	-
		-	0.72 - 2.34	0.95 - 1.64	1.90	0.66	-
	0.318	-	0.78 - 2.51	1.02 - 1.76	2.04	0.71	-
		-	1.17 - 3.79	1.54 - 2.66	3.08	1.07	-
	0.380	-	1.83 - 5.93	2.41 - 4.16	4.83	1.68	-
		-	2.77 - 8.98	3.65 - 6.30	7.30	2.54	-
^{124}Sn	0.270	2.59	-	-	-	0.77	-
		3.88	-	-	-	1.15	-
	0.318	4.18	-	-	-	1.24	-
		6.29	-	-	-	1.87	-
	0.380	9.86	-	-	-	2.93	-
		14.92	-	-	-	4.43	-

Table A.1: (continued)

Isotope	$\sin^2\theta_{12}$	NSM	Tübingen	Jyväskylä	IBM	GCM	PHFB
^{130}Te	0.270	1.58	0.37 - 1.09	0.62 - 0.91	0.67 - 0.97	0.42	0.42 - 1.24
		2.37	0.55 - 1.64	0.93 - 1.37	1.01 - 1.46	0.63	0.63 - 1.86
	0.318	2.55	0.59 - 1.76	1.00 - 1.47	1.08 - 1.57	0.68	0.68 - 2.00
		3.83	0.89 - 2.65	1.51 - 2.22	1.63 - 2.37	1.02	1.03 - 3.01
	0.380	6.01	1.40 - 4.16	2.37 - 3.48	2.56 - 3.71	1.60	1.61 - 4.72
		9.09	2.11 - 6.29	3.58 - 5.26	3.88 - 5.61	2.43	2.44 - 7.14
^{136}Xe	0.270	2.19	0.84 - 3.59	1.34 - 1.86	0.94	0.60	-
		3.29	1.26 - 5.38	2.01 - 2.78	1.40	0.89	-
	0.318	3.54	1.36 - 5.78	2.16 - 2.99	1.51	0.96	-
		5.33	2.04 - 8.71	3.25 - 4.51	2.27	1.45	-
	0.380	8.35	3.21 - 13.65	5.10 - 7.07	3.56	2.27	-
		12.63	4.85 - 20.65	7.72 - 10.70	5.39	3.43	-
^{150}Nd	0.270	-	0.20	-	0.28 - 0.44	0.81	0.17 - 0.60
		-	0.30	-	0.42 - 0.66	1.21	0.26 - 0.90
	0.318	-	0.32	-	0.46 - 0.71	1.30	0.28 - 0.97
		-	0.48	-	0.69 - 1.06	1.96	0.42 - 1.46
	0.380	-	0.76	-	1.08 - 1.67	3.07	0.66 - 2.29
		-	1.14	-	1.63 - 2.52	4.65	0.99 - 3.47

Table A.2: Same as tbl. A.1, but here the required $0\nu\beta\beta$ decay half-life sensitivity in order to *touch* the inverted hierarchy is given. For the pseudo-SU(3) NME for ^{150}Nd we get the values 0.49, 0.72 ($\times 10^{27}$ yrs).

	half-life sensitivity to touch IH [10^{27} yrs]					
Isotope	NSM [105]	Tü [128, 129]	Jy [130]	IBM [106]	GCM [107]	PHFB [108]
^{48}Ca	2.05	-	-	-	0.26	-
	3.03	-	-	-	0.39	-
^{76}Ge	1.91	0.29 - 0.77	0.53 - 0.86	0.51 - 0.70	0.71	-
	2.82	0.42 - 1.13	0.78 - 1.27	0.75 - 1.04	1.05	-
^{82}Se	0.50	0.08 - 0.24	0.25 - 0.40	0.18 - 0.24	0.20	-
	0.74	0.12 - 0.35	0.37 - 0.59	0.26 - 0.36	0.29	-
^{96}Zr	-	0.31 - 0.69	0.17 - 0.22	0.26	0.05	0.14 - 0.33
	-	0.46 - 1.01	0.25 - 0.32	0.39	0.08	0.21 - 0.49
^{100}Mo	-	0.06 - 0.21	0.14 - 0.22	0.12 - 0.16	0.08	0.04 - 0.10
	-	0.09 - 0.32	0.21 - 0.33	0.18 - 0.23	0.12	0.05 - 0.14

Table A.2: (continued)

Isotope	NSM	Tübingen	Jyväskylä	IBM	GCM	PHFB
^{110}Pd	-	-	-	0.51	-	0.08 - 0.24
	-	-	-	0.76	-	0.12 - 0.35
^{116}Cd	-	0.10 - 0.32	0.13 - 0.23	0.26	0.09	-
	-	0.15 - 0.48	0.19 - 0.33	0.39	0.13	-
^{124}Sn	0.54	-	-	-	0.16	-
	0.79	-	-	-	0.24	-
^{130}Te	0.33	0.08 - 0.23	0.13 - 0.19	0.14 - 0.20	0.09	0.09 - 0.26
	0.48	0.11 - 0.33	0.19 - 0.28	0.21 - 0.30	0.13	0.13 - 0.38
^{136}Xe	0.46	0.17 - 0.74	0.28 - 0.39	0.19	0.12	-
	0.67	0.26 - 1.10	0.41 - 0.57	0.29	0.18	-
^{150}Nd	-	0.04	-	0.06 - 0.09	0.17	0.04 - 0.13
	-	0.06	-	0.09 - 0.13	0.25	0.05 - 0.18

Appendix B

Best-Fit Parameters

To reproduce our claimed χ^2 values as reported in chapter 8 the reader can make use of our best-fit parameters which we present in the following. The notation is as in eqn. (5.1) on page 49.

B.1 Minimal Models with $10_H + \overline{126}_H$

Since in these models only the normal neutrino mass hierarchy is viable we give the best-fit parameters only for that case.

M1, no RGE:

$$
\begin{aligned}
r &= 68.9624,\ s = 0.370726 + 0.063044i,\ r_R = 5.242 \times 10^{-14} \\
H &= \begin{pmatrix} 1.22387\times10^{-6} & 0 & 0 \\ 0 & 5.92428\times10^{-5} & 0 \\ 0 & 0 & 6.29473\times10^{-3} \end{pmatrix} \\
F &= \begin{pmatrix} -2.95102\times10^{-6}-3.48291\times10^{-6}i & 1.27484\times10^{-5}-7.53714\times10^{-8}i & 1.07772\times10^{-4}+6.02931\times10^{-5}i \\ 1.27484\times10^{-5}-7.53714\times10^{-8}i & -1.538\times10^{-4}+6.75236\times10^{-5}i & -2.67281\times10^{-4}+2.48978\times10^{-4}i \\ 1.07772\times10^{-4}+6.02931\times10^{-5}i & -2.67281\times10^{-4}+2.48978\times10^{-4}i & -7.38503\times10^{-4}-1.44559\times10^{-3}i \end{pmatrix}.
\end{aligned}
\tag{B.1}
$$

M1, RGE, Yb:

$$
\begin{aligned}
r &= -63.979,\ s = 0.40957 - 0.04238i,\ r_R = 5.68 \times 10^{-14} \\
H &= \begin{pmatrix} 1.28602\times10^{-6} & 0 & 0 \\ 0 & 6.86819\times10^{-5} & 0 \\ 0 & 0 & 6.67018\times10^{-3} \end{pmatrix} \\
F &= \begin{pmatrix} -2.97805\times10^{-6}+7.15644\times10^{-6}i & -1.1859\times10^{-5}+1.38959\times10^{-5}i & -1.52327\times10^{-4}+7.61554\times10^{-5}i \\ -1.1859\times10^{-5}+1.38959\times10^{-5}i & -2.1014\times10^{-4}-1.0501\times10^{-5}i & -3.82533\times10^{-4}-2.10519\times10^{-4}i \\ -1.52327\times10^{-4}+7.61554\times10^{-5}i & -3.82533\times10^{-4}-2.10519\times10^{-4}i & -6.39929\times10^{-4}-7.56101\times10^{-4}i \end{pmatrix}
\end{aligned}
\tag{B.2}
$$

$$
\begin{aligned}
&\underline{\text{MS, } \tan\beta = 50, \text{ no RGE:}} \\
r &= -0.0394977,\ r_R = 2.07005 \times 10^{-12},\ s = 0.347444 + 9.61963 \times 10^{-3} i \\
H &= \begin{pmatrix} -1.49207\times10^{-3} & 0 & 0 \\ 0 & -14.0362 & 0 \\ 0 & 0 & -0.0908578 \end{pmatrix} \\
F &= \begin{pmatrix} 4.32185\times10^{-3}+5.61316\times10^{-3}i & -0.197135-0.117485i & -0.0204746+3.12687\times10^{-3}i \\ -0.197135-0.117485i & 0.851729+2.13093i & 0.528677-0.504235i \\ -0.0204746+3.12687\times10^{-3}i & 0.528677-0.504235i & 0.243146-0.0832618i \end{pmatrix}.
\end{aligned}
\tag{B.3}
$$

$$
\begin{aligned}
&\underline{\text{MS, } \tan\beta = 50, \text{ RGE, Yb:}} \\
r &= 1.87403,\ s = 0.240062 + 0.104276i,\ r_R = -1.83955 \times 10^{-13} \\
H &= \begin{pmatrix} -3.53365\times10^{-5} & 0 & 0 \\ 0 & -6.21061\times10^{-1} & 0 \\ 0 & 0 & 2.86617\times10^{-3} \end{pmatrix} \\
F &= \begin{pmatrix} -2.00425\times10^{-6}-5.84654\times10^{-6}i & 1.82178\times10^{-3}+2.24413\times10^{-3}i & -5.30888\times10^{-4}-4.77251\times10^{-4}i \\ 1.82178\times10^{-3}+2.24413\times10^{-3}i & -9.88137\times10^{-3}+7.39686\times10^{-2}i & -1.91744\times10^{-2}+1.74681\times10^{-2}i \\ -5.30888\times10^{-4}-4.77251\times10^{-4}i & -1.91744\times10^{-2}+1.74681\times10^{-2}i & -9.04751\times10^{-3}+4.41955\times10^{-4}i \end{pmatrix}
\end{aligned}
\tag{B.4}
$$

$$
\begin{aligned}
&\underline{\text{MS, } \tan\beta = 38, \text{ no RGE:}} \\
r &= -0.0444144,\ r_R = 2.23703 \times 10^{-12},\ s = 0.347775 + 7.69997 \times 10^{-3} i \\
H &= \begin{pmatrix} -1.51963\times10^{-3} & 0 & 0 \\ 0 & -12.4872 & 0 \\ 0 & 0 & -0.087355 \end{pmatrix} \\
F &= \begin{pmatrix} 4.60689\times10^{-3}+5.08851\times10^{-3}i & -0.18755-0.102547i & -0.0185995+3.06334\times10^{-3}i \\ -0.18755-0.102547i & 0.751717+1.87754i & 0.495974-0.461167i \\ -0.0185995+3.06334\times10^{-3}i & 0.495974-0.461167i & 0.23599-0.0755543i \end{pmatrix}
\end{aligned}
\tag{B.5}
$$

$$
\begin{aligned}
&\underline{\text{MS, } \tan\beta = 38, \text{ Yb:}} \\
r &= 2.9304,\ r_R = -1.23359 \times 10^{-13},\ s = 0.234158 + 0.116316i \\
H &= \begin{pmatrix} -2.28837\times10^{-5} & 0 & 0 \\ 0 & -0.314998 & 0 \\ 0 & 0 & 1.75335\times10^{-3} \end{pmatrix} \\
F &= \begin{pmatrix} -3.14214\times10^{-6}-2.66257\times10^{-6}i & 1.16818\times10^{-3}+1.29339\times10^{-3}i & -3.56301\times10^{-4}-2.66376\times10^{-4}i \\ 1.16818\times10^{-3}+1.29339\times10^{-3}i & 2.07503\times10^{-3}+0.0332639i & -8.95296\times10^{-3}+0.0105406i \\ -3.56301\times10^{-4}-2.66376\times10^{-4}i & -8.95296\times10^{-3}+0.0105406i & -5.73547\times10^{-3}+6.461\times10^{-4}i \end{pmatrix}
\end{aligned}
\tag{B.6}
$$

$$
\begin{aligned}
&\underline{\text{MS, } \tan\beta = 10, \text{ no RGE:}} \\
r &= -0.0419971,\ r_R = 8.18157 \times 10^{-12},\ s = 0.352986 + 9.48929 \times 10^{-3} i \\
H &= \begin{pmatrix} -1.91347\times10^{-3} & 0 & 0 \\ 0 & -12.9162 & 0 \\ 0 & 0 & -0.100279 \end{pmatrix} \\
F &= \begin{pmatrix} 5.82177\times10^{-3}+5.63088\times10^{-3}i & -0.210036-0.107523i & -0.0200288+2.51356\times10^{-3}i \\ -0.210036-0.107523i & 0.785625+2.00532i & 0.554479-0.479238i \\ -0.0200288+2.51356\times10^{-3}i & 0.554479-0.479238i & 0.275304-0.0811409i \end{pmatrix}
\end{aligned}
\tag{B.7}
$$

$$
\begin{aligned}
&\underline{\text{MS, } \tan\beta = 10, \text{ Yb:}} \\
r &= 12.8528,\ r_R = -9.26868 \times 10^{-14},\ s = 0.231781 + 0.122565i \\
H &= \begin{pmatrix} -5.48738\times10^{-6} & 0 & 0 \\ 0 & -0.0638928 & 0 \\ 0 & 0 & 3.98601\times10^{-4} \end{pmatrix} \\
F &= \begin{pmatrix} -1.1422\times10^{-6}-2.85981\times10^{-7}i & 2.79206\times10^{-4}+2.88156\times10^{-4}i & 8.67453\times10^{-5}+5.53426\times10^{-5}i \\ 2.79206\times10^{-4}+2.88156\times10^{-4}i & 1.39701\times10^{-3}+6.04744\times10^{-3}i & 1.64572\times10^{-3}-2.37702\times10^{-3}i \\ 8.67453\times10^{-5}+5.53426\times10^{-5}i & 1.64572\times10^{-3}-2.37702\times10^{-3}i & -1.34125\times10^{-3}+1.99137\times10^{-4}i \end{pmatrix}
\end{aligned}
\tag{B.8}
$$

B.2 Models with $10_H + \overline{126}_H + 120_H$

B.2.1 Normal Neutrino Mass Hierarchy

$$
\begin{aligned}
&\underline{\text{F1, no RGE:}} \\
r &= 67.1992,\ r_R = -2.68132 \times 10^{-14},\ s = -2.0155,\ t_l = 1.09375, \\
t_u &= -0.973721,\ t_D = -4.11394 \\
H &= \begin{pmatrix} -1.44349\times10^{-3} & 0 & 0 \\ 0 & -2.12083\times10^{-4} & 0 \\ 0 & 0 & 8.38498\times10^{-6} \end{pmatrix} \\
F &= \begin{pmatrix} -3.52616\times10^{-3} & -1.87525\times10^{-5} & -3.01471\times10^{-5} \\ -1.87525\times10^{-5} & -4.43985\times10^{-4} & -2.33814\times10^{-5} \\ -3.01471\times10^{-5} & -2.33814\times10^{-5} & 1.94067\times10^{-6} \end{pmatrix} \\
G &= \begin{pmatrix} 0 & 1.98673\times10^{-3} & 1.36719\times10^{-4} \\ -1.98673\times10^{-3} & 0 & -1.67619\times10^{-5} \\ -1.36719\times10^{-4} & 1.67619\times10^{-5} & 0 \end{pmatrix}
\end{aligned}
\tag{B.9}
$$

$$
\begin{aligned}
&\underline{\text{F1, Yb:}} \\
r &= 64.0686,\ r_R = 2.21836 \times 10^{-16},\ s = 0.52205,\ t_l = 3.62469, \\
t_u &= -0.0599559,\ t_D = -48.4291 \\
H &= \begin{pmatrix} 4.35196\times10^{-6} & 0 & 0 \\ 0 & 6.75021\times10^{-3} & 0 \\ 0 & 0 & 1.61699\times10^{-4} \end{pmatrix} \\
F &= \begin{pmatrix} -7.11126\times10^{-6} & 2.90761\times10^{-5} & 7.12292\times10^{-6} \\ 2.90761\times10^{-5} & -7.59548\times10^{-4} & 5.78627\times10^{-4} \\ 7.12292\times10^{-6} & 5.78627\times10^{-4} & -2.41147\times10^{-4} \end{pmatrix} \\
G &= \begin{pmatrix} 0 & -2.37538\times10^{-5} & 3.60133\times10^{-5} \\ 2.37538\times10^{-5} & 0 & 2.80901\times10^{-5} \\ -3.60133\times10^{-5} & -2.80901\times10^{-5} & 0 \end{pmatrix}
\end{aligned}
\tag{B.10}
$$

FS, $\tan\beta = 50$, no RGE:

$$
\begin{aligned}
r &= -0.209965,\ r_R = -3.59161 \times 10^{-14},\ s = -3.15082,\ t_l = 164.558 \\
t_u &= -18.4887,\ t_D = 1.98859 \\
H &= \begin{pmatrix} -0.0246111 & 0 & 0 \\ 0 & 2.11922 & 0 \\ 0 & 0 & 1.16561\times10^{-3} \end{pmatrix} \\
F &= \begin{pmatrix} -6.79587\times10^{-3} & 0.0141982 & 9.32493\times10^{-6} \\ 0.0141982 & -0.149691 & 4.06145\times10^{-3} \\ 9.32493\times10^{-6} & 4.06145\times10^{-3} & 4.49951\times10^{-4} \end{pmatrix} \\
G &= \begin{pmatrix} 0 & 3.58503\times10^{-3} & 4.93814\times10^{-5} \\ -3.58503\times10^{-3} & 0 & 1.87896\times10^{-4} \\ -4.93814\times10^{-5} & -1.87896\times10^{-4} & 0 \end{pmatrix}
\end{aligned}
\tag{B.11}
$$

FS, $\tan\beta = 50$, Y_B:

$$
\begin{aligned}
r &= -2.26196,\ r_R = -2.3532 \times 10^{-14},\ s = 0.529663,\ t_l = -1.14214, \\
t_u &= 0.653981,\ t_D = -0.196641 \\
H &= \begin{pmatrix} -5.22948\times10^{-4} & 0 & 0 \\ 0 & -0.316395 & 0 \\ 0 & 0 & -0.0129173 \end{pmatrix} \\
F &= \begin{pmatrix} 3.08209\times10^{-4} & 9.844\times10^{-3} & 4.37817\times10^{-3} \\ 9.844\times10^{-3} & -0.293268 & 1.73134\times10^{-3} \\ 4.37817\times10^{-3} & 1.73134\times10^{-3} & -0.0100588 \end{pmatrix} \\
G &= \begin{pmatrix} 0 & -0.0173859 & 1.66654\times10^{-3} \\ 0.0173859 & 0 & -0.138353 \\ -1.66654\times10^{-3} & 0.138353 & 0 \end{pmatrix}
\end{aligned}
\tag{B.12}
$$

B.2.2 Inverted Neutrino Mass Hierarchy

F1, no RGE:

$$
\begin{aligned}
r &= -71.6954,\ r_R = 1.08602 \times 10^{-14},\ s = 0.710962,\ t_l = -11.9888 \\
t_u &= -0.049547,\ t_D = 21.5488 \\
H &= \begin{pmatrix} 6.47261\times10^{-3} & 0 & 0 \\ 0 & 2.64518\times10^{-4} & 0 \\ 0 & 0 & 4.10329\times10^{-5} \end{pmatrix} \\
F &= \begin{pmatrix} -8.37936\times10^{-4} & -8.11918\times10^{-4} & 5.65936\times10^{-6} \\ -8.11918\times10^{-4} & -2.65901\times10^{-4} & 1.47332\times10^{-6} \\ 5.65936\times10^{-6} & 1.47332\times10^{-6} & -5.74189\times10^{-5} \end{pmatrix} \\
G &= \begin{pmatrix} 0 & -9.67226\times10^{-8} & -2.30032\times10^{-5} \\ 9.67226\times10^{-8} & 0 & -2.9926\times10^{-5} \\ 2.30032\times10^{-5} & 2.9926\times10^{-5} & 0 \end{pmatrix}
\end{aligned}
\tag{B.13}
$$

F1, Y_B:

$$
\begin{aligned}
r &= 70.5434,\ r_R = 7.01661 \times 10^{-18},\ s = 0.168991,\ t_l = -5.0025 \\
t_u &= -0.117865,\ t_D = -330.576 \\
H &= \begin{pmatrix} 5.42957\times10^{-6} & 0 & 0 \\ 0 & 7.7751\times10^{-3} & 0 \\ 0 & 0 & 6.62089\times10^{-5} \end{pmatrix} \\
F &= \begin{pmatrix} -2.29305\times10^{-5} & 1.13395\times10^{-5} & 2.01936\times10^{-5} \\ 1.13395\times10^{-5} & -3.39687\times10^{-4} & 3.80432\times10^{-4} \\ 2.01936\times10^{-5} & 3.80432\times10^{-4} & -2.5007\times10^{-4} \end{pmatrix} \\
G &= \begin{pmatrix} 0 & -5.36576\times10^{-5} & 4.07349\times10^{-5} \\ 5.36576\times10^{-5} & 0 & 1.54679\times10^{-4} \\ -4.07349\times10^{-5} & -1.54679\times10^{-4} & 0 \end{pmatrix}
\end{aligned}
\tag{B.14}
$$

FS, $\tan\beta = 50$, no RGE:

$$
\begin{aligned}
r &= 4.05193,\ r_R = 4.5708 \times 10^{-14},\ s = 0.146437,\ t_l = -1.88674 \\
t_u &= -0.143497,\ t_D = -5.43533 \times 10^{-3} \\
H &= \begin{pmatrix} -5.64699\times10^{-5} & 0 & 0 \\ 0 & -0.111019 & 0 \\ 0 & 0 & -9.28316\times10^{-4} \end{pmatrix} \\
F &= \begin{pmatrix} 8.11456\times10^{-7} & 1.29532\times10^{-4} & 3.93343\times10^{-5} \\ 1.29532\times10^{-4} & -0.159366 & 0.0133342 \\ 3.93343\times10^{-5} & 0.0133342 & 4.41386\times10^{-3} \end{pmatrix} \\
G &= \begin{pmatrix} 0 & -3.1015\times10^{-3} & -7.83212\times10^{-4} \\ 3.1015\times10^{-3} & 0 & 1.02167\times10^{-3} \\ 7.83212\times10^{-4} & -1.02167\times10^{-3} & 0 \end{pmatrix}
\end{aligned}
\tag{B.15}
$$

FS, $\tan\beta = 50$, no Y_B:

$$
\begin{aligned}
r &= -2.76923,\ r_R = 9.12617 \times 10^{-14},\ s = 0.239831,\ t_l = -1.23885 \\
t_u &= -0.0166744,\ t_D = 1.12799 \times 10^{-6} \\
H &= \begin{pmatrix} 0.327384 & 0 & 0 \\ 0 & -5.97675\times10^{-7} & 0 \\ 0 & 0 & 2.39637\times10^{-3} \end{pmatrix} \\
F &= \begin{pmatrix} 0.309553 & 3.84441\times10^{-6} & -0.0201878 \\ 3.84441\times10^{-6} & -3.51744\times10^{-10} & 1.65759\times10^{-6} \\ -0.0201878 & 1.65759\times10^{-6} & -6.76014\times10^{-3} \end{pmatrix} \\
G &= \begin{pmatrix} 0 & 1.98713\times10^{-3} & 0.0152033 \\ -1.98713\times10^{-3} & 0 & -1.47992\times10^{-3} \\ -0.0152033 & 1.47992\times10^{-3} & 0 \end{pmatrix}
\end{aligned}
\tag{B.16, B.17}
$$

$$
\begin{aligned}
& \underline{\text{FS, } \tan\beta = 50,\ Y_B\text{:}} \\
r \;&= 3.60572 \times 10^4,\ r_R = 1.3255 \times 10^{-13},\ s = 0.210408,\ t_l = -16.5989 \\
t_u \;&= 0.0303395,\ t_D = -9.12678 \times 10^{-6} \\
H \;&= \begin{pmatrix} -2.39089\times10^{-5} & 0 & 0 \\ 0 & 3.55518 & 0 \\ 0 & 0 & 9.66883\times10^{-6} \end{pmatrix} \\
F \;&= \begin{pmatrix} -7.60456\times10^{-5} & 0.0142587 & -4.52065\times10^{-7} \\ 0.0142587 & 0.190489 & 1.34711\times10^{-4} \\ -4.52065\times10^{-7} & 1.34711\times10^{-4} & -4.66866\times10^{-5} \end{pmatrix} \\
G \;&= \begin{pmatrix} 0 & 0.0194477 & -5.38536\times10^{-5} \\ -0.0194477 & 0 & 2.16164\times10^{-3} \\ 5.38536\times10^{-5} & -2.16164\times10^{-3} & 0 \end{pmatrix}
\end{aligned}
\tag{B.18}
$$

Appendix C

Beta-Functions for RG Evolution

To calculate the RG evolution of observables, RGEs for all parameters of the model under consideration have to be solved simultaneously. Here we summarize 1-loop RGEs for the SM and the MSSM extended by an arbitrary number of right-handed singlet neutrinos. The notation is as in refs. [197, 248]. In particular, we denote a quantity between the nth and $(n+1)$th mass threshold with a superscript (n). For further details including 2-loop beta-functions, we refer the reader to [192, 248, 271–273].

The beta-functions of the gauge couplings are not affected by the additional singlets at 1-loop order. They are given by

$$16\pi^2\,\beta_{g_A} \equiv 16\pi^2\,\mu\frac{g_A}{\mu} = b_A\,g_A^3\,, \tag{C.1}$$

with $(b_{\mathrm{SU(3)_C}}, b_{\mathrm{SU(2)_L}}, b_{\mathrm{U(1)_Y}}) = (-7, -\frac{19}{6}, \frac{41}{10})$ in the SM and $(-3, 1, \frac{33}{5})$ in the MSSM. For the $\mathrm{U(1)_Y}$ charge we use GUT normalization.

C.1 Beta-Functions in the Extended SM

The β-functions governing RG evolution in the SM extended by singlet neutrinos are given by [197, 248, 274]

$$
\begin{aligned}
16\pi^2 \overset{(n)}{\beta}_\kappa &= -\frac{3}{2}(Y_e^\dagger Y_e)^T \overset{(n)}{\kappa} - \frac{3}{2}\overset{(n)}{\kappa}(Y_e^\dagger Y_e) + \frac{1}{2}\big(\overset{(n)}{Y_\nu^\dagger}\overset{(n)}{Y_\nu}\big)^T \overset{(n)}{\kappa} + \frac{1}{2}\overset{(n)}{\kappa}\big(\overset{(n)}{Y_\nu^\dagger}\overset{(n)}{Y_\nu}\big) \\
&\quad + 2\ \mathrm{Tr}(Y_e^\dagger Y_e)\overset{(n)}{\kappa} + 2\ \mathrm{Tr}\big(\overset{(n)}{Y_\nu^\dagger}\overset{(n)}{Y_\nu}\big)\overset{(n)}{\kappa} + 6\ \mathrm{Tr}(Y_u^\dagger Y_u)\overset{(n)}{\kappa} \\
&\quad + 6\ \mathrm{Tr}(Y_d^\dagger Y_d)\overset{(n)}{\kappa} - 3g_2^2\overset{(n)}{\kappa} + \overset{(n)}{\lambda\kappa}\,, && \text{(C.2a)} \\
16\pi^2 \overset{(n)}{\beta}_M &= \big(\overset{(n)}{Y_\nu}\overset{(n)}{Y_\nu^\dagger}\big)\overset{(n)}{M} + \overset{(n)}{M}\big(\overset{(n)}{Y_\nu}\overset{(n)}{Y_\nu^\dagger}\big)^T\,, && \text{(C.2b)} \\
16\pi^2 \overset{(n)}{\beta}_{Y_\nu} &= \overset{(n)}{Y_\nu}\left\{\frac{3}{2}\big(\overset{(n)}{Y_\nu^\dagger}\overset{(n)}{Y_\nu}\big) - \frac{3}{2}(Y_e^\dagger Y_e) + \mathrm{Tr}\big(\overset{(n)}{Y_\nu^\dagger}\overset{(n)}{Y_\nu}\big) + \mathrm{Tr}(Y_e^\dagger Y_e)\right. \\
&\quad \left. + 3\ \mathrm{Tr}(Y_u^\dagger Y_u) + 3\ \mathrm{Tr}(Y_d^\dagger Y_d) - \frac{9}{20}g_1^2 - \frac{9}{4}g_2^2\right\}, && \text{(C.2c)} \\
16\pi^2 \overset{(n)}{\beta}_{Y_e} &= Y_e\left\{\frac{3}{2}Y_e^\dagger Y_e - \frac{3}{2}\overset{(n)}{Y_\nu^\dagger}\overset{(n)}{Y_\nu} - \frac{9}{4}g_1^2 - \frac{9}{4}g_2^2\right. \\
&\quad \left. + \mathrm{Tr}\left[Y_e^\dagger Y_e + \overset{(n)}{Y_\nu^\dagger}\overset{(n)}{Y_\nu} + 3\,Y_d^\dagger Y_d\ + 3\,Y_u^\dagger Y_u\right]\right\}, && \text{(C.2d)} \\
16\pi^2 \overset{(n)}{\beta}_{Y_d} &= Y_d\left\{\frac{3}{2}Y_d^\dagger Y_d - \frac{3}{2}\,Y_u^\dagger Y_u - \frac{1}{4}g_1^2 - \frac{9}{4}g_2^2 - 8\,g_3^2\right. \\
&\quad \left. + \mathrm{Tr}\left[Y_e^\dagger Y_e + \overset{(n)}{Y_\nu^\dagger}\overset{(n)}{Y_\nu} + 3\,Y_d^\dagger Y_d + 3\,Y_u^\dagger Y_u\right]\right\}, && \text{(C.2e)} \\
16\pi^2 \overset{(n)}{\beta}_{Y_u} &= Y_u\left\{\frac{3}{2}Y_u^\dagger Y_u - \frac{3}{2}\,Y_d^\dagger Y_d - \frac{17}{20}g_1^2 - \frac{9}{4}g_2^2 - 8\,g_3^2\right. \\
&\quad \left. + \mathrm{Tr}\left[Y_e^\dagger Y_e + \overset{(n)}{Y_\nu^\dagger}\overset{(n)}{Y_\nu} + 3\,Y_d^\dagger Y_d + 3\,Y_u^\dagger Y_u\right]\right\}, && \text{(C.2f)} \\
16\pi^2 \overset{(n)}{\beta}_\lambda &= 6\,\lambda^2 - 3\,\lambda\left(3g_2^2 + \frac{3}{5}g_1^2\right) + 3\,g_2^4 + \frac{3}{2}\left(\frac{3}{5}g_1^2 + g_2^2\right)^2 \\
&\quad + 4\,\lambda\ \mathrm{Tr}\left[Y_e^\dagger Y_e + \overset{(n)}{Y_\nu^\dagger}\overset{(n)}{Y_\nu} + 3\,Y_d^\dagger Y_d + 3\,Y_u^\dagger Y_u\right] && \text{(C.2g)} \\
&\quad - 8\ \mathrm{Tr}\left[Y_e^\dagger Y_e\, Y_e^\dagger Y_e + \overset{(n)}{Y_\nu^\dagger}\overset{(n)}{Y_\nu}\,\overset{(n)}{Y_\nu^\dagger}\overset{(n)}{Y_\nu} + 3\,Y_d^\dagger Y_d\, Y_d^\dagger Y_d + 3\,Y_u^\dagger Y_u\, Y_u^\dagger Y_u\right].
\end{aligned}
$$

Note our convention that the Higgs self-interaction term in the Lagrangian is $-\frac{\lambda}{4}(\phi^\dagger\phi)^2$.

C.2 Beta-Functions in the Extended MSSM

The 1-loop beta-functions of the MSSM extended by heavy singlets are given by [197, 248, 275]

$$\begin{aligned}
16\pi^2 \overset{(n)}{\beta}_{\kappa} &= (Y_e^\dagger Y_e)^T \overset{(n)}{\kappa} + \overset{(n)}{\kappa} (Y_e^\dagger Y_e) + \left(\overset{(n)}{Y}_\nu^\dagger \overset{(n)}{Y}_\nu\right)^T \overset{(n)}{\kappa} + \overset{(n)}{\kappa} \left(\overset{(n)}{Y}_\nu^\dagger \overset{(n)}{Y}_\nu\right) \\
&\quad + 2\,\mathrm{Tr}\left(\overset{(n)}{Y}_\nu^\dagger \overset{(n)}{Y}_\nu\right) \overset{(n)}{\kappa} + 6\,\mathrm{Tr}(Y_u^\dagger Y_u) \overset{(n)}{\kappa} - \frac{6}{5} g_1^2 \overset{(n)}{\kappa} - 6 g_2^2 \overset{(n)}{\kappa}\,, \qquad \text{(C.3a)} \\
16\pi^2 \overset{(n)}{\beta}_{M} &= 2\left(\overset{(n)}{Y}_\nu \overset{(n)}{Y}_\nu^\dagger\right) \overset{(n)}{M} + 2\,\overset{(n)}{M} \left(\overset{(n)}{Y}_\nu \overset{(n)}{Y}_\nu^\dagger\right)^T, \qquad \text{(C.3b)} \\
16\pi^2 \overset{(n)}{\beta}_{Y_\nu} &= \overset{(n)}{Y}_\nu \left\{ 3 \overset{(n)}{Y}_\nu^\dagger \overset{(n)}{Y}_\nu + Y_e^\dagger Y_e + \mathrm{Tr}\left(\overset{(n)}{Y}_\nu^\dagger \overset{(n)}{Y}_\nu\right) + 3\,\mathrm{Tr}(Y_u^\dagger Y_u) - \frac{3}{5} g_1^2 - 3 g_2^2 \right\}, \qquad \text{(C.3c)} \\
16\pi^2 \overset{(n)}{\beta}_{Y_d} &= Y_d \left\{ 3 Y_d^\dagger Y_d + Y_u^\dagger Y_u + 3\,\mathrm{Tr}(Y_d^\dagger Y_d) + \mathrm{Tr}(Y_e^\dagger Y_e) - \frac{7}{15} g_1^2 - 3 g_2^2 - \frac{16}{3} g_3^2 \right\}, \qquad \text{(C.3d)} \\
16\pi^2 \overset{(n)}{\beta}_{Y_u} &= Y_u \left\{ Y_d^\dagger Y_d + 3 Y_u^\dagger Y_u + \mathrm{Tr}(\overset{(n)}{Y}_\nu^\dagger \overset{(n)}{Y}_\nu) + 3\,\mathrm{Tr}(Y_u^\dagger Y_u) - \frac{13}{15} g_1^2 - 3 g_2^2 - \frac{16}{3} g_3^2 \right\}, \qquad \text{(C.3e)} \\
16\pi^2 \overset{(n)}{\beta}_{Y_e} &= Y_e \left\{ 3 Y_e^\dagger Y_e + \overset{(n)}{Y}_\nu^\dagger \overset{(n)}{Y}_\nu + 3\,\mathrm{Tr}(Y_d^\dagger Y_d) + \mathrm{Tr}(Y_e^\dagger Y_e) - \frac{9}{5} g_1^2 - 3 g_2^2 \right\}. \qquad \text{(C.3f)}
\end{aligned}$$

Bibliography

[1] **Super-Kamiokande** Collaboration, Y. Fukuda *et al.*, "Evidence for oscillation of atmospheric neutrinos," *Phys.Rev.Lett.* **81** (1998) 1562–1567, arXiv:hep-ex/9807003 [hep-ex].

[2] B. Cleveland, T. Daily, J. Davis, Raymond, J. R. Distel, K. Lande, *et al.*, "Measurement of the solar electron neutrino flux with the Homestake chlorine detector," *Astrophys.J.* **496** (1998) 505–526.

[3] G. Bertone and J. Silk, "Particle dark matter,".

[4] M. Milgrom, "A Modification of the Newtonian dynamics as a possible alternative to the hidden mass hypothesis," *Astrophys.J.* **270** (1983) 365–370.

[5] T. Tomoda, "Double beta decay," *Rep. Prog. Phys.* **54** (1991) 53–126.

[6] P. Harrison, D. Perkins, and W. Scott, "Tri-bimaximal mixing and the neutrino oscillation data," *Phys.Lett.* **B530** (2002) 167, hep-ph/0202074.

[7] G. Altarelli and F. Feruglio, "Discrete Flavor Symmetries and Models of Neutrino Mixing," *Rev.Mod.Phys.* **82** (2010) 2701–2729, arXiv:1002.0211 [hep-ph].

[8] M. Abbas and A. Y. Smirnov, "Is the tri-bimaximal mixing accidental?," *Phys.Rev.* **D82** (2010) 013008, arXiv:1004.0099 [hep-ph].

[9] J. Schechter and J. W. F. Valle, "Neutrinoless double-β decay in SU(2)×U(1) theories," *Phys. Rev. D* **25** (1982) 2951–2954.

[10] G. G. Ross, *GRAND UNIFIED THEORIES*. Westview Press, 1985.

[11] P. Minkowski, "$\mu \to e\,\gamma$ at a Rate of One Out of 1-Billion Muon Decays?," *Phys.Lett.* **B67** (1977) 421.

[12] J. E. Kim and M.-S. Seo, "Quark and lepton mixing angles with a dodeca-symmetry," *JHEP* **1102** (2011) 097, arXiv:1005.4684 [hep-ph].

[13] C. H. Albright, A. Dueck, and W. Rodejohann, "Possible Alternatives to Tri-bimaximal Mixing," *Eur.Phys.J.* **C70** (2010) 1099–1110, arXiv:1004.2798 [hep-ph].

[14] A. Dueck, W. Rodejohann, and K. Zuber, "Neutrinoless Double Beta Decay, the Inverted Hierarchy and Precision Determination of theta(12)," *Phys.Rev.* **D83** (2011) 113010, arXiv:1103.4152 [hep-ph].

[15] **DOUBLE-CHOOZ** Collaboration, Y. Abe *et al.*, "Indication for the disappearance of reactor electron antineutrinos in the Double Chooz experiment," *Phys.Rev.Lett.* **108** (2012) 131801, arXiv:1112.6353 [hep-ex].

[16] **DAYA-BAY** Collaboration, F. An *et al.*, "Observation of electron-antineutrino disappearance at Daya Bay," *Phys.Rev.Lett.* **108** (2012) 171803, arXiv:1203.1669 [hep-ex].

[17] **RENO** Collaboration, J. Ahn *et al.*, "Observation of Reactor Electron Antineutrino Disappearance in the RENO Experiment," *Phys.Rev.Lett.* **108** (2012) 191802, arXiv:1204.0626 [hep-ex].

[18] **KamLAND-Zen** Collaboration, A. Gando *et al.*, "Limit on Neutrinoless $\beta\beta$ Decay of Xe-136 from the First Phase of KamLAND-Zen and Comparison with the Positive Claim in Ge-76," arXiv:1211.3863 [hep-ex].

[19] **EXO** Collaboration, M. Auger *et al.*, "Search for Neutrinoless Double-Beta Decay in ^{136}Xe with EXO-200," *Phys.Rev.Lett.* **109** (2012) 032505, arXiv:1205.5608 [hep-ex].

[20] A. Dueck, S. Petcov, and W. Rodejohann, "On Leptonic Unitary Triangles and Boomerangs," *Phys.Rev.* **D82** (2010) 013005, arXiv:1006.0227 [hep-ph].

[21] **ATLAS** Collaboration, G. Aad *et al.*, "Observation of a new particle in the search for the Standard Model Higgs boson with the ATLAS detector at the LHC," *Phys.Lett.* **B716** (2012) 1–29, arXiv:1207.7214 [hep-ex].

[22] **CMS** Collaboration, S. Chatrchyan *et al.*, "Observation of a new boson at a mass of 125 GeV with the CMS experiment at the LHC," *Phys.Lett.* **B716** (2012) 30–61, arXiv:1207.7235 [hep-ex].

[23] **Super-Kamiokande** Collaboration, J. Hosaka *et al.*, "Three flavor neutrino oscillation analysis of atmospheric neutrinos in Super-Kamiokande," *Phys.Rev.* **D74** (2006) 032002, arXiv:hep-ex/0604011 [hep-ex].

[24] **Super-Kamiokande** Collaboration, R. Wendell *et al.*, "Atmospheric neutrino oscillation analysis with sub-leading effects in Super-Kamiokande I, II, and III," *Phys.Rev.* **D81** (2010) 092004, arXiv:1002.3471 [hep-ex].

[25] **GNO** Collaboration, M. Altmann *et al.*, "Complete results for five years of GNO solar neutrino observations," *Phys.Lett.* **B616** (2005) 174–190, arXiv:hep-ex/0504037 [hep-ex].

[26] **Borexino** Collaboration, C. Arpesella *et al.*, "Direct Measurement of the Be-7 Solar Neutrino Flux with 192 Days of Borexino Data," *Phys.Rev.Lett.* **101** (2008) 091302, arXiv:0805.3843 [astro-ph].

[27] **SNO** Collaboration, B. Aharmim *et al.*, "Low Energy Threshold Analysis of the Phase I and Phase II Data Sets of the Sudbury Neutrino Observatory," *Phys.Rev.* **C81** (2010) 055504, arXiv:0910.2984 [nucl-ex].

[28] **CHOOZ** Collaboration, M. Apollonio *et al.*, "Limits on neutrino oscillations from the CHOOZ experiment," *Phys.Lett.* **B466** (1999) 415–430, arXiv:hep-ex/9907037 [hep-ex].

[29] F. Boehm, J. Busenitz, B. Cook, G. Gratta, H. Henrikson, *et al.*, "Search for neutrino oscillations at the Palo Verde nuclear reactors," *Phys.Rev.Lett.* **84** (2000) 3764–3767, arXiv:hep-ex/9912050 [hep-ex].

[30] **KamLAND** Collaboration, S. Abe *et al.*, "Precision Measurement of Neutrino Oscillation Parameters with KamLAND," *Phys.Rev.Lett.* **100** (2008) 221803, arXiv:0801.4589 [hep-ex].

[31] **K2K** Collaboration, M. Ahn *et al.*, "Measurement of Neutrino Oscillation by the K2K Experiment," *Phys.Rev.* **D74** (2006) 072003, arXiv:hep-ex/0606032 [hep-ex].

[32] **MINOS** Collaboration, P. Adamson *et al.*, "A Study of Muon Neutrino Disappearance Using the Fermilab Main Injector Neutrino Beam," *Phys.Rev.* **D77** (2008) 072002, arXiv:0711.0769 [hep-ex].

[33] H. Ishimori, T. Kobayashi, H. Ohki, Y. Shimizu, H. Okada, *et al.*, "Non-Abelian Discrete Symmetries in Particle Physics," *Prog.Theor.Phys.Suppl.* **183** (2010) 1–163, arXiv:1003.3552 [hep-th].

[34] J. Barry and W. Rodejohann, "Deviations from tribimaximal mixing due to the vacuum expectation value misalignment in A_4 models," *Phys.Rev.* **D81** (2010) 093002, arXiv:1003.2385 [hep-ph].

[35] C. H. Albright and W. Rodejohann, "Model-Independent Analysis of Tri-bimaximal Mixing: A Softly-Broken Hidden or an Accidental Symmetry?," *Phys.Lett.* **B665** (2008) 378–383, arXiv:0804.4581 [hep-ph].

[36] C. H. Albright and M.-C. Chen, "Model Predictions for Neutrino Oscillation Parameters," *Phys.Rev.* **D74** (2006) 113006, arXiv:hep-ph/0608137 [hep-ph].

[37] C. H. Albright and M.-C. Chen, "Lepton Flavor Violation in Predictive SUSY-GUT Models," *Phys.Rev.* **D77** (2008) 113010, arXiv:0802.4228 [hep-ph].

[38] C. H. Albright, "Overview of Neutrino Mixing Models and Ways to Differentiate among Them," arXiv:0905.0146 [hep-ph].

[39] S. Goswami, S. T. Petcov, S. Ray, and W. Rodejohann, "Large |U(e3)| and Tri-bimaximal Mixing," *Phys.Rev.* **D80** (2009) 053013, arXiv:0907.2869 [hep-ph].

[40] F. Bazzocchi, L. Merlo, and S. Morisi, "Fermion Masses and Mixings in a S(4)-based Model," *Nucl.Phys.* **B816** (2009) 204–226, arXiv:0901.2086 [hep-ph].

[41] G. Altarelli and D. Meloni, "A Simplest A4 Model for Tri-Bimaximal Neutrino Mixing," *J.Phys.* **G36** (2009) 085005, arXiv:0905.0620 [hep-ph].

[42] G.-J. Ding, "Fermion Masses and Flavor Mixings in a Model with S(4) Flavor Symmetry," *Nucl.Phys.* **B827** (2010) 82–111, arXiv:0909.2210 [hep-ph].

[43] C. Hagedorn, S. F. King, and C. Luhn, "A SUSY GUT of Flavour with S4 x SU(5) to NLO," *JHEP* **1006** (2010) 048, arXiv:1003.4249 [hep-ph].

[44] M. Gonzalez-Garcia, M. Maltoni, J. Salvado, and T. Schwetz, "Global fit to three neutrino mixing: critical look at present precision," arXiv:1209.3023.

[45] G. Fogli, E. Lisi, A. Marrone, D. Montanino, A. Palazzo, *et al.*, "Global analysis of neutrino masses, mixings and phases: entering the era of leptonic CP violation searches," *Phys.Rev.* **D86** (2012) 013012, arXiv:1205.5254 [hep-ph].

[46] D. Forero, M. Tortola, and J. Valle, "Global status of neutrino oscillation parameters after Neutrino-2012," arXiv:1205.4018 [hep-ph].

[47] P. Harrison and W. Scott, "Symmetries and generalizations of tri - bimaximal neutrino mixing," *Phys.Lett.* **B535** (2002) 163–169, arXiv:hep-ph/0203209 [hep-ph].

[48] Z.-z. Xing, "Nearly tri bimaximal neutrino mixing and CP violation," *Phys.Lett.* **B533** (2002) 85–93, arXiv:hep-ph/0204049 [hep-ph].

[49] X. G. He and A. Zee, "Some simple mixing and mass matrices for neutrinos," *Phys.Lett.* **B560** (2003) 87–90, arXiv:hep-ph/0301092 [hep-ph].

[50] W. Grimus and L. Lavoura, "A Discrete symmetry group for maximal atmospheric neutrino mixing," *Phys.Lett.* **B572** (2003) 189–195, arXiv:hep-ph/0305046 [hep-ph].

[51] A. Adulpravitchai, A. Blum, and C. Hagedorn, "A Supersymmetric D4 Model for mu-tau Symmetry," *JHEP* **0903** (2009) 046, arXiv:0812.3799 [hep-ph].

[52] W. Grimus and L. Lavoura, "A Model for trimaximal lepton mixing," *JHEP* **0809** (2008) 106, arXiv:0809.0226 [hep-ph].

[53] W. Grimus and L. Lavoura, "A Three-parameter neutrino mass matrix with maximal CP violation," *Phys.Lett.* **B671** (2009) 456–461, arXiv:0810.4516 [hep-ph].

[54] W. Grimus, L. Lavoura, and A. Singraber, "Trimaximal lepton mixing with a trivial Dirac phase," *Phys.Lett.* **B686** (2010) 141–145, arXiv:0911.5120 [hep-ph].

[55] C. Lam, "Symmetry of Lepton Mixing," *Phys.Lett.* **B656** (2007) 193–198, arXiv:0708.3665 [hep-ph].

[56] C. Lam, "A Bottom-up analysis of horizontal symmetry," arXiv:0907.2206 [hep-ph].

[57] C. H. Albright and W. Rodejohann, "Comparing Trimaximal Mixing and Its Variants with Deviations from Tri-bimaximal Mixing," *Eur.Phys.J.* **C62** (2009) 599–608, arXiv:0812.0436 [hep-ph].

[58] C. D. Carone and R. F. Lebed, "Optimal Parametrization of Deviations from Tribimaximal Form of the Neutrino Mass Matrix," *Phys.Rev.* **D80** (2009) 117301, arXiv:0910.1529 [hep-ph].

[59] Z.-z. Xing, "Tetra-maximal Neutrino Mixing and Its Implications on Neutrino Oscillations and Collider Signatures," *Phys.Rev.* **D78** (2008) 011301, arXiv:0805.0416 [hep-ph].

[60] K. A. Hochmuth and W. Rodejohann, "On Symmetric Lepton Mixing Matrices," *Phys.Lett.* **B644** (2007) 147–152, arXiv:hep-ph/0611030 [hep-ph].

[61] A. S. Joshipura and A. Y. Smirnov, "Quark-lepton universality and large leptonic mixing," *Nucl.Phys.* **B750** (2006) 28–44, arXiv:hep-ph/0512024 [hep-ph].

[62] F. Vissani, "A Study of the scenario with nearly degenerate Majorana neutrinos," arXiv:hep-ph/9708483 [hep-ph].

[63] V. D. Barger, S. Pakvasa, T. J. Weiler, and K. Whisnant, "Bimaximal mixing of three neutrinos," *Phys.Lett.* **B437** (1998) 107–116, arXiv:hep-ph/9806387 [hep-ph].

[64] A. J. Baltz, A. S. Goldhaber, and M. Goldhaber, "The Solar neutrino puzzle: An Oscillation solution with maximal neutrino mixing," *Phys.Rev.Lett.* **81** (1998) 5730–5733, arXiv:hep-ph/9806540 [hep-ph].

[65] H. Georgi and S. Glashow, "Neutrinos on earth and in the heavens," *Phys.Rev.* **D61** (2000) 097301, arXiv:hep-ph/9808293 [hep-ph].

[66] I. Stancu and D. V. a. Ahluwalia, "L / E flatness of the electron - like event ratio in Super-Kamiokande and a degeneracy in neutrino masses," *Phys.Lett.* **B460** (1999) 431–436, arXiv:hep-ph/9903408 [hep-ph].

[67] R. Mohapatra, A. Perez-Lorenzana, and C. A. de Sousa Pires, "Type II seesaw and a gauge model for the bimaximal mixing explanation of neutrino puzzles," *Phys.Lett.* **B474** (2000) 355–360, arXiv:hep-ph/9911395 [hep-ph].

[68] G. Altarelli, F. Feruglio, and L. Merlo, "Revisiting Bimaximal Neutrino Mixing in a Model with S(4) Discrete Symmetry," *JHEP* **0905** (2009) 020, arXiv:0903.1940 [hep-ph].

[69] A. Datta, F.-S. Ling, and P. Ramond, "Correlated hierarchy, Dirac masses and large mixing angles," *Nucl.Phys.* **B671** (2003) 383–400, arXiv:hep-ph/0306002 [hep-ph].

[70] Y. Kajiyama, M. Raidal, and A. Strumia, "The Golden ratio prediction for the solar neutrino mixing," *Phys.Rev.* **D76** (2007) 117301, arXiv:0705.4559 [hep-ph].

[71] L. L. Everett and A. J. Stuart, "Icosahedral (A(5)) Family Symmetry and the Golden Ratio Prediction for Solar Neutrino Mixing," *Phys.Rev.* **D79** (2009) 085005, arXiv:0812.1057 [hep-ph].

[72] W. Rodejohann, "Unified Parametrization for Quark and Lepton Mixing Angles," *Phys.Lett.* **B671** (2009) 267–271, arXiv:0810.5239 [hep-ph].

[73] A. Adulpravitchai, A. Blum, and W. Rodejohann, "Golden Ratio Prediction for Solar Neutrino Mixing," *New J.Phys.* **11** (2009) 063026, arXiv:0903.0531 [hep-ph].

[74] M. Raidal, "Relation between the neutrino and quark mixing angles and grand unification," *Phys.Rev.Lett.* **93** (2004) 161801, arXiv:hep-ph/0404046 [hep-ph].

[75] H. Minakata and A. Y. Smirnov, "Neutrino mixing and quark-lepton complementarity," *Phys.Rev.* **D70** (2004) 073009, arXiv:hep-ph/0405088 [hep-ph].

[76] L. Wolfenstein, "Parametrization of the Kobayashi-Maskawa Matrix," *Phys.Rev.Lett.* **51** (1983) 1945.

[77] **CKMfitter Group** Collaboration, J. Charles *et al.*, "CP violation and the CKM matrix: Assessing the impact of the asymmetric B factories," *Eur.Phys.J.* **C41** (2005) 1–131, arXiv:hep-ph/0406184 [hep-ph].

[78] A. Hocker and Z. Ligeti, "CP violation and the CKM matrix," *Ann.Rev.Nucl.Part.Sci.* **56** (2006) 501–567, arXiv:hep-ph/0605217 [hep-ph].

[79] P. Frampton, S. Petcov, and W. Rodejohann, "On deviations from bimaximal neutrino mixing," *Nucl.Phys.* **B687** (2004) 31–54, arXiv:hep-ph/0401206 [hep-ph].

[80] K. Cheung, S. K. Kang, C. Kim, and J. Lee, "Lepton flavor violation as a probe of quark-lepton unification," *Phys.Rev.* **D72** (2005) 036003, arXiv:hep-ph/0503122 [hep-ph].

[81] K. A. Hochmuth and W. Rodejohann, "Low and High Energy Phenomenology of Quark-Lepton Complementarity Scenarios," *Phys.Rev.* **D75** (2007) 073001, arXiv:hep-ph/0607103 [hep-ph].

[82] S. Antusch, S. F. King, and R. N. Mohapatra, "Quark-lepton complementarity in unified theories," *Phys.Lett.* **B618** (2005) 150–161, arXiv:hep-ph/0504007 [hep-ph].

[83] F. Plentinger, G. Seidl, and W. Winter, "The Seesaw mechanism in quark-lepton complementarity," *Phys.Rev.* **D76** (2007) 113003, arXiv:0707.2379 [hep-ph].

[84] C. I. Low and R. R. Volkas, "Tri-bimaximal mixing, discrete family symmetries, and a conjecture connecting the quark and lepton mixing matrices," *Phys.Rev.* **D68** (2003) 033007, arXiv:hep-ph/0305243 [hep-ph].

[85] S. Pakvasa, W. Rodejohann, and T. J. Weiler, "Unitary parametrization of perturbations to tribimaximal neutrino mixing," *Phys.Rev.Lett.* **100** (2008) 111801, arXiv:0711.0052 [hep-ph].

[86] X.-G. He, S.-W. Li, and B.-Q. Ma, "Triminimal Parametrization of Quark Mixing Matrix," *Phys.Rev.* **D78** (2008) 111301, arXiv:0809.1223 [hep-ph].

[87] X.-G. He, S.-W. Li, and B.-Q. Ma, "Unified triminimal parametrizations of quark and lepton mixing matrices," *Phys.Rev.* **D79** (2009) 073001, arXiv:0903.2880 [hep-ph].

[88] Y. Koide, "Charged Lepton Mass Formula: Development and Prospect," *Int.J.Mod.Phys.* **E16** (2007) 1417–1426, arXiv:0706.2534 [hep-ph].

[89] H. Harari, H. Haut, and J. Weyers, "Quark Masses and Cabibbo Angles," *Phys.Lett.* **B78** (1978) 459.

[90] A. Strumia and F. Vissani, "Neutrino masses and mixings and...," arXiv:hep-ph/0606054 [hep-ph].

[91] J. Vergados, "The Neutrinoless double beta decay from a modern perspective," *Phys.Rept.* **361** (2002) 1–56, hep-ph/0209347.

[92] I. Avignone, Frank T., S. R. Elliott, and J. Engel, "Double Beta Decay, Majorana Neutrinos, and Neutrino Mass," *Rev.Mod.Phys.* **80** (2008) 481–516, arXiv:0708.1033 [nucl-ex].

[93] W. Rodejohann, "Neutrino-less Double Beta Decay and Particle Physics," *Int.J.Mod.Phys.* **E20** (2011) 1833–1930, arXiv:1106.1334 [hep-ph].

[94] W. Rodejohann, "Neutrinoless double beta decay and neutrino physics," arXiv:1206.2560 [hep-ph].

[95] W. Furry, "On transition probabilities in double beta-disintegration," *Phys.Rev.* **56** (1939) 1184–1193.

[96] W. Rodejohann, "Neutrinoless Double Beta Decay in Particle Physics," arXiv:1011.4942 [hep-ph].

[97] S. Pascoli and S. Petcov, "The SNO solar neutrino data, neutrinoless double beta decay and neutrino mass spectrum," *Phys.Lett.* **B544** (2002) 239–250, hep-ph/0205022.

[98] S. Petcov, "Theoretical prospects of neutrinoless double beta decay," *Phys.Scripta* **T121** (2005) 94–101, hep-ph/0504166.

[99] L. Zhan, Y. Wang, J. Cao, and L. Wen, "Determination of the Neutrino Mass Hierarchy at an Intermediate Baseline," *Phys.Rev.* **D78** (2008) 111103, arXiv:0807.3203 [hep-ex].

[100] A. Ghosh, T. Thakore, and S. Choubey, "Determining the Neutrino Mass Hierarchy with INO, T2K, NOvA and Reactor Experiments," arXiv:1212.1305 [hep-ph].

[101] S.-F. Ge, K. Hagiwara, N. Okamura, and Y. Takaesu, "Determination of mass hierarchy with medium baseline reactor neutrino experiments," arXiv:1210.8141 [hep-ph].

[102] K. Hagiwara, T. Kiwanami, N. Okamura, and K.-i. Senda, "Physics potential of neutrino oscillation experiment with a far detector in Oki Island along the T2K baseline," arXiv:1209.2763 [hep-ph].

[103] A. Faessler and F. Simkovic, "Double beta decay," *J. Phys. G: Nucl. Part. Phys.* **24** (1998) 2139–2178.

[104] J. Suhonen and O. Civitarese, "Weak-interaction and nuclear-structure aspects of nuclear double beta decay," *Phys. Rep.* **300** (1998) 123–214.

[105] J. Menéndez, A. Poves, E. Caurier, and F. Nowacki, "Disassembling the nuclear matrix elements of the neutrinoless $\beta\beta$ decay," *Nucl. Phys. A* **818** (2009) 139–151, arXiv:0801.3760v3 [nucl-th].

[106] J. Barea and F. Iachello, "Neutrinoless double-β decay in the microscopic interacting boson model," *Phys. Rev. C* **79** (2009) 044301.

[107] T. R. Rodriguez and G. Martinez-Pinedo, "Energy density functional study of nuclear matrix elements for neutrinoless $\beta\beta$ decay," *Phys. Rev. Lett.* **105** (2010) 252503, arXiv:1008.5260 [nucl-th].

[108] P. K. Rath, R. Chandra, K. Chaturvedi, P. K. Raina, and J. G. Hirsch, "Uncertainties in nuclear transition matrix elements for neutrinoless $\beta\beta$ decay within the projected-Hartree-Fock-Bogoliubov model," *Phys. Rev. C* **82** (2010) 064310.

[109] K. Zuber, "Consensus report of a workshop on matrix elements for neutrinoless double beta decay," nucl-ex/0511009.

[110] A. Faessler, G. Fogli, E. Lisi, V. Rodin, A. Rotunno, *et al.*, "QRPA uncertainties and their correlations in the analysis of 0 nu beta beta decay," *Phys.Rev.* **D79** (2009) 053001, arXiv:0810.5733 [hep-ph].

[111] M. C. Chen, "The SNO liquid scintillator project," *Nucl. Phys. Proc. Suppl.* **145** (2005) 65–68.

[112] D. N. McKinsey and K. J. Coakley, "Neutrino detection with CLEAN," *Astropart. Phys.* **22** (2005) 355–368, astro-ph/0402007.

[113] Y. Huang, R. Lanou, H. Maris, G. Seidel, B. Sethumadhavan, *et al.*, "Potential for Precision Measurement of Solar Neutrino Luminosity by HERON," *Astropart.Phys.* **30** (2008) 1–11, arXiv:0711.4095 [astro-ph].

[114] **LENS** Collaboration, R. Raghavan, "LENS, MiniLENS: Status and outlook," *J.Phys.Conf.Ser.* **120** (2008) 052014.

[115] A. Bandyopadhyay, S. Choubey, and S. Goswami, "Exploring the sensitivity of current and future experiments to Theta(odot)," *Phys. Rev.* **D67** (2003) 113011, hep-ph/0302243.

[116] H. Minakata, H. Nunokawa, W. Teves, and R. Zukanovich Funchal, "Reactor measurement of theta(12): Principles, accuracies and physics potentials," *Phys.Rev.* **D71** (2005) 013005, hep-ph/0407326.

[117] A. Bandyopadhyay, S. Choubey, S. Goswami, and S. Petcov, "High precision measurements of theta(solar) in solar and reactor neutrino experiments," *Phys.Rev.* **D72** (2005) 033013, hep-ph/0410283.

[118] S. Petcov and T. Schwetz, "Precision measurement of solar neutrino oscillation parameters by a long-baseline reactor neutrino experiment in Europe," *Phys.Lett.* **B642** (2006) 487–494, hep-ph/0607155.

[119] A. B. Balantekin, "Significance of neutrino cross-sections for astrophysics," *AIP Conf. Proc.* **1189** (2009) 11–15, arXiv:0909.0226 [hep-ph].

[120] A. Friedland, C. Lunardini, and C. Pena-Garay, "Solar neutrinos as probes of neutrino matter interactions," *Phys.Lett.* **B594** (2004) 347, hep-ph/0402266.

[121] M. Lindner, A. Merle, and W. Rodejohann, "Improved limit on theta(13) and implications for neutrino masses in neutrino-less double beta decay and cosmology," *Phys. Rev.* **D73** (2006) 053005, hep-ph/0512143.

[122] J. Bernabeu, M. Blennow, P. Coloma, A. Donini, C. Espinoza, *et al.*, "EURONU WP6 2009 yearly report: Update of the physics potential of Nufact, superbeams and betabeams," arXiv:1005.3146 [hep-ph].

[123] G. Audi, A. H. Wapstra, and C. Thibault, "The 2003 atomic mass evaluation: (II). Tables, graphs and references," *Nuclear Physics A* **729** (2003) 337–676.

[124] S. M. Bilenky, "Neutrinoless Double Beta-Decay," (2010) , arXiv:1001.1946 [hep-ph].

[125] S. Cowell, "Scaling factor inconsistencies in neutrinoless double beta decay," *Phys. Rev. C* **73** (2006) 028501, nucl-th/0512012.

[126] A. Smolnikov and P. Grabmayr, "Conversion of experimental half-life to effective electron neutrino mass in $0\nu\beta\beta$ decay," *Phys. Rev. C* **81** (2010) 028502.

[127] A. Faessler, G. L. Fogli, E. Lisi, V. Rodin, A. M. Rotunno, and F. Simkovic, "Quasiparticle random phase approximation uncertainties and their correlations in the analysis of $0\nu\beta\beta$ decay," *Phys. Rev. D* **79** (2009) 053001.

[128] F. Simkovic, A. Faessler, H. Muther, V. Rodin, and M. Stauf, "$0\nu\beta\beta$-decay nuclear matrix elements with self-consistent short-range correlations," *Phys. Rev. C* **79** (2009) 055501, arXiv:0902.0331v1 [nucl-th].

[129] D.-L. Fang, A. Faessler, V. Rodin, and F. Simkovic, "Neutrinoless double-β decay of ^{150}Nd accounting for deformation," *Phys.Rev.* **C82** (2010) 051301, arXiv:1009.5579v1 [nucl-th].

[130] O. Civitarese and J. Suhonen, "Nuclear Matrix Elements for Double Beta Decay in the QRPA approach: a critical review," *Journal of Physics: Conference Series* **173** (2009) 012012.

[131] J. G. Hirsch, O. Castanos, and P. Hess, "Neutrinoless double beta decay in heavy deformed nuclei," *Nucl.Phys.* **A582** (1995) 124–140, nucl-th/9407022.

[132] F. Simkovic, G. Pantis, J. D. Vergados, and A. Faessler, "Additional nucleon current contributions to neutrinoless double β decay," *Phys. Rev. C* **60** (1999) 055502.

[133] F. Simkovic, A. Faessler, V. Rodin, P. Vogel, and J. Engel, "Anatomy of the $0\nu\beta\beta$ nuclear matrix elements," *Phys. Rev. C* **77** (2008) 045503, arXiv:0710.2055 [nucl-th].

[134] G. A. Miller and J. E. Spencer, "A survey of pion charge-exchange reactions with nuclei," *Ann. Phys.* **100** (1976) 562–606.

[135] H. Feldmeier, T. Neff, R. Roth, and J. Schnack, "A unitary correlation operator method," *Nucl. Phys. A* **632** (1998) 61–95, nucl-th/9709038.

[136] H. Müther and A. Polls, "Correlations derived from modern nucleon-nucleon potentials," *Phys. Rev. C* **61** (1999) 014304, nucl-th/9908002.

[137] H. Müther and A. Polls, "Two-body correlations in nuclear systems," *Prog. Part. Nucl. Phys.* **45** (2000) 243–334, nucl-th/0001007.

[138] C. Giusti, H. Müther, F. D. Pacati, and M. Stauf, "Short-range and tensor correlations in the ^{16}O$(e, e'pn)$ reaction," *Phys. Rev. C* **60** (1999) 054608, nucl-th/9903065.

[139] A. S. Barabash, "75 years of double beta decay: yesterday, today and tomorrow," arXiv:1101.4502 [nucl-ex].

[140] *See e.g., talks by A. Giuliani at BEYOND 2010 or by C. Nones at NOW 2010* .

[141] H. Ejiri *et al.*, "Spectroscopy of double-beta and inverse-beta decays from Mo-100 for neutrinos," *Phys. Rev. Lett.* **85** (2000) 2917–2920, nucl-ex/9911008.

[142] **NEMO** Collaboration, A. Barabash, "Extrapolation of NEMO technique to future generation of 2beta-decay experiments," *Czech.J.Phys.* **52** (2002) 575–581.

[143] S. Umehara *et al.*, "Neutrino-less double-β decay of ^{48}Ca studied by CaF_2(Eu) scintillators," *Phys. Rev. C* **78** (2008) 058501, arXiv:0810.4746 [nucl-ex].

[144] H. V. Klapdor-Kleingrothaus *et al.*, "Latest Results from the Heidelberg-Moscow Double Beta Decay Experiment," *Eur. Phys. J. A* **12** (2001) 147–154, hep-ph/0103062.

[145] **NEMO** Collaboration, A. S. Barabash and V. B. Brudanin, "Investigation of double beta decay with the NEMO-3 detector," arXiv:1002.2862 [nucl-ex].

[146] J. Argyriades *et al.*, "Measurement of the two neutrino double beta decay half-life of Zr-96 with the NEMO-3 detector," *Nuclear Physics A* **847** (2010) 168–179, arXiv:0906.2694 [nucl-ex].

[147] F. A. Danevich *et al.*, "Search for 2β decay of cadmium and tungsten isotopes: Final results of the Solotvina experiment," *Phys. Rev. C* **68** (2003) 035501.

[148] C. Arnaboldi *et al.*, "Results from a search for the $0\nu\beta\beta$–decay of ^{130}Te," *Phys. Rev. C* **78** (2008) 035502, arXiv:0802.3439 [hep-ex].

[149] R. Bernabei *et al.*, "Investigation of $\beta\beta$ decay modes in ^{134}Xe and ^{136}Xe," *Physics Letters B* **546** (2002) 23–28.

[150] **NEMO** Collaboration, J. Argyriades *et al.*, "Measurement of the double-β decay half-life of ^{150}Nd and search for neutrinoless decay modes with the NEMO-3 detector," *Phys. Rev. C* **80** (2009) 032501, arXiv:0810.0248 [hep-ex].

[151] **IGEX** Collaboration, C. Aalseth *et al.*, "The IGEX Ge-76 neutrinoless double beta decay experiment: Prospects for next generation experiments," *Phys.Rev.* **D65** (2002) 092007, hep-ex/0202026.

[152] H. Klapdor-Kleingrothaus and I. Krivosheina, "The evidence for the observation of neutrinoless double beta decay: The identification of neutrinoless double beta events from the full spectra," *Mod.Phys.Lett.* **A21** (2006) 1547–1566.

[153] S. Umehara, T. Kishimoto, I. Ogawa, R. Hazama, S. Yoshida, *et al.*, "CANDLES for double beta decay of Ca-48," *J.Phys.Conf.Ser.* **39** (2006) 356–358.

[154] I. Abt *et al.*, "A new 76Ge double beta decay experiment at LNGS," hep-ex/0404039.

[155] **Majorana** Collaboration, C. E. Aalseth *et al.*, "The Majorana neutrinoless double-beta decay experiment," *Phys. Atom. Nucl.* **67** (2004) 2002–2010, hep-ex/0405008.

[156] K. Zuber, "COBRA–double beta decay searches using CdTe detectors," *Physics Letters B* **519** (2001) 1–7, nucl-ex/0105018.

[157] C. Arnaboldi *et al.*, "CUORE: a cryogenic underground observatory for rare events," *Nucl. Instrum. Meth. A* **518** (2004) 775–798, nucl-ex/0212053.

[158] M. Danilov *et al.*, "Detection of very small neutrino masses in double–beta decay using laser tagging," *Phys. Lett. B* **480** (2000) 12–18, hep-ex/0002003.

[159] Y. Takeuchi, "Recent status of the XMASS project," *Prepared for ICHEP 04, Beijing, China, 16-22 Aug 2004,* (2004) 324–327.

[160] **KamLAND** Collaboration, A. Terashima *et al.*, "R & D for possible future improvements of KamLAND," *J.Phys.Conf.Ser.* **120** (2008) 052029.

[161] **NEXT** Collaboration, . F. Granena *et al.*, "NEXT, a HPGXe TPC for neutrinoless double beta decay searches," arXiv:0907.4054 [hep-ex].

[162] N. Ishihara, T. Inagaki, T. Ohama, K. Omata, S. Takeda, *et al.*, "A Separation method of 0 neutrino and 2 neutrino events in double beta decay experiments with DCBA," *Nucl.Instrum.Meth.* **A443** (2000) 101–107.

[163] **SNO+** Collaboration, M. C. Chen, "The SNO+ Experiment," arXiv:0810.3694 [hep-ex].

[164] R. Slansky, "Group Theory for Unified Model Building," *Phys.Rept.* **79** (1981) 1–128.

[165] G. Senjanovic, "SO(10): A Theory of fermion masses and mixings," hep-ph/0612312.

[166] B. Bajc, A. Melfo, G. Senjanovic, and F. Vissani, "Yukawa sector in non-supersymmetric renormalizable SO(10)," *Phys.Rev.* **D73** (2006) 055001, hep-ph/0510139.

[167] R. Peccei and H. R. Quinn, "CP Conservation in the Presence of Instantons," *Phys.Rev.Lett.* **38** (1977) 1440–1443.

[168] A. S. Joshipura and K. M. Patel, "Fermion Masses in SO(10) Models," *Phys.Rev.* **D83** (2011) 095002, arXiv:1102.5148 [hep-ph].

[169] H. Fritzsch, "Weak Interaction Mixing in the Six - Quark Theory," *Phys.Lett.* **B73** (1978) 317–322.

[170] M. Shin, "The Phenomenological Predictions of Fritzsch Type Quark Mass Matrices and the Underlying Structure of Particle Physics Beyond the Standard Model," *Phys.Lett.* **B145** (1984) 285.

[171] P. H. Frampton, S. L. Glashow, and D. Marfatia, "Zeroes of the neutrino mass matrix," *Phys.Lett.* **B536** (2002) 79–82, hep-ph/0201008.

[172] Z.-z. Xing, "Texture zeros and Majorana phases of the neutrino mass matrix," *Phys.Lett.* **B530** (2002) 159–166, hep-ph/0201151.

[173] B. R. Desai, D. Roy, and A. R. Vaucher, "Three neutrino mass matrices with two texture zeros," *Mod.Phys.Lett.* **A18** (2003) 1355–1366, hep-ph/0209035.

[174] K. Matsuda and H. Nishiura, "Can four-zero-texture mass matrix model reproduce the quark and lepton mixing angles and CP violating phases?," *Phys.Rev.* **D74** (2006) 033014, hep-ph/0606142.

[175] S. Dev, S. Kumar, S. Verma, and S. Gupta, "Phenomenological implications of a class of neutrino mass matrices," *Nucl.Phys.* **B784** (2007) 103–117, hep-ph/0611313.

[176] S. Dev, S. Kumar, S. Verma, and S. Gupta, "Phenomenology of two-texture zero neutrino mass matrices," *Phys.Rev.* **D76** (2007) 013002, hep-ph/0612102.

[177] G. Branco, R. Gonzalez Felipe, F. Joaquim, and T. Yanagida, "Removing ambiguities in the neutrino mass matrix," *Phys.Lett.* **B562** (2003) 265–272, hep-ph/0212341.

[178] B. C. Chauhan, J. Pulido, and M. Picariello, "Neutrino mass matrices with vanishing determinant," *Phys.Rev.* **D73** (2006) 053003, hep-ph/0602084.

[179] E. Ma, "Connection between the neutrino seesaw mechanism and properties of the Majorana neutrino mass matrix," *Phys.Rev.* **D71** (2005) 111301, hep-ph/0501056.

[180] E. Lashin and N. Chamoun, "Zero minors of the neutrino mass matrix," *Phys.Rev.* **D78** (2008) 073002, arXiv:0708.2423 [hep-ph].

[181] E. Lashin and N. Chamoun, "One vanishing minor in the neutrino mass matrix," *Phys.Rev.* **D80** (2009) 093004, arXiv:0909.2669 [hep-ph].

[182] T. Araki, J. Heeck, and J. Kubo, "Vanishing Minors in the Neutrino Mass Matrix from Abelian Gauge Symmetries," arXiv:1203.4951 [hep-ph].

[183] D. Black, A. H. Fariborz, S. Nasri, and J. Schechter, "Complementary Ansatz for the neutrino mass matrix," *Phys.Rev.* **D62** (2000) 073015, hep-ph/0004105.

[184] X.-G. He and A. Zee, "Neutrino masses with 'zero sum' condition: m(nu(1)) + m(nu(2)) + m(nu(3)) = 0," *Phys.Rev.* **D68** (2003) 037302, hep-ph/0302201.

[185] W. Rodejohann, "Neutrino mass matrices leaving no trace," *Phys.Lett.* **B579** (2004) 127–139, hep-ph/0308119.

[186] H. Fritzsch and Z.-z. Xing, "Mass and flavor mixing schemes of quarks and leptons," *Prog.Part.Nucl.Phys.* **45** (2000) 1–81, hep-ph/9912358.

[187] K. Matsuda, T. Fukuyama, and H. Nishiura, "SO(10) GUT and quark lepton mass matrices," *Phys.Rev.* **D61** (2000) 053001, arXiv:hep-ph/9906433 [hep-ph].

[188] T. Fukuyama, K. Matsuda, and H. Nishiura, "Zero texture model and SO(10) GUT," *Int.J.Mod.Phys.* **A22** (2007) 5325–5343, hep-ph/0702284.

[189] S. Dev, S. Kumar, S. Verma, S. Gupta, and R. Gautam, "Four Zero Texture Fermion Mass Matrices in SO(10) GUT," *Eur.Phys.J.* **C72** (2012) 1940, arXiv:1203.1403 [hep-ph].

[190] W. Grimus, "Neutrino mass matrices, texture zeros, and family symmetries," *PoS* **HEP2005** (2006) 186, hep-ph/0511078.

[191] W. Grimus and H. Kühböck, "Fermion masses and mixings in a renormalizable SO(10) x Z(2) GUT," *Phys.Lett.* **B643** (2006) 182–189, hep-ph/0607197.

[192] C. Das and M. Parida, "New formulas and predictions for running fermion masses at higher scales in SM, 2 HDM, and MSSM," *Eur.Phys.J.* **C20** (2001) 121–137, hep-ph/0010004.

[193] Z.-z. Xing, H. Zhang, and S. Zhou, "Updated Values of Running Quark and Lepton Masses," *Phys.Rev.* **D77** (2008) 113016, arXiv:0712.1419 [hep-ph].

[194] G. Ross and M. Serna, "Unification and fermion mass structure," *Phys.Lett.* **B664** (2008) 97–102, arXiv:0704.1248 [hep-ph].

[195] G. Altarelli and G. Blankenburg, "Different $SO(10)$ Paths to Fermion Masses and Mixings," *JHEP* **1103** (2011) 133, arXiv:1012.2697 [hep-ph].

[196] F. Vissani and A. Y. Smirnov, "Neutrino masses and b - tau unification in the supersymmetric standard model," *Phys.Lett.* **B341** (1994) 173–180, hep-ph/9405399.

[197] S. Antusch, J. Kersten, M. Lindner, and M. Ratz, "Neutrino mass matrix running for non-degenerate see-saw scales," *Phys.Lett.* **B538** (2002) 87–95, hep-ph/0203233.

[198] F. Buccella, D. Falcone, C. S. Fong, E. Nardi, and G. Ricciardi, "Squeezing out predictions with leptogenesis from SO(10)," *Phys.Rev.* **D86** (2012) 035012, arXiv:1203.0829 [hep-ph].

[199] S. Bertolini, L. Di Luzio, and M. Malinsky, "Intermediate mass scales in the non-supersymmetric SO(10) grand unification: A Reappraisal," *Phys.Rev.* **D80** (2009) 015013, arXiv:0903.4049 [hep-ph].

[200] H. Goh, R. Mohapatra, and S. Nasri, "SO(10) symmetry breaking and type II seesaw," *Phys.Rev.* **D70** (2004) 075022, arXiv:hep-ph/0408139 [hep-ph].

[201] A. Melfo, A. Ramirez, and G. Senjanovic, "Type II see-saw dominance in SO(10)," *Phys.Rev.* **D82** (2010) 075014, arXiv:1005.0834 [hep-ph].

[202] S. Bertolini, L. Di Luzio, and M. Malinsky, "On the vacuum of the minimal nonsupersymmetric SO(10) unification," *Phys.Rev.* **D81** (2010) 035015, arXiv:0912.1796 [hep-ph].

[203] S. Bertolini, T. Schwetz, and M. Malinsky, "Fermion masses and mixings in SO(10) models and the neutrino challenge to SUSY GUTs," *Phys.Rev.* **D73** (2006) 115012, arXiv:hep-ph/0605006 [hep-ph].

[204] K. Babu and R. Mohapatra, "Predictive neutrino spectrum in minimal SO(10) grand unification," *Phys.Rev.Lett.* **70** (1993) 2845–2848, arXiv:hep-ph/9209215 [hep-ph].

[205] L. Lavoura, "Predicting the neutrino spectrum in minimal SO(10) grand unification," *Phys.Rev.* **D48** (1993) 5440–5443, arXiv:hep-ph/9306297 [hep-ph].

[206] B. Bajc, G. Senjanovic, and F. Vissani, "How neutrino and charged fermion masses are connected within minimal supersymmetric SO(10)," arXiv:hep-ph/0110310 [hep-ph].

[207] B. Bajc, G. Senjanovic, and F. Vissani, "b - tau unification and large atmospheric mixing: A Case for noncanonical seesaw," *Phys.Rev.Lett.* **90** (2003) 051802, arXiv:hep-ph/0210207 [hep-ph].

[208] H. Goh, R. Mohapatra, and S.-P. Ng, "Minimal SUSY SO(10), b tau unification and large neutrino mixings," *Phys.Lett.* **B570** (2003) 215–221, arXiv:hep-ph/0303055 [hep-ph].

[209] H. Goh, R. Mohapatra, and S.-P. Ng, "Minimal SUSY SO(10) model and predictions for neutrino mixings and leptonic CP violation," *Phys.Rev.* **D68** (2003) 115008, arXiv:hep-ph/0308197 [hep-ph].

[210] C. S. Aulakh, B. Bajc, A. Melfo, G. Senjanovic, and F. Vissani, "The Minimal supersymmetric grand unified theory," *Phys.Lett.* **B588** (2004) 196–202, arXiv:hep-ph/0306242 [hep-ph].

[211] C. S. Aulakh and A. Girdhar, "SO(10) MSGUT: Spectra, couplings and threshold effects," *Nucl.Phys.* **B711** (2005) 275–313, arXiv:hep-ph/0405074 [hep-ph].

[212] S. Bertolini, M. Frigerio, and M. Malinsky, "Fermion masses in SUSY SO(10) with type II seesaw: A Non-minimal predictive scenario," *Phys.Rev.* **D70** (2004) 095002, arXiv:hep-ph/0406117 [hep-ph].

[213] B. Bajc, A. Melfo, G. Senjanovic, and F. Vissani, "The Minimal supersymmetric grand unified theory. 1. Symmetry breaking and the particle spectrum," *Phys.Rev.* **D70** (2004) 035007, arXiv:hep-ph/0402122 [hep-ph].

[214] B. Bajc, G. Senjanovic, and F. Vissani, "Probing the nature of the seesaw in renormalizable SO(10)," *Phys.Rev.* **D70** (2004) 093002, arXiv:hep-ph/0402140 [hep-ph].

[215] C. S. Aulakh and S. K. Garg, "MSGUT : From bloom to doom," *Nucl.Phys.* **B757** (2006) 47–78, arXiv:hep-ph/0512224 [hep-ph].

[216] K. Babu and C. Macesanu, "Neutrino masses and mixings in a minimal SO(10) model," *Phys.Rev.* **D72** (2005) 115003, arXiv:hep-ph/0505200 [hep-ph].

[217] S. Bertolini and M. Malinsky, "On CP violation in minimal renormalizable SUSY SO(10) and beyond," *Phys.Rev.* **D72** (2005) 055021, arXiv:hep-ph/0504241 [hep-ph].

[218] B. Bajc, A. Melfo, G. Senjanovic, and F. Vissani, "Fermion mass relations in a supersymmetric SO(10) theory," *Phys.Lett.* **B634** (2006) 272–277, arXiv:hep-ph/0511352 [hep-ph].

[219] C. S. Aulakh and S. K. Garg, "Correcting alpha(3)(M(Z)) in the NMSGUT," *Mod.Phys.Lett.* **A24** (2009) 1711–1719, arXiv:0710.4018 [hep-ph].

[220] B. Bajc, I. Dorsner, and M. Nemevsek, "Minimal SO(10) splits supersymmetry," *JHEP* **0811** (2008) 007, arXiv:0809.1069 [hep-ph].

[221] K. Matsuda, Y. Koide, T. Fukuyama, and H. Nishiura, "How far can the SO(10) two Higgs model describe the observed neutrino masses and mixings?," *Phys.Rev.* **D65** (2002) 033008, arXiv:hep-ph/0108202 [hep-ph].

[222] B. Dutta, Y. Mimura, and R. Mohapatra, "Neutrino masses and mixings in a predictive SO(10) model with CKM CP violation," *Phys.Lett.* **B603** (2004) 35–45, hep-ph/0406262.

[223] W. Grimus and H. Kuhbock, "A renormalizable SO(10) GUT scenario with spontaneous CP violation," *Eur.Phys.J.* **C51** (2007) 721–729, hep-ph/0612132.

[224] C. S. Aulakh and S. K. Garg, "The New Minimal Supersymmetric GUT : Spectra, RG analysis and fitting formulae," arXiv:hep-ph/0612021 [hep-ph].

[225] C. Aulakh and R. N. Mohapatra, "Implications of supersymmetric SO(10) grand unification," *Phys.Rev.* **D28** (1983) 217.

[226] T. Clark, T.-K. Kuo, and N. Nakagawa, "An SO(10) supersymmetric grand unified theory," *Phys.Lett.* **B115** (1982) 26.

[227] C. S. Aulakh, B. Bajc, A. Melfo, A. Rasin, and G. Senjanovic, "SO(10) theory of R-parity and neutrino mass," *Nucl.Phys.* **B597** (2001) 89–109, arXiv:hep-ph/0004031 [hep-ph].

[228] N. Oshimo, "Antisymmetric Higgs representation in SO(10) for neutrinos," *Phys.Rev.* **D66** (2002) 095010, arXiv:hep-ph/0206239 [hep-ph].

[229] N. Oshimo, "Model for neutrino mixing based on SO(10)," *Nucl.Phys.* **B668** (2003) 258–272, arXiv:hep-ph/0305166 [hep-ph].

[230] C. S. Aulakh, "Pinning down the new minimal supersymmetric GUT," *Phys.Lett.* **B661** (2008) 196–200, arXiv:0710.3945 [hep-ph].

[231] C. S. Aulakh and S. K. Garg, "The New Minimal Supersymmetric GUT : Spectra, RG analysis and Fermion Fits," *Nucl.Phys.* **B857** (2012) 101–142, arXiv:0807.0917 [hep-ph].

[232] A. S. Joshipura and K. M. Patel, "Viability of the exact tri-bimaximal mixing at M_{GUT} in SO(10)," *JHEP* **1109** (2011) 137, arXiv:1105.5943 [hep-ph].

[233] S. Davidson, E. Nardi, and Y. Nir, "Leptogenesis," *Phys.Rept.* **466** (2008) 105–177, arXiv:0802.2962 [hep-ph].

[234] J. Nelder and R. Mead, "A simplex method for function minimization," *Comp. J.* **7** (1965) 308–313.

[235] W. H. Press, S. A. Teukolsky, W. T. Vetterling, and B. P. Flannery, *NUMERICAL RECIPES. The Art of Scientific Computing*. Cambridge University Press, 3rd ed., 2007.

[236] M. Glassi *et al.*, *GNU Scientific Library Reference Manual*. Network Theory Ltd, 3rd ed., 2009.

[237] H. E. Haber, R. Hempfling, and A. H. Hoang, "Approximating the radiatively corrected Higgs mass in the minimal supersymmetric model," *Z.Phys.* **C75** (1997) 539–554, hep-ph/9609331.

[238] **CMS** Collaboration, V. Khachatryan *et al.*, "Search for Supersymmetry in pp Collisions at 7 TeV in Events with Jets and Missing Transverse Energy," *Phys.Lett.* **B698** (2011) 196–218, arXiv:1101.1628 [hep-ex].

[239] **ATLAS** Collaboration, G. Aad *et al.*, "Search for supersymmetry using final states with one lepton, jets, and missing transverse momentum with the ATLAS detector in sqrts = 7 TeV pp," *Phys.Rev.Lett.* **106** (2011) 131802, arXiv:1102.2357 [hep-ex].

[240] O. Buchmueller, R. Cavanaugh, D. Colling, A. de Roeck, M. Dolan, *et al.*, "Implications of Initial LHC Searches for Supersymmetry," *Eur.Phys.J.* **C71** (2011) 1634, arXiv:1102.4585 [hep-ph].

[241] L. J. Hall, D. Pinner, and J. T. Ruderman, "A Natural SUSY Higgs Near 126 GeV," *JHEP* **1204** (2012) 131, arXiv:1112.2703 [hep-ph].

[242] S. Heinemeyer, O. Stal, and G. Weiglein, "Interpreting the LHC Higgs Search Results in the MSSM," *Phys.Lett.* **B710** (2012) 201–206, arXiv:1112.3026 [hep-ph].

[243] M. Carena, S. Gori, N. R. Shah, and C. E. Wagner, "A 125 GeV SM-like Higgs in the MSSM and the $\gamma\gamma$ rate," *JHEP* **1203** (2012) 014, arXiv:1112.3336 [hep-ph].

[244] P. Draper, P. Meade, M. Reece, and D. Shih, "Implications of a 125 GeV Higgs for the MSSM and Low-Scale SUSY Breaking," *Phys.Rev.* **D85** (2012) 095007, arXiv:1112.3068 [hep-ph].

[245] D. Carmi, A. Falkowski, E. Kuflik, T. Volansky, and J. Zupan, "Higgs After the Discovery: A Status Report," arXiv:1207.1718 [hep-ph].

[246] R. Benbrik, M. G. Bock, S. Heinemeyer, O. Stal, G. Weiglein, *et al.*, "Confronting the MSSM and the NMSSM with the Discovery of a Signal in the two Photon Channel at the LHC," arXiv:1207.1096 [hep-ph].

[247] P. Nath, "Higgs Physics and Supersymmetry," arXiv:1210.0520 [hep-ph].

[248] S. Antusch, J. Kersten, M. Lindner, M. Ratz, and M. A. Schmidt, "Running neutrino mass parameters in see-saw scenarios," *JHEP* **0503** (2005) 024, hep-ph/0501272.

[249] P. H. Chankowski and S. Pokorski, "Quantum corrections to neutrino masses and mixing angles," *Int.J.Mod.Phys.* **A17** (2002) 575–614, hep-ph/0110249.

[250] L. J. Hall, R. Rattazzi, and U. Sarid, "The Top quark mass in supersymmetric SO(10) unification," *Phys.Rev.* **D50** (1994) 7048–7065, arXiv:hep-ph/9306309 [hep-ph].

[251] M. S. Carena, M. Olechowski, S. Pokorski, and C. Wagner, "Electroweak symmetry breaking and bottom - top Yukawa unification," *Nucl.Phys.* **B426** (1994) 269–300, arXiv:hep-ph/9402253 [hep-ph].

[252] R. Hempfling, "Yukawa coupling unification with supersymmetric threshold corrections," *Phys.Rev.* **D49** (1994) 6168–6172.

[253] T. Blazek, S. Raby, and S. Pokorski, "Finite supersymmetric threshold corrections to CKM matrix elements in the large tan Beta regime," *Phys.Rev.* **D52** (1995) 4151–4158, arXiv:hep-ph/9504364 [hep-ph].

[254] A. Freitas, E. Gasser, and U. Haisch, "Supersymmetric large tan(beta) corrections to DeltaM(d, s) and B(d, s) $\to \mu^+\mu^-$ revisited," *Phys.Rev.* **D76** (2007) 014016, arXiv:hep-ph/0702267 [HEP-PH].

[255] S. Antusch and M. Spinrath, "Quark and lepton masses at the GUT scale including SUSY threshold corrections," *Phys.Rev.* **D78** (2008) 075020, arXiv:0804.0717 [hep-ph].

[256] M. Fukugita and T. Yanagida, "Baryogenesis Without Grand Unification," *Phys.Lett.* **B174** (1986) 45.

[257] V. Kuzmin, V. Rubakov, and M. Shaposhnikov, "On the Anomalous Electroweak Baryon Number Nonconservation in the Early Universe," *Phys.Lett.* **B155** (1985) 36.

[258] J. P. Kneller and G. Steigman, "BBN for pedestrians," *New J.Phys.* **6** (2004) 117, arXiv:astro-ph/0406320 [astro-ph].

[259] W. Hu and S. Dodelson, "Cosmic microwave background anisotropies," *Ann.Rev.Astron.Astrophys.* **40** (2002) 171–216, arXiv:astro-ph/0110414 [astro-ph].

[260] **SDSS** Collaboration, M. Tegmark *et al.*, "Cosmological parameters from SDSS and WMAP," *Phys.Rev.* **D69** (2004) 103501, arXiv:astro-ph/0310723 [astro-ph].

[261] L. Covi, E. Roulet, and F. Vissani, "CP violating decays in leptogenesis scenarios," *Phys.Lett.* **B384** (1996) 169–174, arXiv:hep-ph/9605319 [hep-ph].

[262] W. Buchmuller, R. Peccei, and T. Yanagida, "Leptogenesis as the origin of matter," *Ann.Rev.Nucl.Part.Sci.* **55** (2005) 311–355, arXiv:hep-ph/0502169 [hep-ph].

[263] Message Passing Interface Forum, *MPI: A Message-Passing Interface Standard, Version 2.2*. High Performance Computing Center Stuttgart (HLRS), 2009. Available online at http://www.mpi-forum.org/docs/mpi-2.2/mpi22-report.pdf; visited on November 19th 2012.

[264] C. Giunti and C. W. Kim, *Fundamentals of Neutrino Physics and Astrophysics*, ch. 6, p. 239. OXFORD UNIVERSITY PRESS, 2007.

[265] D. E. Knuth, *Seminumerical Algorithms*, vol. 2 of *The Art of Computer Programming*, pp. 1–44. Addison-Wesley, 1969.

[266] T. Wang, "Integer Hash Function." Available online at http://www.concentric.net/~ttwang/tech/inthash.htm; visited on November 19th 2012.

[267] S. Garfinkel and G. Spafford, *Practical UNIX and Internet Security*, ch. 23.8. O'Reilly Media, 1996. Available online at http://www.diablotin.com/librairie/networking/puis/ch23_08.htm; visited on November 19th 2012.

[268] D. E. Knuth, *Sorting and Searching*, vol. 3 of *The Art of Computer Programming*, pp. 506–542. Addison-Wesley, 1973.

[269] M. Holthausen, K. S. Lim, and M. Lindner, "Planck scale Boundary Conditions and the Higgs Mass," *JHEP* **1202** (2012) 037, arXiv:1112.2415 [hep-ph].

[270] U. Langenfeld, S. Moch, and P. Uwer, "Measuring the running top-quark mass," *Phys.Rev.* **D80** (2009) 054009, arXiv:0906.5273 [hep-ph].

[271] M. E. Machacek and M. T. Vaughn, "Two Loop Renormalization Group Equations in a General Quantum Field Theory. 1. Wave Function Renormalization," *Nucl.Phys.* **B222** (1983) 83.

[272] M. E. Machacek and M. T. Vaughn, "Two Loop Renormalization Group Equations in a General Quantum Field Theory. 2. Yukawa Couplings," *Nucl.Phys.* **B236** (1984) 221.

[273] M. E. Machacek and M. T. Vaughn, "Two Loop Renormalization Group Equations in a General Quantum Field Theory. 3. Scalar Quartic Couplings," *Nucl.Phys.* **B249** (1985) 70.

[274] B. Grzadkowski and M. Lindner, "Nonlinear evolution of Yukawa couplings," *Phys.Lett.* **B193** (1987) 71.

[275] B. Grzadkowski, M. Lindner, and S. Theisen, "Nonlinear evolution of Yukawa couplings in the double Higgs and supersymmetric extensions of the standard model," *Phys.Lett.* **B198** (1987) 64.